ADDIS ABABA SCIENCE AND TECHNOLOGY UNIVERSTIY

COLLEGE OF ARCHITECTURE AND CIVIL ENGINEERING

DEPARTMENT OF CIVIL ENGINERING

(GEOTECHNICAL ENGINEERING)

ASSESSMENT ON THE EFFECT OF DYNAMIC LOADS ON AIRPORT PAVEMENT STRUCTURE: A CASE STUDY AT BOLE INTERNATIONAL AIRPORT

A Thesis Submitted to the Department of Civil Engineering, College of Architecture and Civil Engineering in Partial Fulfillment of the Requirement for a Master of Science Degree in Geotechnical Engineering

BY KIRUBEL TEFERA

Advisor: Yoseph Birru Gebregiorgis (PhD)

June, 2018

ADDIS ABABA SCIENCE AND TECHNOLOGY UNIVERSTIY

APPROVED BY BOAED OF EXAMINERS

APPROVAL PAGE

This MSc thesis Proposal entitled with **"ASSESSMENT ON TH EEFFECT OF DYNAMIC LOADS ON AIRPORT PAVEMENT STRUCTURE: A CASE STUDY AT BOLE INTERNATIONAL AIRPORT"** has been approved by the following examiners after the Thesis presentation for the Master of Science in Geotechnical Engineering.

Date of Defense: 16/06/2018

Yoseph Birru Gebregiorgis (PhD)	_____	_____
Advisor	Signature	Date
Dr.Avinash M.Potdar	_____	_____
Internal Examiner	Signature	Date
Dr. Argaw Asha	_____	_____
External Examiner	Signature	Date
Dr. Melaku Sisay	_____	_____
ERA PG, Program Coordinator	Signature	Date
Mr. Simon G/Egziabher	_____	_____
Head, Civil Engineering Department	Signature	Date
Dr. Brook Abate	_____	_____
Dean, College of Architecture and Civil Engineering	Signature	Date

DECLARATION

Hereby declare that the work which is being presented in this thesis entitles "**Assessment on the Effect of Dynamic Loads on Airport pavement Structures: A Case Study at Bole International Airport**" is original work of my own, has not been presented for a degree in any university and that all sources of materials used for this thesis duly acknowledge.

Name: Kirubel Tefera

Signature: _____

Place: Addis Ababa Science and Technology University

College of Architecture and Civil Engineering

Geotechnical Engineering

Date: May, 2018

ACKNOWLEDGEMENT

I would like to thank my almighty God who is always with me in each and every step of my life. I wish to express my sincere and deepest gratitude to my advisor Dr. Yosef Birru for all his guidance, support and supervision my research work. I would like to thank Ethiopian Roads Authority and Addis Ababa Science and Technology University (AASTU) for making me part of this postgraduate scholarship program. I gratefully acknowledge The Ethiopian Airport Enterprise works, especially Tariku Gebrehiwot and Mengistu Gebrekiros during collection of soil samples and data from different location. They definitely provide me with the tool that I need to choose and the right path I should follow to successful completion of this thesis. Finally, my deep and sincere gratitude to my family for their love, help and support and encouraging me and this journey would not have been possible if not for them, and I want to thank my friends and colleagues.

TABLE OF CONTENTS

LIST OF SYMBOLS AND ABRIVATIONS

ET: Ethiopian Airlines (Ethiopian)

FAA: Federal Aviation Administration

MEPDG: Mechanistic-Empirical Pavement Design Guide

CBR: California Bearing Ratio

NAFEC: National Aviation Facilities Experimental Center

NAPTF: National Airport Pavement Test Facility

ASGs: Asphalt Strain Gages

ESALs: Equivalent Standard Axle Loads

S: Aircraft Speed

FAARFIELD: Federal Aviation Administration Rigid and Flexible Iterative Elastic Layered Design

KN: Kilo Newton

AC: Asphalt concrete

AC CDF: Asphalt concrete cumulative damage factor

ESG =Resilient Modulus of the Subgrade

K= Foundation Modulus of the Subgrade

NDT: Nondestructive Testing

DCP: Dynamic Cone Penetrometer tests

NDT: Nondestructive testing

NCHRP: National Cooperative Highway Research Program

LLNL: Lawrence Livermore National Laboratory

LEAF: Layered Elastic Computational Program Implemented

TC: Standard Traffic Cycle

FWD: Falling-Weight Deflectometer

NAFEC: National Aviation Facilities Experimental Center

AASTU: Addis Ababa Science and Technology University

LIST OF TABLES

LIST OF FIGURES

LIST OF ANNEX

ABSTRACT

This research was aim to assess the effect of dynamic load on airport pavement structures in general and Airport pavements in particular. The proper assessment on the effect of dynamic loads on airport pavement structures shall be important for understanding the mechanisms and effects of dynamic loads on such structures. The primary aim of this research was to assess the effects of dynamic loads on Airport pavements taking the Addis Ababa Bole International Airport as a sample.

Sieve analysis, compaction and Californian bearing ratio was conducted at Addis Ababa Bole international site. To identify mechanism and the effect of dynamic load on airport pavement structure analysis was made for load duration, static deflection, dynamic deflection, maximum deflection and impact factor. Finally, federal aviation administration rigid and flexible iterative (FAARFIELD) software was used for conducted to analyses of cumulative damage factor (CDF) value for subgrade. It consists of automatic calculation based on elastic and linear multilayer structural model for flexible pavements. Potential applicability of this new method for Airport pavement design has been evaluated considering Bole international airport as case study. The data used for traffic and pavement structures were obtained from the project document for the Expansion of Addis Ababa Bole international airport.

It is concluded that federal aviation administration rigid and flexible iterative (FAARFIELD) is more detailed and controllable. The results are more conservative when pavements are at the limit of its service capacity and align reasonably when dealing with new pavements or with pavements having high load capacity. In general, the results of the study show that load duration, maximum deflection (response) have inverse relation with the aircraft speed. On the other hand, dynamic deflection (response) and impact factor have direct relation with the aircraft speed. Subgrade cumulative damage factor (CDF) value decreases with increase in Californian bearing ratio (CBR) value and finally goes to zero. This show that for flexible pavement subgrade cumulative damage factor (CDF)-value, foundation modulus of subgrade (k)-value and natural frequency approaches to zero as time goes to infinity.

Key Words: Dynamic Load**;** Airport Pavements; Subgrade cumulative damage factor(CDF); Resilient Modulus(R); Foundation Modulus (K); Elastic modulus (E); federal aviation administration rigid and flexible iterative (FAARFIELD) Software

CHAPTER ONE

INTRODUCTION

1.1 Background

Ethiopian Airlines (Ethiopian) (ET) is a government owned company found in the capital city of Ethiopia, Addis Ababa, with its head office located at Bole International Airport (Ethiopian Fact Sheet 2011). The airline, which was established on 1945, is one of the worlds and Africa's oldest airlines, with over sixty years of existence (Iches et.al 2005). On April 08, 1946, the airline started operation by making its first domestic flight to Gondar and international flight to Cairo (Saunders 1971). This makes the airline to take the pioneer position in African air transport industry (Bahru 1988).

Air transport provides several far reaching benefits to different countries worldwide (Aviation n.d.). Explicitly, it is essential to create employment opportunity, growth and sustainability of tourism, fast and efficient trade, sustainable economic growth and the likes (Aviation n.d.). In this regard, Ethiopian Airlines provides several benefits to the country as well as to different stakeholders through the provision of different services to its customers (Civil Aviation Authority 2007). For instance, by being source of direct and indirect employment and hiring essential amount of human resource, it plays a significant role in an attempt to overcome the problem of high unemployment in the country (Nyaringo 1964). Besides, it encourages the national tourism sector by facilitating transportation for a number of tourists from different parts of the world, and it also has other benefits (African Aviation 2006; Civil Aviation Authority 2011).

1.2. Statement of the Problem

The Ethiopian Airport enterprise has Aircraft and Machines. But during the operation of the Aircraft on runways, and operation of machine in maintenance room, it produces the dynamic load. These loads have direct and indirect contact with the airport pavement structure such as Airport flexible pavement. These loads also have the negative effect on the Airport pavement structure especially on Airport flexible pavement. For example overloading of the pavements can result either from loads too large or from a substantially increased application rate or from both. Loads and pressure larger than the defined (design or evaluation) load, it shortens

the design life engineering structure, whilst smaller loads extend it. With the exception of massive overloading, pavements in their structural behavior are not subjected to particular limiting load above which they suddenly or catastrophically fail. This failure on the airport pavement structure occurs due to the failure on the foundation or subgrade which supports Airport pavement structure. Also, the dynamic loads have negative effect on subgrade and the foundation material which supports that airport pavement structure.

Therefore, the purpose of this research was to search the problems related with the dynamic load effect on the Airport pavement structure especially Airport flexible in case Bole International Airport. It should indicate the problem if exist, and provide specific measurement. Finally we would compare the result for different condition of dynamic load generating and recommend the specific solution for specific problem as Engineer.

1.3. Objectives

1.3.1 General Objective

The main objective of this research was to assess the effect and mechanism by which a dynamic load can affect Airport pavement structures, taking Addis Ababa Bole International Airport as a sample.

1.3.2 Specific Objectives

- To determine the properties of soil.
- To identify dynamic loads based on site features
- To Analysis the effect of dynamic load on the Airport pavement structure and the mechanisms considering type of structures, size and typology with corresponding foundation types.
- To propose remedial measures. This shall consider for both existing and new structures

1.4 Research Question

Therefore, the researcher motivated to assess the effect of dynamic load on Airport pavement structures in particular by answering the following basic questions:

1. How to identify dynamic loads based on site features?
2. What are the effect of dynamic load on the airport pavement structure in general and Airport pavements in particular?
3. How to identify the effect of dynamic load on the airport pavement structure in in general and Airport pavements in particular, and the mechanisms considering type of structures, size and typology with corresponding foundation types ?
4. How to Analysis the effect of dynamic load on the airport pavement structure in general and Airport pavements in particular, and the mechanisms considering type of structures, size and typology with corresponding foundation types?

1.5 Scope of the Study

This study will be conducted in Addis Ababa Bole International Airport. The assessment was on the effect of dynamic loads effects on airport pavement structure, and mechanism by which the dynamic load can affect the airport pavement structure.

Figure1-1 Site Location on Google Earth Map

1.6 Structure of the Thesis

This thesis contains six Chapters and appendices. The first Chapter contains introduction, Background, statement of the problem, objectives, scope of the study and structure of the thesis. Chapter two covers a literature review containing Introduction, Effect of Dynamic Load, Effect of Dynamic Load on airport pavement Structure, Effect of Dynamic Load on Subgrades, Analyzing the Effect of Dynamic (Moving) Loads, Subgrade Behavior, Subgrade Behavior under Airport Flexible Pavement, Laboratory and Field Test, Laboratory and Field Test for Pavement and Correlations with Other Tests. In the third Chapter, the general description of the study area under which contain about site information such as General, Soil, Classification System , Subgrade Support, Drainage , Soil Conditions , Site Investigation , Procedures , Soil Maps , Aerial Photography, Geography, Climate. The materials and method presented in chapter four. In fifth chapter laboratory test results and discussions are presented. In chapter six conclusion and recommendation are given. Reference materials used in the research work are appropriately sited and listed. The thesis ends with appendices which contain detail experimental results of laboratory investigation.

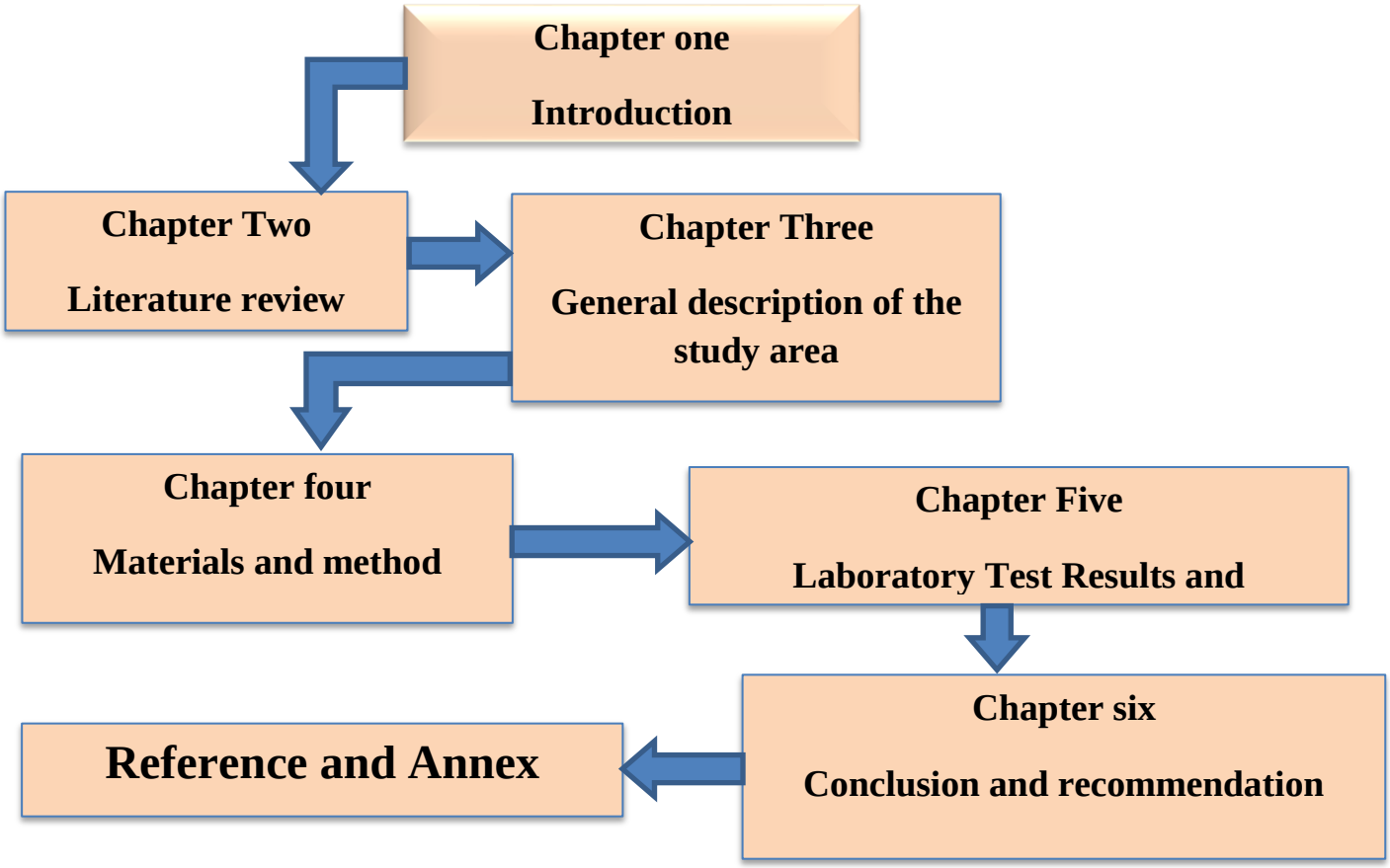

Figure 1-2 : Outline of the Thesis

CHAPTER TWO

LITERATURE REVIEW

2.1 Introduction

The objective of this research is to examine the effect of dynamic load by introducing the aircraft loads on the airport flexible pavement.

2.2 Effect of Dynamic Load

2.2.1 Effect of Dynamic Load on Airport Pavement Structure

Increase in the weight and number of aircrafts that use the existing airport asphalt pavements has focused the light on the ability of these pavements to serve efficiently. The fast deterioration of airport asphalt pavements in comparison with their design life encourages the researchers to assess the effect of dynamic load on the existing airport pavement. The effect of aircraft impact, aircraft movement, and aircraft braking forces on airport asphalt pavement were studied. It was found that all the known design methods of airport asphalt pavements are underestimate the actual dynamic effects of aircraft loads. (Richard H. Ledbetter) When the impact factor is 1.5 of the actual wheel load, the wheel load factor for rutting criterion is from 3.96-4.49 for standard single wheel loads of 200-500kN respectively. Also, when the braking forces are 50% of the standard single wheel loads, the wheel load factor for fatigue criterion is from 6.64-7.66 for single wheel loads of 133.6-334kN respectively. The pavement structure optimization as recommended by most design methods should be re-considered due to the considerable effects of dynamic loads of aircraft maneuvers.

Yoder and Witczak reported that historically, all airfield pavement designs have been based upon the most critical areas being the primary taxiway and runway ends, the introduction of jet aircraft and the possibility of greater dynamic responses due to such features as acceleration, deceleration, reverse thrust, "spike" load at the point of rotation have resulted in the reevaluation of design principles to examine what is the critical airfield area. They mentioned that there is no current field evidence, however, available on large scale, to conclude that dynamic aircraft effects are more critical from a design viewpoint than the conditions assumed for static and slowly moving aircraft at or near maximum takeoff weight.

Huang reported that all methods discussed so far are based on static without considering the inertia effects due to dynamic loads**.** The inclusion of inertial effect for routine pavement design involving nonlinear elastic and visco-elastic materials is still a dream to be realized in the future. Seong et al. (2002) reported that the pavement responses have often been analyzed with static loads, but the pavement critical responses are induced by moving dynamic loads. In their research the airport pavements have been modeled using a plate of infinite extent on a visco-elastic foundation. They modeled moving aircraft loads as a twin-tandem main gear with constant load amplitude or harmonic amplitude variations. Their analysis results considering visco-elasticity of the foundation showed significant differences from those obtained with an elastic system. Without viscous damping, they reported, the effects of aircraft speed and load frequency, within practical ranges, on the deflection and stress are negligible; however, with viscous damping, those effects are significant. Yadav and Shukla (2012) stated that an estimation of the runway pavement deflection during landing for design purposes has been a challenging problem for engineers. Their model showed that the dynamic deflection increases with an increase in vertical velocity and contact pressure. Likewise, the impact factor, which is defined as the ratio of the dynamic deflection to static deflection, also increases with an increase in vertical velocity for a given value of the contact pressure. They found that irrespective of contact pressure values, the impact factor for zero vertical velocity is 2 under elastic runway pavement conditions. The FAA advisory circular (2009) is based on new geotechnical research and experience, and has completely revised the previous pavement design procedures. The new aircraft live load distributions recognize much heavier aircraft takeoff weights, but also do not overload existing runway designs.

Two series of full-scale tests using instrumented aircraft and runways were made (Richard H. Ledbetter, U.S. Army Engineer Waterways Experiment Station, and Vicksburg, Mississippi). Among the results were that (a) both types of pavements exhibited both elastic and inelastic responses; (b) these types of responses must be separated to interpret the data; (c) two different types of displacement responses (inertial and non-inertial) are present;(d) bow waves and elastic vertical expansions about the wheels occur in both types of pavements; (e) the vertical pressures in both types of pavements are totally recoverable and elastic; (f) no basic aircraft ground operating mode induces pavement responses greater than those occurring for static load conditions, although under unusual conditions, such responses might occur; (g) pavement thicknesses can be reduced in the interiors of runways, but the pavement in exit areas of flexible runways should be stronger than that of main runways; (h) inelastic

behavior is highly dependent on temperature, rate of load application, and load history; (i) in the velocity range of static load to low-speed taxi, inelastic displacements can be larger than elastic ones; and (j) the elastic behavior of stiff pavements is almost constant. Because the elastic and inelastic displacement behavior of pavements correlates to the behavior of the Waterways Experiment Station pavements test sections under simulated aircraft loads and wheel configurations and distributed traffic to the behavior of actual pavements under actual aircraft operations, further investigations of dynamic load effects can probably be conducted on pavement test sections of limited size.

Because of reports of pavement distress resulting from current commercial aircraft loads and growing concern over the possibility of further detrimental aircraft dynamic-load effects on airport pavements. The study consisted of a literature survey, computer analyses to determine aircraft-loads and pavement responses, scaled pavement tests, and correlations between experimental and analytical data. In general, it was concluded that aircraft dynamic wheel loads have had a significant effect on portions of airport pavements. Specifically, the study showed that the primary effects that influence pavement response to dynamic loads are the increased magnitudes of aircraft wheel loads that result from aircraft modes of operation, pavement unevenness, and aircraft structural characteristics during moving ground operations and the dynamic load phenomena associated with the materials used in the construction of both flexible pavements. For a given aircraft and level of pavement unevenness, the loads imposed on a runway can be accurately defined for various ground operations. On the other hand, there has been a serious lack of the information necessary to obtain an accurate description of pavement response to dynamic loads. (Richard H. Ledbetter)

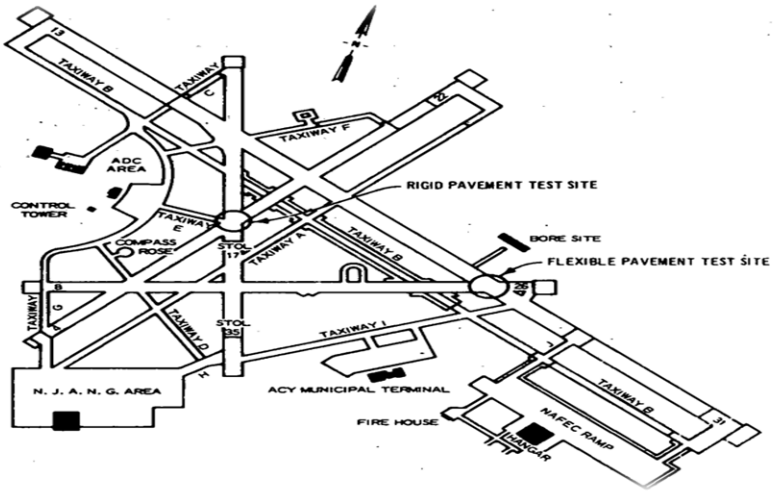

Figure 2-1 Test Sites at NAFEC Airport (Richard H. Ledbetter)

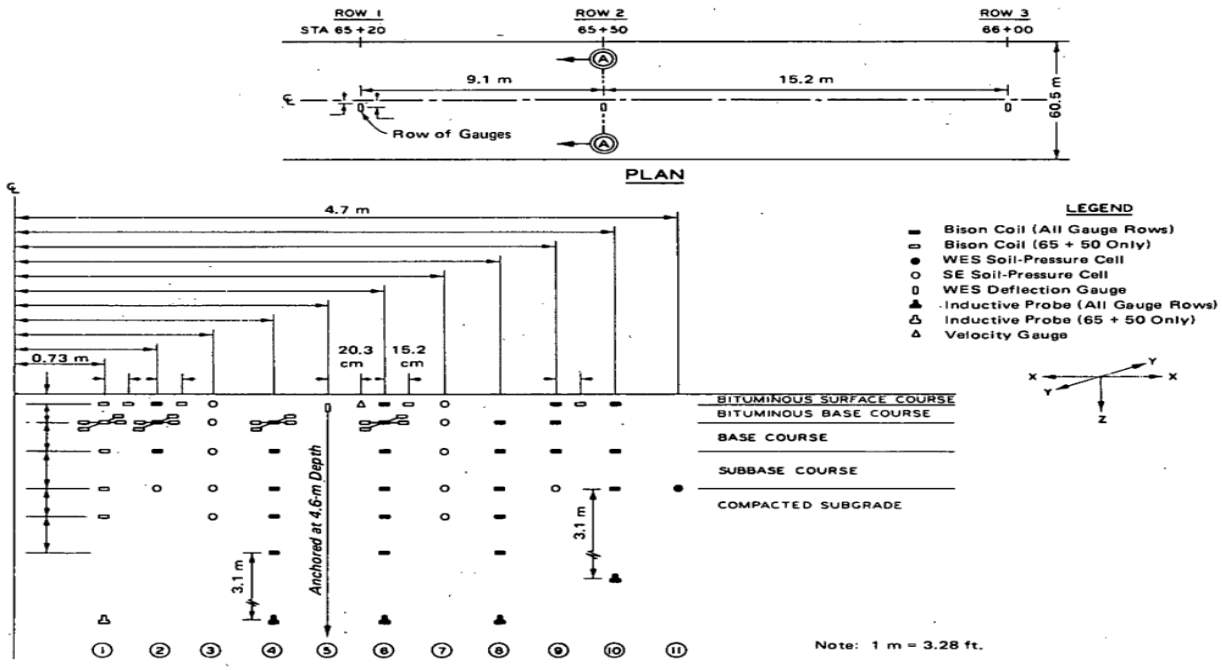

Figure 2-2 Arrangement of Flexible Pavement Instrumentation (Richard H. Ledbetter)

AC fatigue cracking and rutting are among the most common distresses in airport flexible pavements. The main focus of the NAPTF traffic test program was to evaluate these two pavement performance characteristics: rutting and AC fatigue cracking.

2.2.2 Effect of Dynamic Load on Subgrades

Subgrade is the foundation layer for supporting highways. One of the influential parameters on stiffness modulus is dynamic loading characteristics in investigating the stiffness modulus, dynamic loading components including loading waveform, loading time and rest period should be taken into account.

2.2.2.1 Importance of Stiffness Modulus of Subgrade

Determination of pavement layer thickness is governed by the stiffness of subgrade and granular layers, thus information on the stiffness modulus of subgrade and granular layers is required before designing any pavement. These parameters are necessary to determine the thickness of the pavement layers in order to achieve an optimum economic design. If the stiffness value of base, subbase and subgrade layers is high, it means that these layers have higher stress distribution ability. Accordingly, the required thickness of pavement can be reduced using the stiffer layers. Thus, it gives a considerable cost saving in terms of construction beside the optimum design. In this paper the main focus is on subgrade layer. Barksdale and Itani (1989) indicated that uncrushed gravels have a lower stiffness modulus

than crushed stones making them more susceptible to rutting. In addition, Zakaria and Leest (1996) reported that pavement strain is strongly dependent on aggregate type, fines content, moisture content, compaction and load applications. Giroud and Han (2004) stated that, bearing capacity failure of the base course or subgrade after repeated traffic loads is the main cause of surface rutting. Xu and Huang (2011) concluded that most rutting is related to the weakness in the middle and lower layers. In addition, in the Mechanistic-Empirical Pavement Design Guide (MEPDG) the total rut depth in the pavement structure is equal to the sum of rut depths in each layer and the rutting of underlying layers should not be overlooked. Consequently, Jegede (2000) stated that stabilization could improve the California Bearing Ratio (CBR) when facing poor soil properties. This concurs with Van Zyl and Maree (1983) conclusion that increasing density (that is, increased stiffness) significantly reduces plastic deformation. In terms of fatigue failure, Mulungye et al. (2007) stated that even in weak soil layers, fatigue cracking occurred before rutting. Based on the studies done by Cardone et al. (2011), the stiffness of the soil and granular layer must be sufficiently high to avoid fatigue cracking. Finally, a critical overview of the literature indicates the significance of using appropriate stiffness for underlying layers including subgrade.

2.2.2.2 Necessity of Using Stiffness Modulus for Design

Currently, flexible pavements are designed generally based on static properties such as CBR and soil support values. These methods are unable to represent the real response of pavement layers under traffic loading, since they are based on static conditions which are different from actual conditions (dynamic loading). Stochastic dynamic loads are increase pavement damage about 20 to 30% more than static loads (Divne, 1998; Cebon, 1998; Yong et al., 2010). Although, researchers have long been aware of the effect of dynamic loading on road damage (Gillespie, 1992; Lu and Xueju, 1996) the actual pavement design was limited to static loading based on the experience. Recognizing this deficiency, engineers are recommended to use stiffness modulus for design and characterizing the pavement layers (M-EPDG guide and AASHTO, 2002). Three important aspects of dynamic loading include:

i. Loading waveform,
ii. Loading time,
iii. Rest period.

2.2.2.3 Loading Waveform for Subgrade Layer

Moving traffic applies continuous stress pulses to the material comprising each layer. Type, magnitude, and duration of the induced pulses depend on traffic volume, aircraft type, speed, pavement structure, type of materials, and element position (Huang, 2004). Square loading, haversine and sinusoidal loading waveforms have been used for characterizing the stiffness modulus. In the current MEPDG program, haversine loading waveform is used for testing pavement structure because of its similarity to the field condition. In a study by Zhou et al. (2010), a three-layered pavement structure consisting of a Hot Mix Asphalt (HMA) surface layer, base layer, and subgrade was analyzed under a standard 80kN single axle (dual-tire) load with a uniform contact pressure of 689.476kpa.

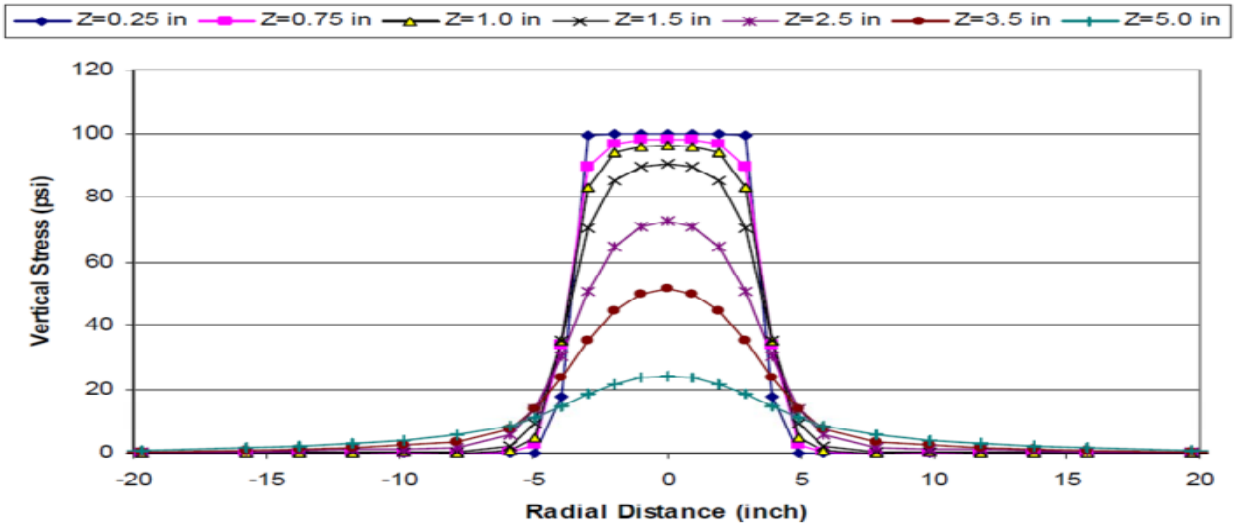

Figure 2-3: Vertical Stress Distributions at Different Depths of Pavement. (Zhou Et al.2010)

Figure 2.4 illustrates the computed vertical stress distributions at different depths in this study. They concluded that the square waveform loading represents the vertical stress distribution in the top one inch of pavement structure more realistically. Similar findings were reported in other pavement structures as well. Consequently, with increase in depth, haversine loading waveform can better present what practically occurs in the field compare to the square waveform. Therefore, for the subgrade layer, haversine loading waveform is recommended.

2.2.2.4 Loading Time for Subgrade Layer

The duration of loading pulse used for stiffness modulus determination should simulate the existing traffic condition in the field. Based on the literature (NCHRP 1- 37A, 2004; Zhou et al., 2010; Huang, 2004), it has been well established that the loading time duration depends on the aircraft speed and the depth of the desirable point below the pavement surface. Based on studies by Zhou et al. (2010); they emphasized and recommended the use of modulus ratio (the modulus ratio between each desired layer and the underneath layer) in order to characterize the loading time more realistically. They stated that even if the Aircraft speed and the depth beneath the pavement surface are the same, the loading times may differ significantly. A lower value of modulus ratio (R) indicates stiffer underneath materials and higher load distributing ability of the layer. As it can be seen from Table 2-1, the calculated loading times at different depths of the pavement structure match reasonably well to the measured values in the field by Loulizi et al. (2002) at the Virginia Smart Road project. Therefore, the loading time is mostly dependent on the depth, aircraft speed, and the stiffness modulus of the underneath layers. Loading time increases with depth and reduces with high speed traffic volume and stiffer underneath material. Consequently for subgrade layer, the effect of loading time is intensified due to the increase in depth and decrease in the quality of the materials.

2.2.2.5 Determination of Rest Period for Subgrade Layer

Traffic loading is not continuously applied to a pavement structure in the field but a rest period occurs corresponding to the traffic volume. Lytton et al. (1993) reported the rest period (t rest), between traffic loading passes as the number of seconds in a day divided by daily traffic (N) in Equivalent Standard Axle Loads (ESALs) (t rest = 86400/N). For pure elastic material, the rest period has no effect on the stiffness modulus (stress-strain relationship). Therefore, for subgrade material with elasto-plastic response, significant influence of the rest period on the layer stiffness modulus should be considered and AASHTO T307 has approved this statement.

2.2.2.6 Boundary of Stiffness Modulus for Various Soils

The preferred method for characterizing the stiffness of unbound pavement materials is the resilient modulus (Mr). The AASHTO 1993 Pavement Design Guide has recommended the resilient modulus for characterizing subgrade stiffness for flexible pavements. The resilient modulus test applies a repeated axial cyclic stress with fixed magnitude, load duration and

cycle duration to a cylindrical soil specimen. While the specimen is subjected to this dynamic loading, it is also subjected to a static confining stress provided by a triaxial pressure chamber. It is essentially a cyclic version of a triaxial compression test. Resilient modulus can be estimated from soil classification and soil unit weight. Table 2.2 summarizes the resilient modulus of different soils depending on soil classification for subgrade applications.

Table 2-1: The Measured Vs. the Predicted Loading Times at the Virginia Smart Road. (NCHRP 1-37A, 2004)

Truck speed Km/h	Deep (mm)	Measured loading time (sec)- smart road by(loulizi al,.. 2002)	Modulus ratio (R)	Predicted loading time by (Zhou et al..,2010)
	40	0.019	1	0.015
	190	0.031	2.66	0.036
75	267	0.054	0.17	0.046
	419	0.113	36	0.121
	597	0.142	1.18	0.144
	40	0.06	1	0.046
	190	0.09	2.66	0.119
25	267	0.14	0.17	0.120
	419	0.33	36	0.335
	597	0.42	1.18	0.402

Table 2-2 Default Mr. Values For Unbound Granular And Subgrade Materials At Optimum Moisture Content And Density Conditions (NCHRP 1-37A, 2004).

AASTO soil class	**Resilient modulus range (psi)**	**Type resilient modulus(psi)**
A-1-a	38,500 - 42,000	40,000
A-1-b	35,500 - 40,000	38,000
A-2-4	28,000 - 37,500	32,000
A-2-5	24,000 - 33,000	28,000
A-2-6	21,500 - 31,000	26,000
A-2-7	21,500 - 28,000	24,000
A-3	24,500 - 35,500	29,000

A-4	21,500 - 29,000	24,000
A-5	17,000 - 25,500	20,000
A-6	13,500 - 24,000	17,000
A-7-5	8,000 - 17,500	12,000
A-7-6	5,000 - 13,500	8,000

In many cases, fatigue or rutting failure in pavements occur due to inaccurate determination of stiffness modulus in subgrade layer. Improper stiffness modulus may rise from the difference between loading parameters in the laboratory testing condition and the field condition. In this paper, significant loading parameters including loading waveform, loading time, and rest time was expressed in subgrade layer. It was concluded that haversine loading waveform can better present what practically occurs in the field compare to the square waveform for subgrade layer. Furthermore, for this layer, the effect of loading time is intensified due to the increase in depth and decrease in the quality of the materials. In addition, because of elasto-plastic response of subgrade material, the rest period should be considered in determination of stiffness modulus.

2.2.3 Analyzing the Effect of Dynamic (Moving) Loads

Yadav and Shukla (2012) stated that an estimation of the runway pavement deflection during landing for design purposes has been a challenging problem for engineers. The elastic-viscoelastic correspondence principle can be applied directly to moving loads, as indicated by Perloff and Moavenzadeh (1967) for determining the surface deflection of a viscoelastic half-space, by Chou and Larew (1969) for the stresses and displacements in a viscoelastic two-layer system, by Elliott and Moavenzadeh (1971) in a three-layer system, and by Huang (1973b) in a multilayer system . The complexities of the analysis and the large amount of computer time required make these methods unsuited for practical use. Therefore, a simplified method has been used in both VESYS and KENLAYER.

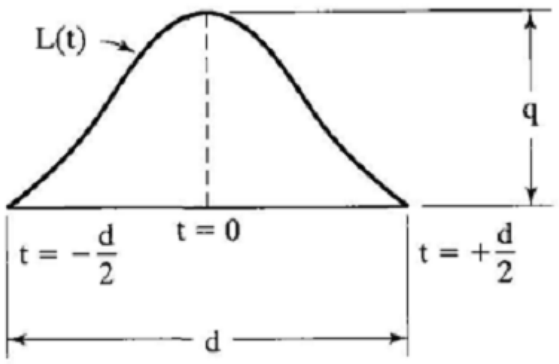

Figure 2-4 Moving Load as a Function of Time (Huang, 2004)

$$L(t) = qsin^2\left(\frac{\pi}{2} + \frac{\pi t}{d}\right) \ldots\ldots\ldots\ldots\ldots\ldots\ldots\ldots (2.1)$$

In this method, it is assumed that the intensity of load varies with time according to a haversine function, as shown in Figure 2.6 With t=0 at the peak, the load function is expressed as in which d is the duration of load . When the load is at a considerable distance from a given point, or t = ±d/2, the load above the point is zero, or $L(t) = 0$. When the load is directly above the given point, or t=0, the load intensity is q.

The duration of load depends on the aircraft speed "S" and the tire contact radius a. A reasonable assumption is that the load has practically no effect when it is at a distance of 6a from the point, or

$$d = \frac{12a}{S} \ldots\ldots\ldots\ldots\ldots\ldots\ldots\ldots\ldots\ldots\ldots\ldots\ldots\ldots (2.2)$$

If a=152.4mm and s=64 km/h = 17.9m/s d=0.1s.The response under static load can be expressed as a Dirichlet series:

$$R(t) = \sum_{i=1}^{7} C_i exp\left(-\frac{t}{T_i}\right) \ldots\ldots\ldots\ldots\ldots\ldots\ldots\ldots\ldots\ldots\ldots\ldots\ldots\ldots (2.3)$$

The response under moving load can be obtained by Boltzmann's superposition principle:

$$R = \int_{d/2}^{0} R(t)\frac{dL}{dt}dt \ldots\ldots\ldots\ldots\ldots\ldots\ldots\ldots\ldots\ldots\ldots (2.4)$$

$$\frac{dL}{dt} = \frac{q\pi}{d} sin\left(\frac{2\pi t}{d}\right) \ldots\ldots\ldots\ldots\ldots\ldots\ldots\ldots (2.5)$$

and integrating yields

$$R = \frac{q\pi^2}{2} \sum_{i=1}^{n} C_i \frac{1 + \exp(-d/2T_i)}{\pi^2 + (d/2T_i)^2} \ldots\ldots\ldots\ldots (2.6)$$

Assuming that the half-space has Poisson ratio 0.45 and is subjected to a circular load with contact radius 152mm and contact pressure 552kPa, as shown in Figure 2-6, determine the maximum surface time of 0.1s by deflection after a loading the collocation method

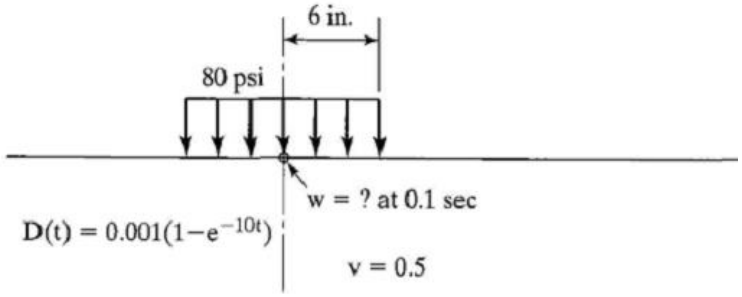

Figure 2-5 (1in=25.4mm, 1psi=6.9kpa). (Huang, 2004)

But the load is moving at 64 km/h to determine the maximum deflection according to Eq.2.7, the surface deflection under a static load can be expressed as

$$\omega = 0.72(1 - e^{-10t}) \ldots\ldots\ldots\ldots\ldots\ldots\ldots\ldots\ldots\ldots\ldots\ldots\ldots\ldots (2.7)$$

The first term is independent of time and therefore remains the same regardless of whether the load is moving. From Eq.2.6, the second term with T=0.1 and d=0.1s for 64km/h should be changed to 0.5 x π^2 x 0.72 (1+$e^{-0.5}$)/ (π^2+0.25) = 14.3mm, so maximum deflection = 0.72 - 0.564=3.96mm

2.3 Federal Aviation Administration Rigid and Flexible Iterative Elastic Layered Design (FAARFIELD) Software

FAARFIELD is based on the cumulative damage factor (CDF) concept, in which the contribution of each aircraft in a given traffic mix to total damage is separately analyzed. Therefore, the FAARFIELD program should not be used to compare individual aircraft pavement thickness requirements with the design methods contained in previous versions of the AC that are based on the "design aircraft" concept. Likewise, due care should be used when using FAARFIELD to evaluate pavement structures originally designed with the thickness design curves in previous versions of this AC. Any comparison between FAARFIELD and the design curve methodology from previous versions of this AC must be performed using the entire traffic mix.

The design procedure presented in this chapter provides a method of design based on layered elastic and three-dimensional finite element-based structural analysis developed to calculate design thicknesses for airfield pavements. Layered elastic and three-dimensional finite element-based design theories were adopted to address the impact of new complex gear and wheel arrangements. The design method is computationally intense, so the FAA developed a computer program called FAARFIELD to help pavement engineers implement it.

The structural computations are performed by two subprograms within FAARFIELD. These subprograms are called LEAF and NIKE3D_FAA. LEAF is a layered elastic computational program implemented as a Microsoft Windows TM dynamic link library written in Visual Basic TM 2005. NIKE3D_FAA is a three-dimensional finite element computational program implemented as a dynamic link library written in FORTRAN. NIKE3D_FAA is a modification of the NIKE3D program originally developed by the Lawrence Livermore National Laboratory (LLNL) of the U.S. Department of Energy and is distributed in compiled form under a software sharing agreement between LLNL and the FAA.

A wide variety of aircrafts with pertinent pavement design characteristics are stored in the program library. The FAARFIELD internal aircraft library is divided into six aircraft groups: Generic, Airbus, Boeing, Other Commercial, General Aviation, and Military. The designer has considerable latitude in selecting and adjusting aircraft weights and frequencies.

The pavement design method is based on the gross weight of the aircraft. The pavement should be designed for the maximum anticipated takeoff weight of the aircraft at the anticipated facility. The design procedure assumes 95 percent of the gross weight is carried by the main landing gears and 5 percent is carried by the nose gear. FAARFIELD provides manufacturer recommended gross operating weights for many civil and military aircraft. The FAA recommends using the maximum anticipated takeoff weight, which provides some degree of conservatism in the design. This will allow for changes in operational use and forecast traffic. The conservatism is offset somewhat by ignoring arriving traffic.

Gear type and configuration dictate how aircraft weight is distributed to a pavement and how the pavement will respond to aircraft loadings. Table 2.3 shows typical gear configurations and new gear designations in accordance with FAA Order 5300.7, Standard Naming Convention for Aircraft Landing Gear Configurations (Appendix 2).Tire pressure varies depending on gear configuration, gross weight, and tire size. Tire pressure has significantly more influence on strains in the asphalt surface layer than at the subgrade. Tire pressures in excess of 1.5MPa may be safely exceeded if the pavement surface course and base course meet the minimum design requirements for pavement loading along with a high stability asphalt surface.

Forecasts of annual departures by aircraft type are needed for pavement design. Information on aircraft operations is available from Airport Master Plans, Terminal Area Forecasts, the National Plan of Integrated Airport Systems, Airport Activity Statistics, and FAA Air Traffic Activity Reports. Pavement engineers should consult these publications when developing forecasts of annual departures by aircraft type.

Table 2-3 Standard Naming Convention for Common Aircraft Gear Configurations (O'Donnell, 2009)

Gear Designation	Gear Designation	Airplane Example
S	 Single	Sngl Whl-45
D	 Dual	B737-100
2S	 2 Singles in Tandem	C-130
2D	 2 Duals in Tandem	B767-200
3D	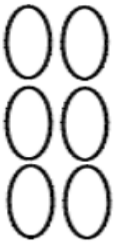 3 Duals in Tandem	B777-200
2T	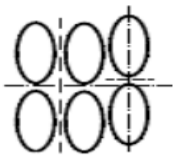 Two Triple Wheels in Tandem	C-17A

Table 2-4 Standard Naming Convention for Common Aircraft Gear Configurations (Continued) (O'Donnell, 2009)

Gear Designation	Gear Designation	Airplane Example
2D/D1	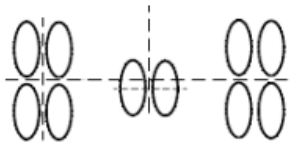 Two Dual Wheels in Tandem Main Gear/Dual Wheel Body Gear	DC10-30/40
2D/2D1	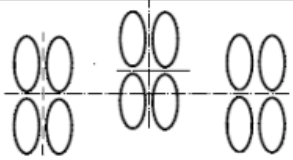 2D/2D1 Two Dual Wheels in Tandem Main Gear/Two Dual Wheels in Tandem Body Gear	A340-600 std
2D/2D2	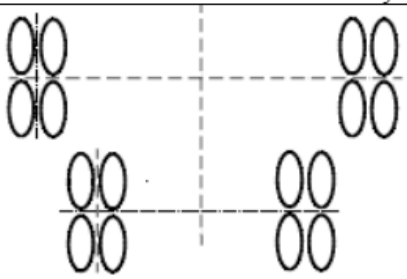 Two Dual Wheels in Tandem Main Gear/Two Dual Wheels in Tandem Body Gear	B747-400
2D/3D2	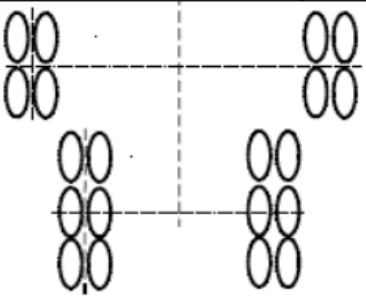 Two Dual Wheels in Tandem Main Gear/Three Dual Wheels in Tandem Body Gear	A380-800
5D	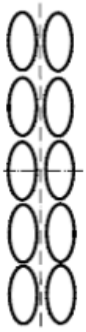 Five Dual Wheels in Tandem Main Gear	An-124

The program may be operated with U.S. customary or metric dimensions. FAARFIELD can be downloaded from the Office of Airport Safety and Standards website. (http://www.faa.gov/airports/). The internal help file for FAARFIELD contains a user's manual, which provides detailed information on proper execution of the program. The

manual also contains additional technical references for specific details of the FAARFIELD design procedure. FAARFIELD was developed and calibrated specifically to produce pavement thickness designs consistent with previous methods based on a mixture of different aircraft rather than an individual aircraft. If a single aircraft is used for design, a warning will appear in the Aircraft Window indicating a non-standard aircraft list is used in the design. This warning is intended to alert the user that the program was intended for use with a mixture of different aircraft types. Nearly any traffic mix can be developed from the aircraft in the program library. Solution times are a function of the number of aircrafts in the mix. The FAARFIELD design procedure deals with mixed traffic differently than did previous design methods. Determination of a design aircraft is not required to operate FAARFIELD. Instead, the program calculates the damaging effects of each aircraft in the traffic mix. The damaging effects of all aircrafts are summed in accordance with Miner's law. When the cumulative damage factor (CDF) sums to a value of 1.0, the design conditions have been satisfied.

There are distinct differences between the previous FAA design methodology and the methodology contained in FAARFIELD. These differences, along with some common design assumptions between the two methods, are discussed below. The FAA design standard for pavements is based on a 20-year design life. The computer program is capable of considering other design life time frames, but the use of a design life other than 20 years constitutes a deviation from FAA standards.

The design procedures in previous versions of this AC required the traffic mixture to be converted into a single design aircraft and all annual departures converted to equivalent annual departures of the design aircraft. The design aircraft was determined by selecting the most damaging aircraft based on the anticipated gross weight and the number of departures for each aircraft. The FAARFIELD design program does not convert the traffic mixture to equivalent departures of a design aircraft. Instead, it analyzes the damage to the pavement for each aircraft and determines a final thickness for the total cumulative damage. FAARFIELD considers the placement of each aircraft's main gear in relationship to the pavement centerline. It also allows the pavement damage associated with a particular aircraft to be completely isolated from one or more of the other aircrafts in the traffic mixture.

As an aircraft moves along a pavement section it seldom travels in a perfectly straight path or along the exact same path as before. This lateral movement is known as aircraft wander and is modeled by a statistically normal distribution. As an aircraft moves along a taxiway or runway, it may take several trips or passes along the pavement for a specific point on the pavement to receive a full-load application. The ratio of the number of passes required to apply one full load application to a unit area of the pavement is expressed by the pass to coverage (P/C) ratio. It is easy to observe the number of passes an aircraft may make on a given pavement, but the number of coverage must be mathematically derived based upon the established P/C ratio for each aircraft. By definition, one coverage occurs when a unit area of the pavement experiences the maximum response (strain for flexible pavement) induced by a given aircraft. For flexible pavements, coverage is a measure of the number of repetitions of the maximum strain occurring at the top of subgrade.

Airport pavement design using FAARFIELD considers only departures and ignores the arrival traffic when determining the number of aircraft passes. This is because in most cases aircrafts arrive at an airport at a significantly lower weight than at takeoff due to fuel consumption. During touchdown impact, remaining lift on the wings further alleviates the dynamic vertical force that is actually transmitted to the pavement through the landing gears. The FAA has defined a standard traffic cycle (TC) as one takeoff and one landing of the same aircraft. In the situation described above, one traffic cycle produces one pass of the aircraft which results in a pass to-traffic cycle ratio (P/TC) of 1. To determine annual departures for pavement design purposes multiply the number of departing aircrafts by the P/TC. For most airport pavement design purposes, a P/TC of 1 may be used. In cases where the landing weight is not significantly less than the takeoff weight or in a case where the aircraft must travel along the pavement more than once, it may be appropriate to adjust the number of annual departures used for thickness design to reflect a different pass-to-traffic cycle (P/TC) ratio. For example, in the case of a runway with a central taxiway configuration the aircraft is required to traffic a large part of the runway during the taxi movement. In this case the aircraft must travel along the same portion of the runway pavement two times during the takeoff operation. For this scenario a P/TC ratio of 2 would be used (assuming that the aircraft obtains fuel at the airport), and the number of annual departures used for design should accordingly be increased by a factor of 2. Additional definitions and guidance on determining the P/TC ratio may be found in AC 150/5335-5, “Standardized Method of Reporting Airport Pavement Strength – PCN,” Appendix1.

In FAARFIELD, the "design aircraft" concept has been replaced by design for fatigue failure expressed in terms of a cumulative damage factor (CDF) using Miner's rule, CDF is the amount of the structural fatigue life of a pavement that has been used up. It is expressed as the ratio of applied load repetitions to allowable load repetitions to failure. For a single aircraft and constant annual departures, CDF is expressed as

$$\text{CDF} = \frac{\text{number of load applied repetations}}{\text{number of allowable reptations to failure}} \ldots\ldots\ldots\ldots\ldots\ldots\ldots\ldots\ldots\ldots\ldots\ldots\ldots 2.8(a)$$

Or

$$\text{CDF} = \frac{(\text{anual departures})\text{x}(\text{life in years})}{\left({}^{\text{pass}}/_{\text{coverage ratio}}\right)\text{x}(\text{coverage to fuilure})} \ldots\ldots\ldots\ldots\ldots\ldots\ldots 2.8(b)$$

Or

$$\text{CDF} = \frac{\text{applied coverage}}{\text{coverages to fuilure}} \ldots\ldots\ldots\ldots\ldots\ldots\ldots\ldots\ldots 2.8(c)$$

Table 2-5 Describes Pavement Condition for Different Values of CDF (O'Donnell, 2009)

CDF value	Pavement Remaining Life
1	The pavement has used up all of its fatigue life.
<1	The pavement has some life remaining, and the value of CDF gives the fraction of then life used.
>1	The pavement has exceeded its fatigue life.

In the program implementation, CDF is calculated for each 254mm wide strip along the pavement over a total width of 20828 mm. Pass-to-coverage ratio is computed for each strip based on a normally distributed aircraft wander pattern with standard deviation of 773mm (equivalent to aircraft operation on a taxiway) and used in the above equation for Miner's rule. The CDF for design is taken to be the maximum over all 82 strips. Even with the same gear geometry, therefore, aircrafts with different main gear track widths will have different pass-to-coverage ratios in each of the 254mm strips and may show little cumulative effect on the maximum CDF. Removing the aircrafts with the lowest stress or strain may then have

little effect on the design thickness, depending on how close the gear tracks are to each other and the number of departures.

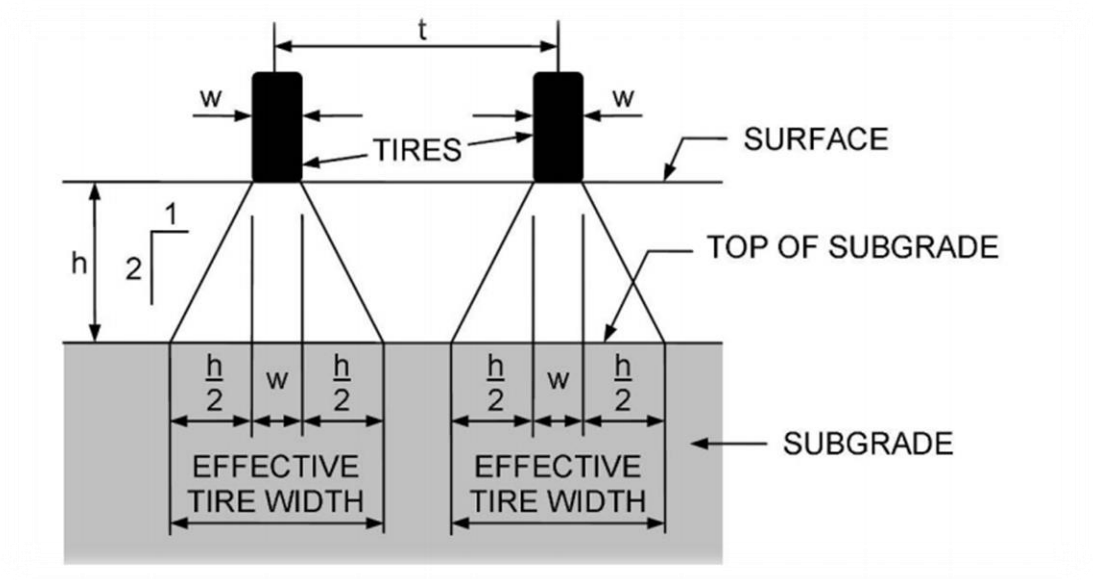

Figure 2-6 Two Effective Tire Widths - No Overlap (O'Donnell, 2009)

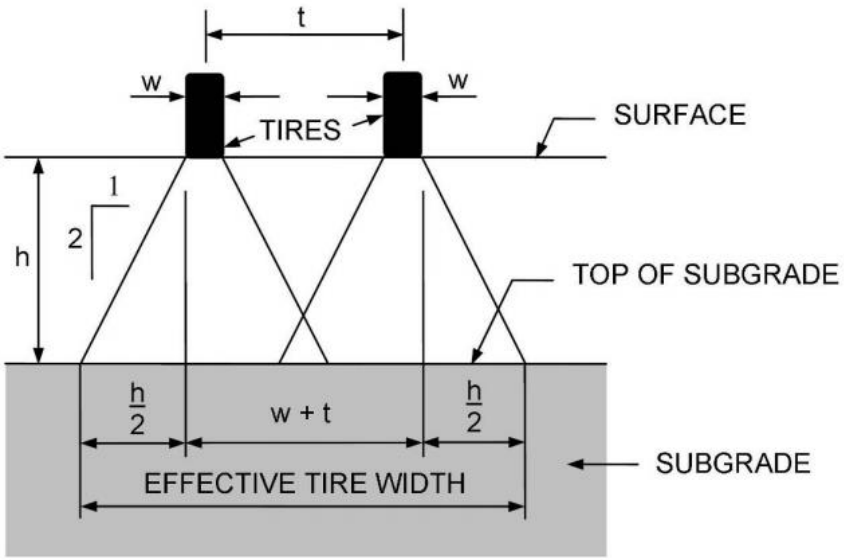

Figure 2-7 One Effective Tire Width–Overlap (O'Donnell, 2009)

To illustrate the results of CDF calculations, an existing taxiway pavement composed of the following section was assumed: the subgrade k-value is 38.4MN/m3, equivalent to an *E* modulus of 103.42MPa, the PCC surface course is 386mm thick, the P-306 concrete base

course is 152 mm thick, and the P-209 crushed aggregate subbase course is 152mm. The pavement is designed for the following aircraft mix: B747-200B Combi Mixed weighing 836,000 pounds (379,203kg) at an annual departure level of 1,200, B777-200 ER weighing 657,000 pounds (298,010kg) at an annual departure level of 1,200, and DC8-63/73 weighing 358,000 pounds (162,386kg) at an annual departure level of 1,200. The CDF contributions for each individual aircraft and the cumulative CDF across the pavement section are shown on figure 2-9. Values of individual aircraft contributions depend on several factors of which the most important are annual departure level and aircraft gross weight.

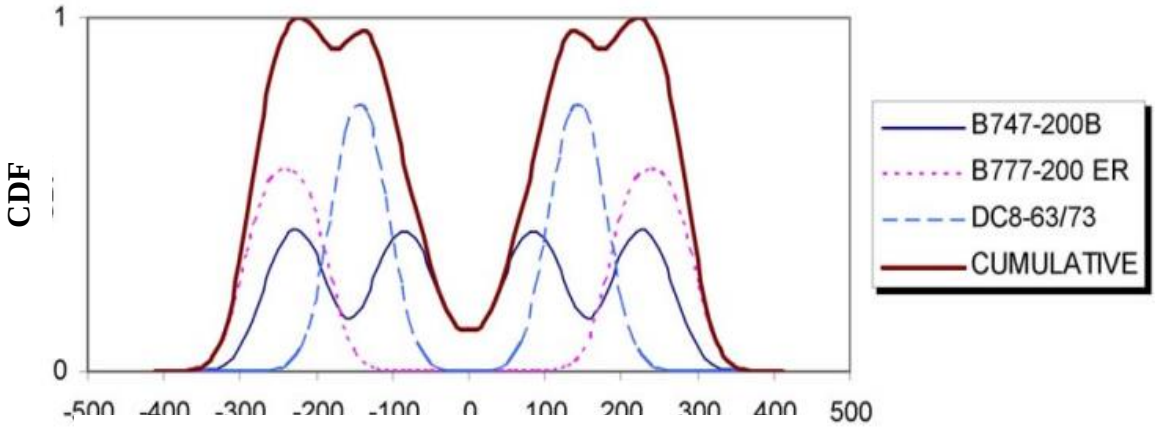

Figure 2-8 CDF Contribution for aircraft Mix (O'Donnell, 2009)

In the FAARFIELD design procedure, pavement layers are assigned a thickness, elastic modulus, and Poisson's ratio. The same layer properties are used in layered elastic and finite element analysis mode. Layer thicknesses can be varied, subject to minimum thickness requirements. Elastic moduli are either fixed or variable, depending on the material. The permissible range of variability for elastic moduli is fixed to ensure reasonable values. Poisson's ratio for all materials is fixed. Materials are identified by their corresponding FAA specification designations; for example, crushed stone base course is identified as Item P-209. The list of materials contains an undefined layer with variable properties. If an undefined layer is used, a warning will appear in the Structure Window stating that a non-standard material has been selected and its use in the structure will require FAA approval.

When used in accordance with the user's manual, FAARFIELD will automatically establish the minimum layer thickness for each layer, as required. However, it is recommended that the user consult the applicable paragraphs of this AC for design of new flexible is obtained.

2.4 Subgrade Behavior under Airport Flexible Pavement

Subgrade soil is the soil that forms the foundation for the pavement. It is the soil directly beneath the pavement structure. It should be remembered that the subgrade soil ultimately provides support for the pavement and the imposed loads. The pavement serves to distribute the imposed load to the subgrade over an area greater than that of the tire contact area. The greater the thickness of pavement, the greater is the area over which the load on the subgrade is distributed. It follows, therefore, that the more unstable the subgrade soil, the greater is the required area of load distribution and consequently the required thickness of pavement is greater. The soils having the best engineering characteristics encountered in the grading and excavating operations should be incorporated in the upper layers of the subgrade by selective grading. The strength of materials intended for use in flexible pavement structures is measured by the CBR tests.. Each of these tests is discussed in greater detail below. Elastic modulus is estimated from CBR and k using the correlations $E=1500\times CBR$ and $E=26\times k^{1.284}$

For flexible pavement design, FAARFIELD uses the maximum vertical strain at the top of the subgrade and the maximum horizontal strain at the bottom of the asphalt surface layer as the predictors of pavement structural life. FAARFIELD provides the required thickness for all individual layers of flexible pavement (surface, base, and subbase) needed to support a given aircraft traffic mix over a particular subgrade.

The subgrade soils are subjected to lower stresses than the surface, base, and subbase courses. Subgrade stresses attenuate with depth, and the controlling subgrade stress is usually at the top of the subgrade, unless unusual conditions exist. Unusual conditions such as a layered subgrade or sharply varying water contents or densities can change the location of the controlling stress. The ability of a particular soil to resist shear and deformation vary with its density and moisture content. Such unusual conditions should be revealed during the soils investigation. Specification Item P-152, Excavation and Embankment, covers the construction and density control of subgrade soils. Table 2-6 shows depths below the subgrade surface to which compaction controls apply. To use table 2-6, consider the mix of the aircrafts that will be using the pavement feature under consideration. The aircraft in the mix that should be used to determine compaction requirements is the aircraft requiring the

maximum compaction depth from table 2-6, regardless of the anticipated number of operations.

A loss of structural capacity can result from contamination of base or subbase elements with fines from underlying subgrade soils. This contamination occurs during pavement construction and during pavement loading. Aggregate contamination results in a reduced ability of the aggregate to distribute and reduce stresses applied to the subgrade. Fine grained soils are most likely to contaminate pavement aggregate. This process is not limited to soft subgrade conditions. Problematic soils may be cohesive or noncohesive and usually exhibit poor drainage properties. Chemical and mechanical stabilization of the subbase or subgrade can be effectively used to reduce aggregate contamination (refer to paragraph 206). Geosynthetics are effective at providing separation between fine-grained soils and overlying pavement aggregates (FHWA-HI-95-038) (see Appendix 4). In this application, the Geosynthetics is not considered to act as a structural element within the pavement. For separation applications the geosynthetic is designed based on survivability properties. Refer to FHWA-HI-95-038 (see Appendix 4) for additional information about design and construction using separation geosynthetic.

An apron extension is to be built to accommodate the following aircraft mix: B767-200 (154,221kg), B757-200 (1,161,200kg), and A310-200 (142,900kg). A soils investigation has shown the subgrade will be noncohesive. In-place densities of the soils have been determined at even foot increments below the ground surface. Design calculations indicate that the top of subgrade in this area will be approximately 10 inches (254mm) below the existing grade. Depths and densities may be tabulated as follows in table 2-6.

Table 2-6 Subgrade Compaction Requirements for Flexible Pavements (O'Donnell, 2009)

GEAR TYPE	GROSS WEIGHT(Lb)	NON-COHESIVE SOILS Depth of Compaction, inch				COHESIVE SOILS Depth of Compaction, inch			
		100%	**95%**	**90%**	**85%**	**100%**	**95%**	**90%**	**85%**
S	30,000	8	8-18	18-32	32-44	6	6-9	9-12	12-17
	50,000	10	10-24	24-36	36-48	6	6-9	9-16	16-20
	75,000	12	12-30	30-40	40-52	6	6-12	10-19	19-25
D (incls.2S)	50,000	12	12-28	28-38	38-50	6	6-10	10-17	17-22
	100,000	17	17-30	30-42	42-55	6	6-12	12-19	19-25
	150,000	19	19-32	32-46	46-60	7	6-14	14-21	21-28
	200,000	21	21-37	37-53	53-59	9	7-16	16-24	24-32
2D (incls. B757, B767,A-300, DC-10-10, L1011)	100,000	14	14-26	26-38	38-49	5	9-10	10-17	17-22
	200,000	17	17-30	30-43	43-56	5	6-12	12-18	18-26
	300,000	20	20-34	34-48	48-63	7	7-14	14-22	22-29
	400,000-600,000	23	23-41	41-59	59-76	9	9-18	18-27	27-36
2D/D1,2D/2D1(incls. MD11, A340,DC10-30/40)	500,000-600,000	23	23-41	41-59	59-76	9	9-18	18-27	27-36
2D/2D2 (incls. B747 series)	800,000	23	23-41	41-59	59-76	9	9-18	18-27	27-36
	975,000	24	24-44	44-62	62-78	10	10-20	20-28	20-28
3D (incls. B777 series)	550,000	20	20-36	36-52	52-67	6	6-14	14-21	14-21

	650,000	22	22-39	39-56	56-70	7	7-16	16-22	16-22
	750,000	24	24-42	42-57	57-71	8	8-17	17-23	17-23
2D/3D2 (incls. A380 series)	1,250,000	24	24-42	42-61	61-78	9	9-18	18-27	18-27
	1,350,000	25	25-44	44-64	64-81	10	10-20	20-29	20-27

Notes:

- Noncohesive soils, for the purpose of determining compaction control, are those with a plasticity index of less than 3.
- Tabulated values denote depths below the finished subgrade above which densities should equal or exceed the indicated percentage of the maximum dry density as specified in Item P-152.
- The subgrade in cut areas should have natural densities shown or should (a) be compacted from the surface to achieve the required densities, (b) be removed and replaced at the densities shown, or (c) when economics and grades permit, be covered with sufficient select or subbase material so that the uncompacted subgrade is at a depth where the in-place densities are satisfactory.
- For intermediate aircraft weights, use linear interpolation.
- 1inch = 25.4 mm, 1 pound. = 0.454 kg

Table 2-7 Densities for Subgrade (O'Donnell, 2009)

Depth Below Existing Grade	Depth Below Finished Grade	In-Place Density
1′ (0.3 m)	2″ (50 mm)	70%
2′ (0.6 m)	14″ (0.36 m)	84%
3′ (0.9 m)	26″ (0.66 m)	86%
4′ (1.2 m)	38″ (0.97 m)	90%
5′ (1.5 m)	50″ (1.27 m)	93%

The B767-200 gives the maximum required compaction values from table 2-3. Using table 2-6 for non-cohesive soils and applying linear interpolation, obtain the following compaction requirements as shown in table 2-8.

Table 2-8 Compaction Requirements (O'Donnell, 2009)

100%	95%	90%
0-21	21-37	37-52

Comparison of the tabulations show that for this example in-place density is satisfactory at a depth of 0.97m, being 90 percent within the required 90 percent zone. It will be necessary to compact an additional 0.03m at 95 percent. Therefore, compact the top 0.53m of subgrade at 100 percent density and the 533.4mm to 965.2mm at 95 percent density.

Subgrade soils are usually rather variable and the selection of a design CBR value requires some judgment. The design CBR value should be equal to or less than 85 percent of all the 27 AC 150/5320-6E 9/30/2009 subgrade CBR values. This corresponds to a design value of one standard deviation below the mean. In some cases subgrade soils that are significantly different in strength occur in different layers. In these instances several designs should be examined to determine the most economical pavement section. It may be more economical to remove and replace a weak layer than to design for it. On the other hand, circumstances may be such that designing for the weakest layer is more economical. Local conditions will dictate which approach should be used.

Subgrade soils are usually rather variable and the selection of a design CBR value requires some judgment. The design CBR value should be equal to or less than 85 percent of all the subgrade CBR values. This corresponds to a design value of one standard deviation below the mean. In some cases subgrade soils that are significantly different in strength occur in different layers. In these instances several designs should be examined to determine the most economical pavement section. It may be more economical to remove and replace a weak layer than to design for it. On the other hand, circumstances may be such that designing for the weakest layer is more economical. Local conditions will dictate which approach should be used.

The design process for flexible pavement considers two modes of failure for flexible pavement: vertical strain in the subgrade and horizontal strain in the asphalt layer. Limiting vertical strain in the subgrade is intended to preclude failure by subgrade rutting. Limiting horizontal strain at the bottom of the asphalt surfacing layer guards is against pavement failure initiated by cracking of the asphalt surface layer. By default, FAARFIELD computes only the vertical subgrade strain for flexible pavement thickness design. However, the user has the option of enabling the asphalt strain computation by deselecting the "No AC CDF" checkbox in the FAARFIELD options screen. In most cases the thickness design is governed by the subgrade strain criterion. The user has the option of performing the asphalt strain check for the final design, and it is good engineering practice to do so.

The subgrade is assumed to be infinite in thickness and is characterized by either a modulus or CBR value. Subgrade modulus values for flexible pavement design can be determined in a number of ways. The procedure that will be applicable in most cases is to use available CBR values and substitute in the relationship: $E = 1500 \times CBR$, (E in psi) this method will provide designs compatible with the previous FAA design procedure based on the CBR equation. Although FAARFIELD requires input of the material elastic modulus, direct input of CBR values is also acceptable.

As an example of the use of the FAARFIELD, assume a flexible pavement is to be designed for the aircraft traffic mix in table 2-9. The subgrade CBR is 8 (E=12,000psi). Since the traffic mix includes jet aircrafts weighing 45,359kg or more, an asphalt stabilized base will be used. The pavement layer thicknesses obtained from the design software FAARFIELD are listed in table 2-10.

Table 2-9 aircraft Traffic Mix

No.	Name	Gross Weight, lb	Annual Departures	Annual Growth, %
1	A320-100	150,796	600	0.00
2	A340-600 std	805,128	1,000	0.00
3	A340-600 std Belly	805,128	1,000	0.00
4	A380-800	1,239,000	300	0.00
5	B737-800	174,700	2,000	0.00
6	B747-400	877,000	400	0.00
7	B747-400ER	913,000	300	0.00
8	B757-300	271,000	1,200	0.00
9	B767-400 ER	451,000	800	0.00
10	B777-300 ER	777,000	1,000	0.00
11	B787-8	478,000	600	0.00

Table 2-10 Pavement Structure Information for Design

No.	Type	Thickness, in	Modulus, psi	Poisson's Ratio
1	P-401/ P-403 AC Surface	5.00	200,000	0.35
2	P-401/ P-403 St (flex)	11.06	400,000	0.35
3	P-209 Cr Ag	18.78	51,440	0.35
4	Subgrade	0.00	12,000	0.35

The screenshot from the design software showing final thickness design is shown below:

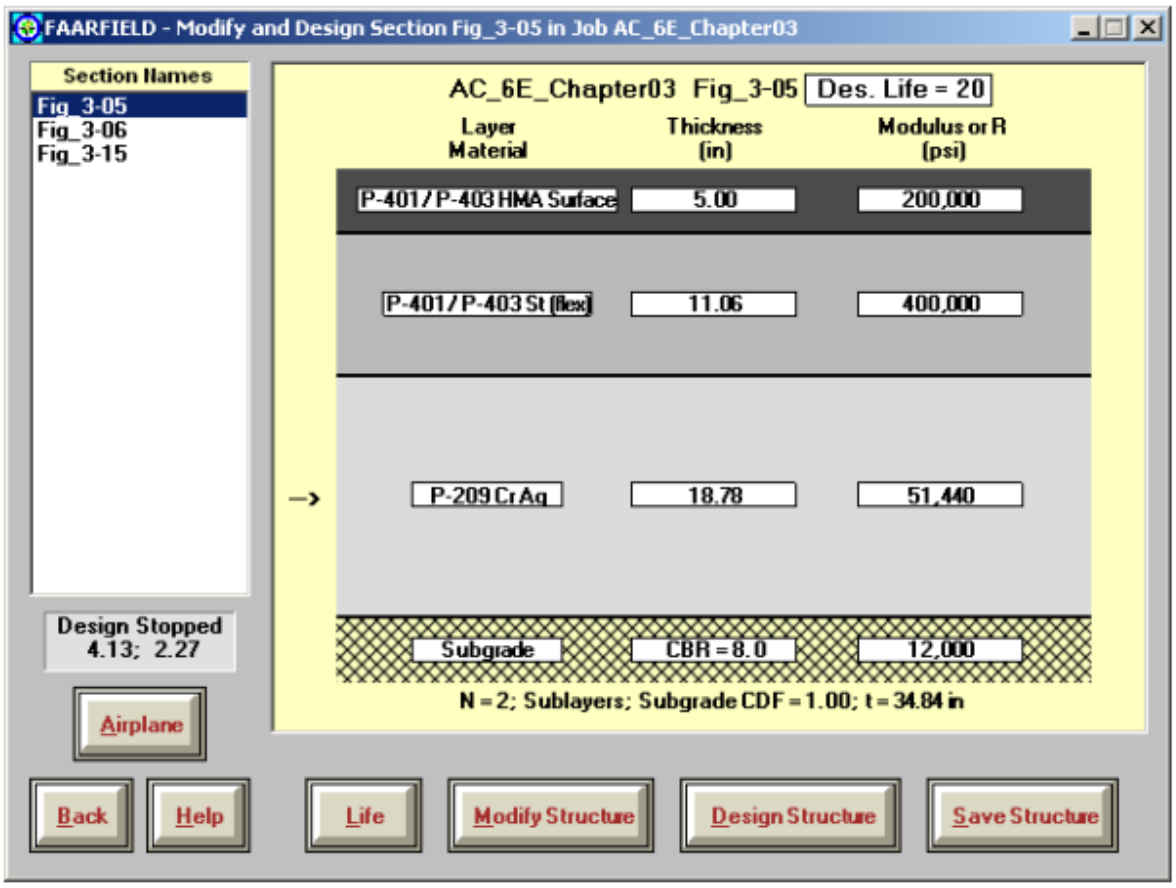

Figure 2-9 FAARFIELD Screenshot Showing Final Pavement Thickness Design

The pavement thickness design software also provides information on the damage caused by individual aircrafts. This additional information is provided in the Notes and aircrafts Windows. For the given example, the additional aircraft information is listed in table 2-8 Notes those two fields are provided for CDF information. Each field contains different information. “CDF Contribution” lists the contribution of the aircrafts to the total CDF calculated at the critical offset. This column should sum to 1.00 for a completed design, although due to rounding error and internal tolerances the sum may be slightly greater than or less than 1.00. “CDF Max for aircrafts” lists the maximum CDF over all offsets calculated for the aircrafts, whether or not these occur at the critical offset. The sum of the values in this column should be greater than or equal to 1.00 for a completed design.”

Table 2-11 Additional aircraft Information for Design (O'Donnell, 2009)

No.	Name	CDF Contribution	CDF Max for aircrafts	P/C Ratio
1	A320-100	0.00	0.00	1.21
2	A340-600 std	0.04	0.05	0.59
3	A340-600 std Belly	0.00	0.03	0.57
4	A380-800	0.01	0.01	0.42
5	B737-800	0.00	0.00	1.22
6	B747-400	0.01	0.01	0.57
7	B747-400ER	0.01	0.02	0.57
8	B757-300	0.00	0.00	0.73
9	B767-400 ER	0.04	0.05	0.60
10	B777-300 ER	0.86	0.86	0.40
11	B787-8	0.03	0.03	0.57

Table 2-11 shows that the pavement thickness design in this example is controlled primarily by the B777-300 ER, which contributes 86 percent of the CDF.

2.5. Laboratory and Field Test

2.5.1 Laboratory and Field Test for Pavement

The instrumentation packages were installed in the pavement structures of runways 04-22 and 13-31 at the National Aviation Facilities Experimental Center (NAFEC) Airport, Atlantic City, New Jersey, at the sites indicated in Figure 2.13. A 24.4rn long segment of runway 13-31 located at its intersection with runway 8-26 was selected as the flexible pavement test site. This test site allowed the collection of typical response measurements during landing and at the point of rotation for takeoff as well as during low- and high-speed taxiing, braking, and turning operations. This particular site was in a portion of the runway that was being reconstructed, which was of great advantage for the installation of the instrumentation. After the reconstruction, the flexible pavement in this area consisted of 7.6cm of bituminous surface course, 15.2cm of bituminous base course, and 22.9cm of base course consisting of the crushed and mixed original pavement surface and base courses, and 30.5cm of subbase course constructed from the original subbase course over a compacted subgrade.

Data were collected for 408 aircraft operations during the cold weather tests. Of this total, 203 operations were on the flexible pavement test site. During the warm weather tests, data were collected for 281 aircraft operations on the flexible pavement test site. The following types of tests were performed during both cold and warm weather tests:

Static load tests: - the aircraft was positioned over each gauge row and data collected to provide a base for comparison with the data from the dynamic load tests and a verification of the capability of the instrumentation system.

Dynamic load tests :- Various aircraft ground operations were conducted on the test sites, and the pavement responses and aircraft dynamic loads were determined for the following aircraft operating modes: (a) creep-speed taxi at 5.6 to 14.8 km/h, (b) low speed taxi at 27.8 to 55.6 km/h, (c) medium-speed taxi at 83.4 to 148.2 km/h, (d) high-speed taxi at 157.5 to 240.9 km/h, (e) high-speed braking at 240.9 to 83.4 km/h, (f) takeoff rotation at 157.5 to 240.9 km/h, (g) touchdown, (h) high speed braking with reverse thrust, and (i) turning at 7.4 to 55.6 km/h.

The NAPTF is located at the FAA's William J. Hughes Technical Center, Atlantic City International Airport, New Jersey. It was constructed to generate full-scale test data needed to develop pavement design

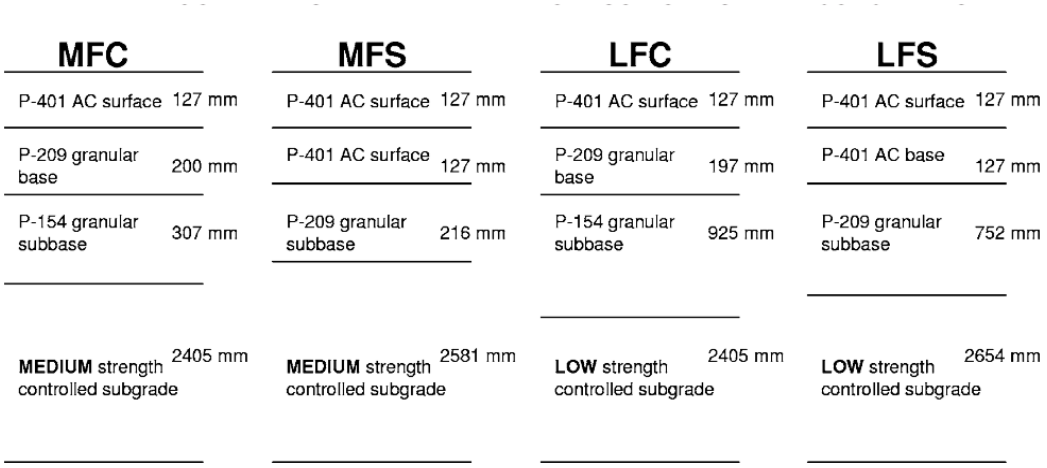

Figure 2-10: NAPTF of Flexible Test Sections. (Thompson, 2006)

Each NAPTF test section is designated using a three-character code MFC, LFS, etc., where the first character indicates the subgrade strength "L" for low, "M" for medium, and "H" for high, the second character indicates the test pavement type "F" for flexible and "R" for rigid, and third character signifies whether the base course material is conventional C unbound granular material or asphalt-stabilized S. Procedures for the new generation of large civil transport aircraft, including the Boeing 777 B777 and Boeing 747 B74. The NAPTF test pavement area is 274.3 m (900ft) long and 18.3 m 60ft wide. The first set of test pavements included a total of nine test sections six flexible and three rigid built on three different

subgrade materials: low-strength target California Bearing Ratio CBR of 4, medium-strength target CBR of 8, and high-strength target CBR of 20.

According to the FAA, the primary objective of the NAPTF trafficking tests was to determine the number of load applications to cause shear failure in the subgrade. Per NAPTF failure criterion, this is reflected as 25.4-mm surface upheaval adjacent to the traffic lane.

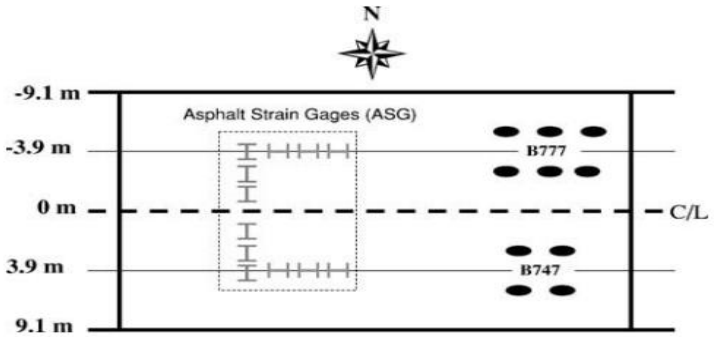

Figure 2-11: AC Strain Gage Installation at NAPTF. (Thompson, 2006)

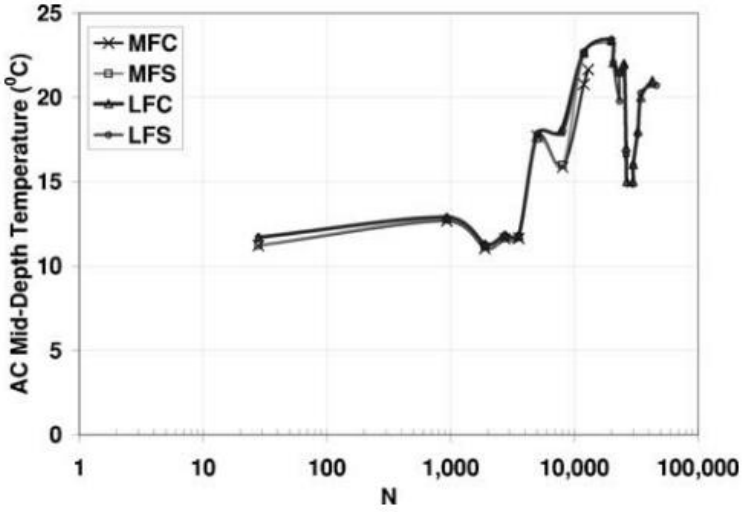

Figure 2-12 Variations in AC Temperature during NAPTF (Thompson, 2006)

After the completion of NAPTF traffic testing, trench studies were conducted to investigate the failure mechanism of the pavement structures. In the medium-strength flexible test sections MFC and MFS, rutting was primarily contributed by the subgrade and P-154 subbase layer. Subgrade intrusion into the P-154 subbase layer was observed. In both the low-strength subgrade test sections LFC and LFS, rutting was observed in the P-401 AC layer, P-209 base

layer, and P-154 subbase layers in both the traffic paths. Shoving occurred in the P-401 AC layer 35–38. The trench study findings also confirmed that the surface cracks in the NAPTF test pavements were all top-down cracks.

While the medium-strength subgrade test sections were declared to be failed at the subgrade level as per NAPTF failure criterion, the LFC and LFS sections failed in the surface layers, signifying tire pressure or other upper layer failure effects, but not subgrade level failure 36. According to Hayhoe , full structural failure did not occur in the LFC and LFS test sections, probably because the subgrade material contained a significant amount of silt and the upper layers of the subgrade dried somewhat over the long period of time between construction and starting of traffic testing.

The investigation of the relations between the pavement response and the aircraft dynamic loads found the following results: The B-727 aircraft dynamic load tests in 1972 (cold weather) and 1974 (warm weather) on the non-conditioned flexible pavement structure showed that none of the basic aircraft ground operating modes induced pavement responses (elastic plus inelastic) greater than those occurring for static load conditions, even though the aircraft dynamic loads were as much as 1.2 times the static load. That indicate the impact factor is 1.2. The elastic response alone also generally indicates this to be true. The pavement surfaces were relatively smooth in the test site areas. The tests showed that inelastic behavior is highly dependent on temperature, rate of load application, and load history (magnitude of load and lateral position of aircraft).

The elastic and inelastic displacement behavior directly correlates the behavior of the WES pavement test sections under simulated aircraft loads and wheel configurations and distributed (not conditioning) traffic to the behavior of an actual pavement under actual aircraft operations (NAFEC tests). This correlation means that any further investigation of dynamic load effects can probably be conducted on pavement test sections of limited size. Inelastic behavior occurred in both the non-conditioned flexible and may possibly be a common characteristic that links the performance of all types of pavement. In fact, it may be the major controlling factor or mechanism for pavement performance and life because it can be the primary movement for static and low-speed operations. (O'Donnell, 2009)

The thickness required of pavements subjected to parked or slow-moving aircraft should be based on the static mass of the aircraft, as is the current practice. This applies to the parking aprons, taxiways other than high speed exit areas, and runway ends. In high-speed exit areas,

runway interiors, and other areas that are subjected to high-speed aircraft operations only, the design should be based on an analysis of the design loading.

2.5.2 Correlations with Other Tests

Various empirical tests have been used to determine the material properties for pavement design. Most of these tests measure the strength of the material and are not a true representation of the resilient modulus. An extensive study was made by Van Til et al. (1972) to relate the resilient modulus and other test parameters to the soil support value or the layer coefficient employed in the AASHO design equation. These correlations can be used as a guide if other, more reliable, information is not available. It should be noted that any empirical correlation is based on a set of local conditions. The correlation is not valid if the actual conditions are different from those under which the correlation is established. Therefore, great care must be exercised in the judicious selection of the resilient modulus from these correlations. Figure 2.13 shows a correlation chart that can be used to estimate the resilient modulus of subgrade soils from the R value, CBR, Texas triaxial classification, and group index.

The R value is the resistance value of a soil determined by a stabilometer. The stabilometer test was developed by the California Division of Highways and measures basically the internal friction of the material; the cohesion for bonded materials is measured by the cohesiometer test. Figure 2.14 is a schematic diagram of stabilometer, which is a closed-system triaxial test. A vertical pressure of 1.1MPa is applied to a sample, 102mm in diameter and about 114mm in height, and the resulting horizontal pressures induced in the fluid within the rubber membrane are measured. The resistance value is computed as

$$R = 100 - \frac{100}{(2.5/D_2)\,(P_V/P_h - 1) + 1} \quad \ldots\ldots\ldots\ldots\ldots\ldots\ldots\ldots\ldots\ldots\ldots\ldots\ldots\ldots\ldots\ldots (2.11)$$

in which R is the resistance value; Pv is the applied vertical pressure of 1.1MPa; P_h is the transmitted horizontal pressure at Pv of 1.1 MPa; and D_2 is the displacement of stabilometer fluid necessary to increase horizontal pressure from 35 to 690 KPa, measured in revolutions of a calibrated pump handle. The value of D_2 is determined after the maximum vertical pressure of 1.1 MPa is applied. If the sample is a liquid with no shear resistance, then $P_h = P_{v,}$ or from Eq.7.5, R=0. If the sample is rigid with no deformation at all, then P_h=0, or R=100.

Therefore, the R value ranges from 0 to 100. To ensure that the sample is saturated; California used an exudation pressure of 1.7 MPa, whereas Washington used 2.1MPa.

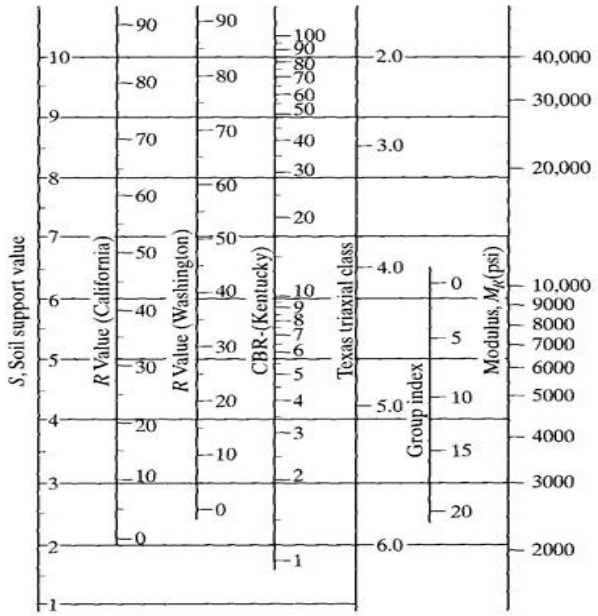

Figure 2-13 Correlation Chart for Estimating Resilient Modulus of Subgrade Soils (1psi=6.9kpa). (After Van Til Et Al. (1972)) (Huang, 2004)

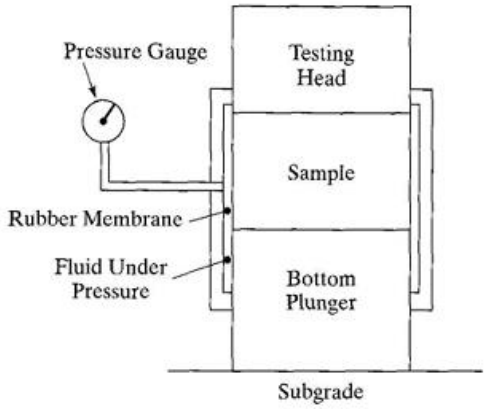

Figure 2-14 Schematic Diagram of Stabilometer (Huang, 2004)

The California Bearing Ratio test (CBR) is a penetration test, wherein a standard piston, having an area of 1935mm^2, is used to penetrate the soil at a standard rate of 1.3mm per minute. The pressure at each 2.5mm penetration up to 12.7mm is recorded and its ratio to the

bearing value of a standard crushed rock is termed as the CBR. The standard values of a high-quality crushed rock are as follows (Huang, 2004)

Figure 2-15, the Standard Values of a High-Quality Crushed Rock (Huang, 2004)

Penetration	Pressure
2.5mm	6.9MPa
5.0mm	10.4MPa
7.6mm	13.1MPa
10.2mm	15.9MPa
12.7mm	17.9 MPa

In most cases, CBR decreases as the penetration increases, so the ratio at the 2.5mm penetration is used as the CBR. In some cases, the ratio at 5.0mm will be greater than that at 2.5mm. If this occurs, the ratio at 5.0mm should be used. In the Kentucky method, the specimen is molded at or near to the optimum moisture as determined by the standard proctor method. However, the sample is placed in a mold, 152mm in diameter and 117mm in height, and com paced in five equal layers, each subjected to 10 blows of a 4.5kg hammer at 457mm drop. The specimen is soaked for 4 days before testing.

The Texas triaxial test is used to classify soils on the basis of the location of Mohr's envelope. The apparatus consists of a stainless cylinder with an inside diameter of 171mm fitted with a tubular rubber membrane 152mm in diameter. The lateral pressure σ_3 is applied by compressed air between the cylinder and the rubber membrane. The major principal stress is the applied stress because the confining pressure is not applied to the top of the specimen. From the principal stresses at the time of failure, Mohr's circles for several tests with different confining pressures are constructed. Mohr's failure envelope is transferred to a classification chart, as shown in Figure 2.19, and the strength class of the material is determined to the nearest tenth. The group index, which ranges from 0 to 20, is used in the AASH TO soil classification system. The values vary with the percentage passing through a No.200 sieve, the plasticity index, and the liquid limit and can be found from charts or formulas. In addition to Figure 2.13, other correlations between M_R, CBR, and R values are also available. These correlations could be quite different from those shown in Figure 2.19

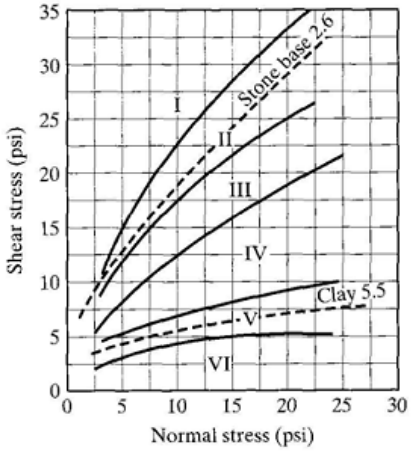

Figure 2-16 Chart for Classification of Subgrade and Base by Texas Triaxial Test (1psi=6.9kpa). (Huang, 2004)

Table 2-12: Comparison of CBR, R Value, and Resilient Modulus (Huang, 2004)

Soil Type	CBR test		R value test		Triaxial test
Soil description	CBR	MR (psi) by eq.7.6	R	M_R (psi) by eq.7.7	M_R (psi)
Sand	31	46,500	60	34,500	16,900
Silt	20	30,000	59	33,900	11,200
Sandy loam	25	37,500	21	12,800	11,600
Silt-clay loam	25	37,500	21	12,800	17,600
Silty clay	7.6	11,400	18	11,000	8200
Heavy clay	5.2	7800	<5	<3900	14,700

Note . Source : After AI (1982)

Heukelom and Klomp (1962), show that in which M_R is the resilient modulus in psi.

$$M_R = 1500(\text{CBR}) \ldots\ldots\ldots\ldots\ldots\ldots\ldots\ldots\ldots\ldots\ldots\ldots\ldots\ldots\ldots\ldots\ldots\ldots\ldots.. (2.12)$$

The coefficient, 1500, could vary from 750 to 3000, with a factor of 2. Available data indicate that Equation 2.13 provides better results at values of CBR less than about 20. In other words, the correlation appears to be more reasonable for fine-grained soils and fine sands than for granular materials.

The Asphalt Institute (1982) proposed the following correlation between M_R and the R value:

$$\text{M}_R = 1155 + 555R \ldots\ldots\ldots\ldots\ldots\ldots\ldots\ldots\ldots\ldots\ldots\ldots\ldots\ldots\ldots (2.13)$$

Laboratory data obtained from six different soil samples were used by the Asphalt Institute (1982) to illustrate the relationships. The R values were obtained at an exudation pressure of 1.7MPa. The CBR samples were compacted at optimum moisture content to maximum density and soaked before testing. The repeated load triaxial tests were performed at optimum conditions using a deviator stress of 41kPa and a confining pressure of 14kPa.

Table 2-13: Correlation between CBR and Resilient Modulus

Soil Type	CBR = 30			CBR = 80		
Location	R value	Texas classification	M_R (psi)	R value	Texas classification	M_R (psi)
Base 29,	65	3.2	20,000	83	2.1	000
Subbase	61	3.4	14,700	85	2.3	20,000
Subgrade	64	3.2	19,000	83	2.1	39,000

Note. 1psi=6.9 kPa

CHAPTER THREE

GENERAL DESCRIPTION OF THE STUDY AREA

Accurate identification and evaluation of pavement foundations is necessary. The following sections highlight some of the more important aspects of soil mechanics that are important to the geotechnical and pavement engineers.

3.1 Location

Addis Ababa is located at the center of Ethiopia between latitude of $8^0$50′11″-$9^0$05′29″North and longitude of 38039′40″-38054′57″East on Universal Transverse Mercator projection. The capital lies at the foot of Mount Entoto which is 3400m above sea level and extends south wards to its lowest point near to 2000m above sea level around Akaki i.e. south most edge of the city. The project site is located in Addis Ababa, Bole Sub-City, in bole international airport. The project site is characterized by flat to rolling ground with an average elevation of 2320.558m a.s.l.

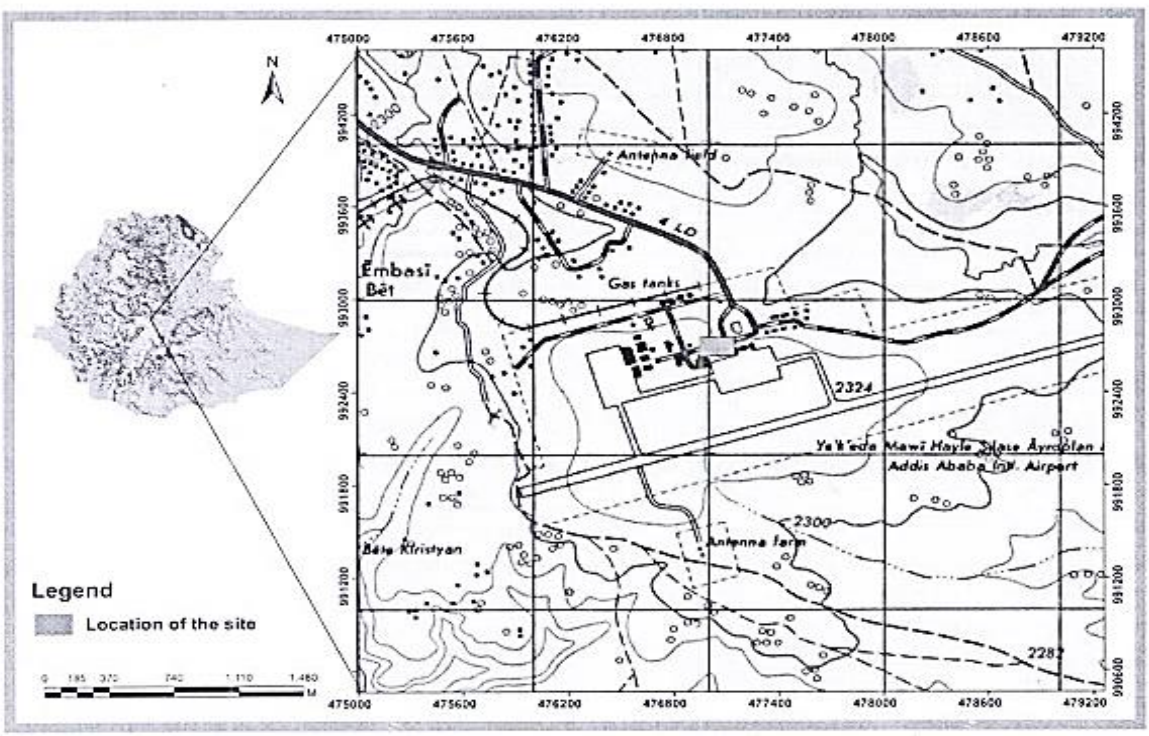

Figure 3-1 Location Map of Addis Ababa Bole International Terminal Expansion Site (Google map)

3.2 Soil Conditions and Drainage

For engineering purposes, soil includes all natural deposits that can be moved and manipulated with earth moving equipment, without requiring blasting or ripping. The soil profile is the vertical arrangement of individual soil layers exhibiting physical properties different than the adjacent layer. Subgrade soil is the soil layer that forms the foundation for the pavement structure; it is the soil directly beneath the pavement structure. Subsurface soil conditions include the elevation of the water table, the presence of water bearing strata, and the field properties of the soil. Field properties include the density, moisture content, frost susceptibility, and typical depth of frost penetration.

The subgrade soil provides the ultimate support for the pavement and the imposed loads. The pavement structure serves to distribute the imposed load to the subgrade over an area greater than the tire contact area. The available soils with the best engineering characteristics should be incorporated in the upper layers of the subgrade.

The design value for subgrade support should be conservatively selected to ensure a stable subgrade and should reflect the long term subgrade support that will be provided to the pavement. The Federal Airport Aviation (FAA) recommends selecting a value that is one standard deviation below the mean. Where the mean subgrade strength is lower than a California Bearing Ratio **(**CBR) of 5, it may be necessary to improve the subgrade through stabilization or other means in order to facilitate compaction of the subbase. When the design CBR is lower than 3, it is required to improve the subgrade through stabilization or other means. Soil conditions impact the size, extent, and nature of surface and subsurface drainage structures and facilities. For detailed guidance on design of subsurface drainage layers, refer to AC 150/5320-5, Airport Drainage Design, and Appendix G.

3.3 Aerial Photography

Relief, drainage, and soil patterns may be determined from aerial photography. A review of historical aerial site photographs may reveal prior drainage patterns and deposits of different soil types. Many websites now provide access to aerial photographs and maps useful for preliminary site investigations. Center: (8.9800689 ,38.7989319), Borders: (8.9787199, 38.7975829) Addis Ababa Airport map, Addis Ababa Airport topography, Addis Ababa Airport elevation, Addis Ababa Airport relief, Ethiopia, Oromia, North Shewa (R4), Addis Ababa, point of interest

Figure 3-2: Aerial Photography of Addis Ababa Bole International Terminal (Addis Ababa Bole international airport file)

3.4 Geography

The predominant climate type is tropical monsoon, with wide topographic induced variation. The Ethiopian Highlands cover most of the country and have a climate which is generally considerably cooler than other regions at similar proximity to the Equator. Most of the country's major cities are located at elevations of around 2,000-2,500m above sea level, including historic capitals such as Gondar and Axum.

3.5 Climate

The modern capital, Addis Ababa, is situated on the foothills of Mount Entoto at an elevation of around 2,400meters. It experiences a mild climate year round. With temperatures fairly uniform year round, the seasons in Addis Ababa are largely defined by rainfall: a dry season from October to February, a light rainy season from March to May, and a heavy rainy season from June to September. The average annual rainfall is approximately 1,200mm.

There are on average Seven hours of sunshine per day. The dry season is the sunniest time of the year, though even at the height of the rainy season in July and August there are still usually several hours per day of bright sunshine. The average annual temperature in Addis Ababa is 16°C, with daily maximum temperatures averaging 20-25°C throughout the year, and overnight lows averaging 5-10°C

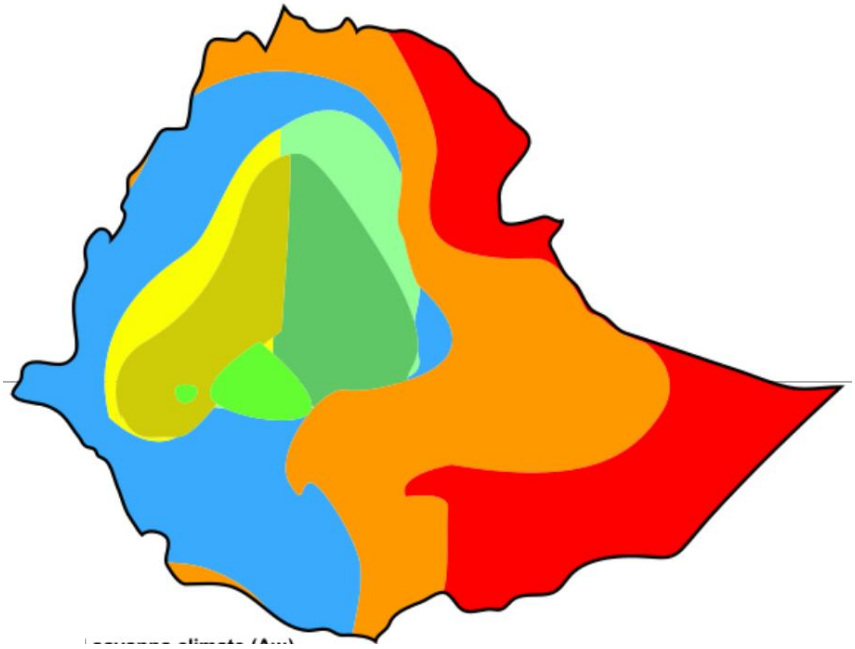

Legends:-

- **Tropical savanna climate**
- **Warm desert climate**
- **Warm semi-Arid climate**
- **Warm Mediterranean climate**
- **Temperate Mediterranean climate**
- **Temperate oceanic climate**
- **Humid subtropical climate**
- **Humid subtropical climate / Sub-topical oceanic highland climate**

Figure 3-3 Climate Map of Ethiopia (Ethiopian Meteorological Agency, , 2015)

Because Addis Ababa is located around the equator its temperature stays nearly constant month to month with no more than 10^0C change and a temperate climate due to its high altitude location in the subtropics. The average minimum and maximum temperature of each month is presented in the following graph. The graph is generated from the raw data obtained from Ethiopian Meteorological Agency.

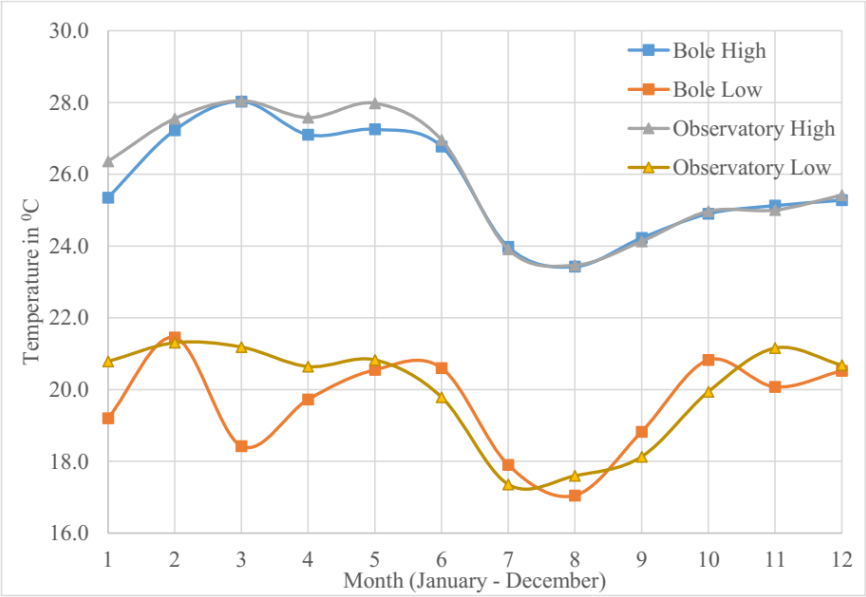

Figure 3-4 Average High and Low Temperature of Bole and Observatory Gauging Stations (Ethiopian Meteorological Agency, , 2015)

Addis Ababa has a pronounced rainfall peak during the summer season locally known as Kiremt which is from June to September. It also exhibits a considerable amount of rainfall during February to May locally known as Belg, Bega being between October and January with minimum rainfall record. Daily rainfall records of stations in Addis Ababa as obtained from National Metrological Agency depict that the rainfall distribution is bimodal in nature.

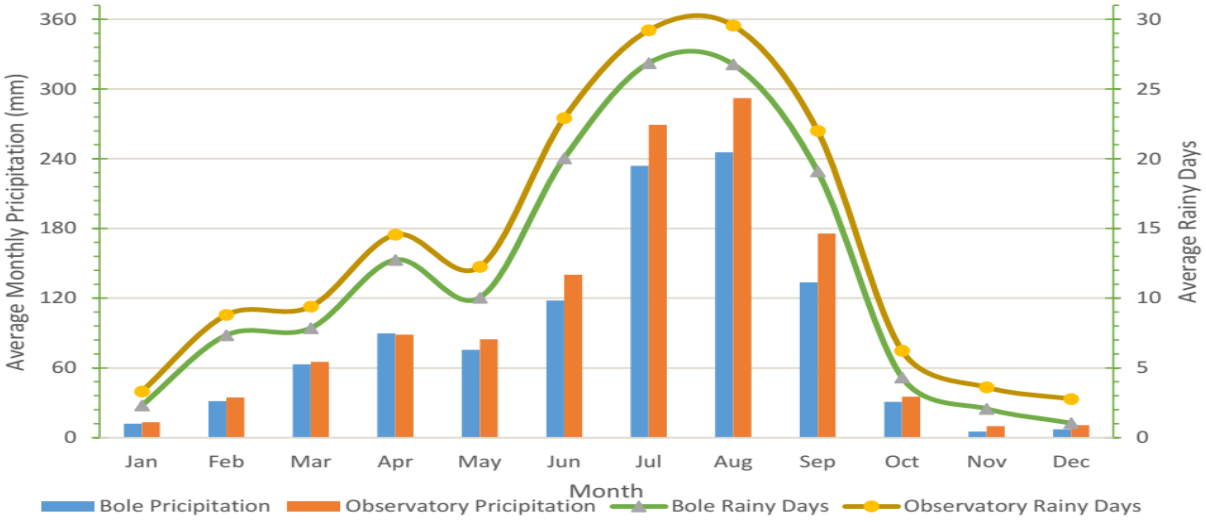

Figure 3-5 Average Monthly Rainfall Depth and Rainy Days of Bole and Observation Stations (Ethiopian Meteorological Agency, , 2015)

CHAPTER FOUR

MATERIALS AND METHODS

4.1 General Research Approach

To achieve the objectives of this thesis, the following methodologies have been followed. Literature review, Field work, laboratory test and analysis of the result. On the field, four sampling areas were collected. The sampling site was located four direction of the airport pavement part. That direction was East direction (Gorro Sefera), North direction (Bole Homes), West (Bole Mikael) and Southern direction is (Bole Bulbula around Solo Le Hotel).

4.2 Surveying and Sampling

4.2.1 Subsurface Borings and Pavement Cores of Existing Pavement.

The initial step in an investigation of subsurface conditions is a soil survey to determine the quantity and extent of the different types of soil, the arrangement of soil layers, and the depth of any subsurface water. Profile borings are usually obtained to determine the soil or rock profile and its lateral extent. The spacing of borings cannot always be definitely specified by rule or preconceived plan because of the variations at a site. Sufficient borings should be taken to identify the extent of soils encountered.

Additional steps that may be taken to characterize the subsurface include: Nondestructive testing (NDT) and Dynamic Cone Penetrometer (DCP) tests. Nondestructive testing (NDT), as described in Appendix C, can be used to evaluate subgrade strength and to assist with establishing locations for soil borings as well as sampling locations for evaluation of existing pavements. Dynamic Cone Penetrometer (DCP) tests, per ASTM D 6951 Standard Test Method for Use of the Dynamic Cone Penetrometer in Shallow Pavement Applications, provide useful information. DCP tests can easily be run as each soil layer is encountered as boring progresses or DCP tests can be run after taking pavement cores of existing pavements. DCP results can provide a quick estimate of subgrade strength with correlations between DCP and CBR. In addition, plots of DCP results provide a graphical representation of the relative strength of subgrade layers. Boring logs from original construction and prior

evaluations can also provide useful information. Cores of existing pavement provide information about the existing pavement structure. It is recommended to take color photographs of pavement cores and include with the geotechnical report.

4.2.2 Number of Borings, Locations, and Depths.

The locations, depths, and numbers of borings should be sufficient to determine and map soil variations. If past experience indicates that settlement or stability in deep fill areas at the location may be a problem, or if in the opinion of the geotechnical engineer more investigations are warranted, additional and/or deeper borings may be required to determine the proper design, location, and construction procedures. Where uniform soil conditions are encountered, fewer borings may be acceptable. Suggested criteria for the location, depth, and number of borings for new construction are given in Table 4-1. Wide variations in these criteria can be expected due to local conditions.

Table 4-1 Typical Subsurface Boring Spacing and Depth (O'Donnell, 2009)

Area	**Spacing**	**Depth**
Runways, Taxiways and Taxi lanes	Random Across Pavement at 60 m Intervals	Cut Areas - 3m Below Finished Grade Fill Areas- 3m Below Existing Ground
Other Areas of Pavement	1Boring per 930sqm of Area	Cut Areas-3m Below Finished Grade Fill Areas-3m Below Existing Ground
Borrow Areas	Sufficient Tests to Clearly Define the Borrow Material	To Depth of Borrow Excavation

Boring depths should be sufficient to determine if consolidation and/or location of slippage planes will impact the pavement structure.

4.2.3 Boring Log.

The results of the soil explorations should be summarized in boring logs. A typical boring log includes location of the boring, date performed, type of exploration, surface elevation, depth of materials, sample identification numbers, classification of the material, water table, and standard penetration resistance. Refer to ASTM D 1586 Standard Test Method for Standard Penetration Test (SPT) and Split Barrel Sampling of Soils. Representative samples of the different soil layers encountered should be obtained and tested in the laboratory to determine their physical and engineering properties. If samples not obtained with split barrel, e.g. grab

sample from flight auger extreme care should be used to assure that sample is representative and not a mixture of layers. In-situ properties, such as in-place moisture, density, shear strength, consolidation characteristics etc., may require obtaining “undisturbed” core samples per ASTM D 1587 Standard Practice for Thin-Walled Tube Sampling of Fine Grained Soils for Geotechnical Purposes. Because test results only represent the sample being tested, it is important that each sample be representative of a particular soil type and not be a mixture of several materials. Identification of soil properties from composite bag samples can lead to misleading representation of soil properties.

4.2.4 In-place Testing.

Pits, open cuts, or both may be required for making in-place bearing tests, taking undisturbed samples, charting variable soil strata, etc. This type of soil investigation may be necessary for projects involving in-situ conditions that warrant a high degree of accuracy.

4.2.5 Number of Cores

Sufficient cores should be taken to evaluate condition of existing pavement to help characterize extent and possible causes of distress. Cores of existing pavement structure aid in the determination of the extent of rehabilitation and/or reconstruction required to correct the distress. The soil specimens for this thesis work were collected from different point which found around Addis Ababa bole international airport pavements parts. Prior to sampling, visual site investigations were made to consider the different soil types. Accordingly, four test pits were selected from around different locations Airport pavement.

Figure 4-1 Sample Location and Test Pit Distribution of Addis Ababa Bole International Airport on Google Image

4.3 Sample Preparation and Laboratory Test Procedure

Soil samples were prepared for the test by air drying and sieving to the required size. For the selected samples the following laboratory tests were conducted.

- Sieve Analysis (ASTM D 422)
- Compaction test (ASTM D 698 and ASTM D 1557)
- California Bearing Ratio test (ASTM D 1883)

4.3.1 Sieve analysis (Dry and Wet)

This test method covers a procedure the quantitative determination of the distribution of particle sizes in soils. Either of the two methods of sieving is applicable according to the soil's cohesiveness nature. Dry sieve is applicable for non-cohesive soils whereas wet sieve is for cohesive soils to separate individual particles. ASTM D 422 is Standard Test Method for Laboratory Determination of Particle-Size Analysis of Soils.

4.3.2 Compaction Test (Water Content –Dry Density Relation)

ASTM D698: Standard Test Method for Laboratory Compaction Characteristics of Soil Using Standard Effort 600kN-m/m^3, and ASTM D1557: Test Method for Laboratory Compaction Characteristics of Soil Using Standard Effort 2,700kN-m/m^3

4.3.3 California Bearing Ratio Test (CBR TEST) (ASTM D 1883)

Standard Method of Test for the California Bearing Ratio ASTM D in this research two kinds of CBR test are conducted to compare laboratory determined CBR at two different conditions. These are the soaked CBR test and Unsoaked CBR test. In this research, this test method covers the determination of the California Bearing Ratio (CBR) of the locally subgrade materials from laboratory compacted specimens. This is aimed to measure the strength of a subgrade soil at its OMC.

4.4 Work Flow Chart

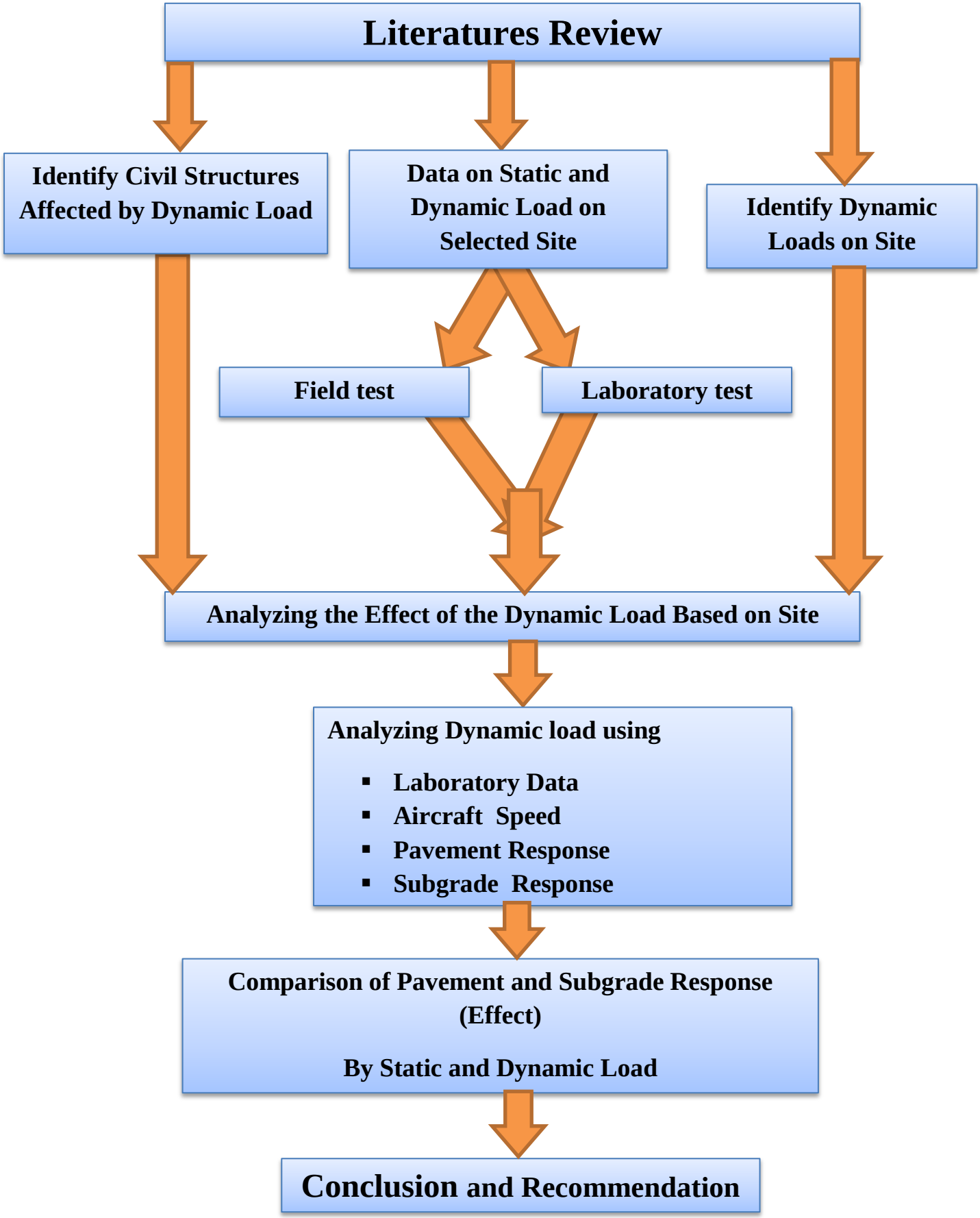

CHAPTER FIVE

RESULT AND DISCUSSIONS

5.1 Laboratory Test and Results

According to the ERA grading limit, the material shall have a smooth continuous grading within the limits for grading A, B or C and the sub-base material shall comply with one of the grading given below in Table 5.1

Table 5-1 the specification of grain size analysis of ERA grading chart (ERA, 2013)

SIEVE SIZE (mm)	Mass Percent Passing			
	A	B	C	D
63	100			
50	90-100	100	100	
37.5			80-100	
25	51-80	55-85		100
20			60-100	
9.5		40-70		51-85
5			30-100	
4.75	35-70	30-60		35-65
2		20-51		25-51
1.18			17-75	
0.425		10-31		15-30
0.3			9-50	
0.075	5-15	5-15	5-25	5-15

Among the grading limits, grade B has almost a complete specification of percent mass passing for each sieve size. Taking these advantages this thesis work is made based on grading B specification.

Penetration and Loading Relation

Table 5-2 Penetration and Loading Relation

Penetration / No of layer	0.00	0.64	1.27	1.91	2.54	3.81	5.08	7.62
	mm	mm	mm	mm	mm	mm	mm	mm
10	0	1171	1579	1986	2546	3005	3463	4278
30	0	1528	1986	2445	3107	3514	4074	4533
65	0	5561	6845	8556	10410	12549	13832	14545

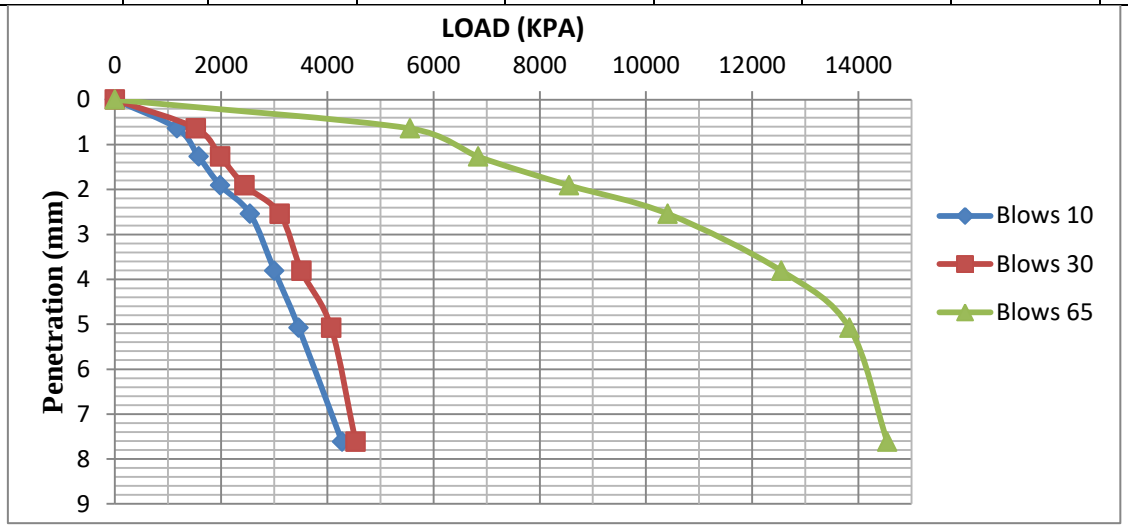

Figure 5-1 Penetration and Loading Relation

The test result on table 5.3 shows that laboratory result of subgrade materials

Table 5-3 Laboratory Test Results

CBR			
No. of blows	10	30	65
No. of layers	5	5	5
Dry unit weight (g/cm3)	1.76	1.83	1.91
CBR (%)	29	35	122
Absorptivity(g)	180	122	77
Swell (%)	1.24	0.97	0.63

Moisture Density Relations(Proctor)						
Proctor modify	1	2	3	4	5	OPM

Moisture content (%)	6.1	9.7	12.0	16.2	/	11.6
Dry density (g/cm3)	1.84	1.87	1.90	1.82	/	1.90

Sieve Analysis

Sieve size (mm)	50	37.5	20	5	2	1.18	0.425	0.3	0.075	Soil sort
Percentage passing (%)	86.7	79.7	47.7	23.4	18.2	17.0	15.1	14.6	13.2	Course-Grained

Remarks:	
Conclusion	All the indicator meet the technical requirements of Backfill
Idea of the material Engineer consultant	Upon examination, the material can be used for every region of subgrade

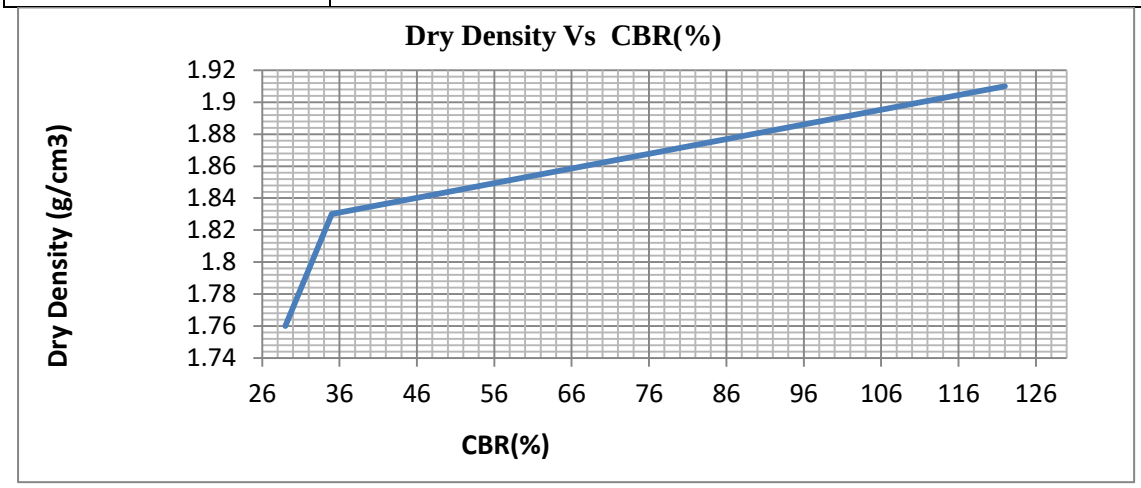

Figure 5-2 Graph of Dry Density - CBR (%)

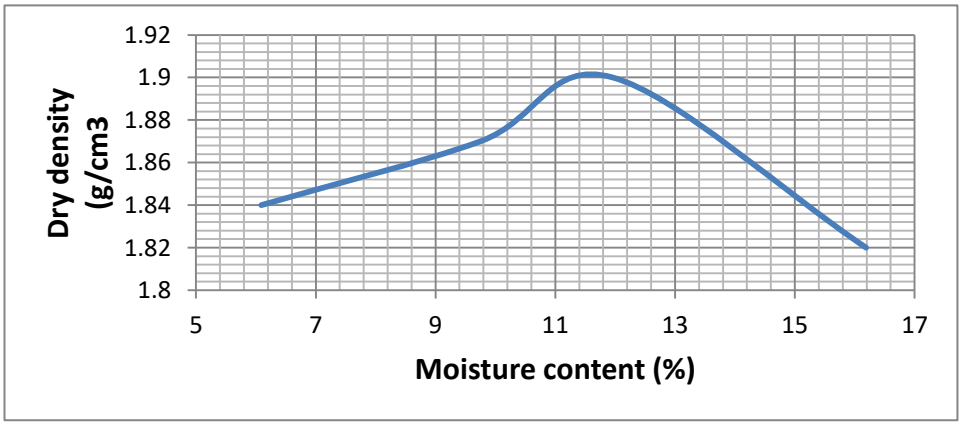

Figure 5-3: Moisture – Dry Density

5.2 Analysis of Dynamic (Moving) Loads

5.2.1 Analysis of Load Duration

Boeing 737 Rides on 27x7.75 R15 Rubber. In English, That means it is 27 inches (68.58cm) in diameter, i.e. 19.72cm (0.1972m) in radius 7.75 inches (19.685Cm) Wide, And Wrapped around A 15-Inch Wheel. [Ref. aircraft tires Don't Explode on Landing because they are pumped!]

Table 5-4 aircraft creep-speed taxi and load duration

aircraft Speed (m/sec)	1.56	2.06	2.56	3.06	3.56	4.06	4.11	1.56	2.06
Load Duration (Sec)	1.517	1.149	0.924	0.773	0.665	0.583	0.576	1.517	1.149

$$d = 12a/s \ldots\ldots\ldots\ldots\ldots\ldots\ldots\ldots\ldots\ldots\ldots\ldots\ldots\ldots\ldots\ldots\ldots\ldots\ldots 5.1$$

a. If a = 19.72cm (0.1972m) in radius and creep-speed taxi at 5.6(***1.56m/s***) to 14.8 km/h(***4.11m/s***) (3 to 8 knots),

➔If a = 19.72cm (0.1972m) in radius and S=1.56m/s

$$d = \frac{12a}{s} \quad , \mathbf{d} = \frac{\mathbf{12x0.1972m}}{\mathbf{1.56m/s}} = \mathbf{1.5sec}$$

➔If a = 19.72cm (0.1972m) in radius and S=17.9m/s

$$d = \frac{12a}{s} \quad , \mathbf{d} = \frac{\mathbf{12x0.1972m}}{\mathbf{4.11m/s}} = \mathbf{0.576sec}$$

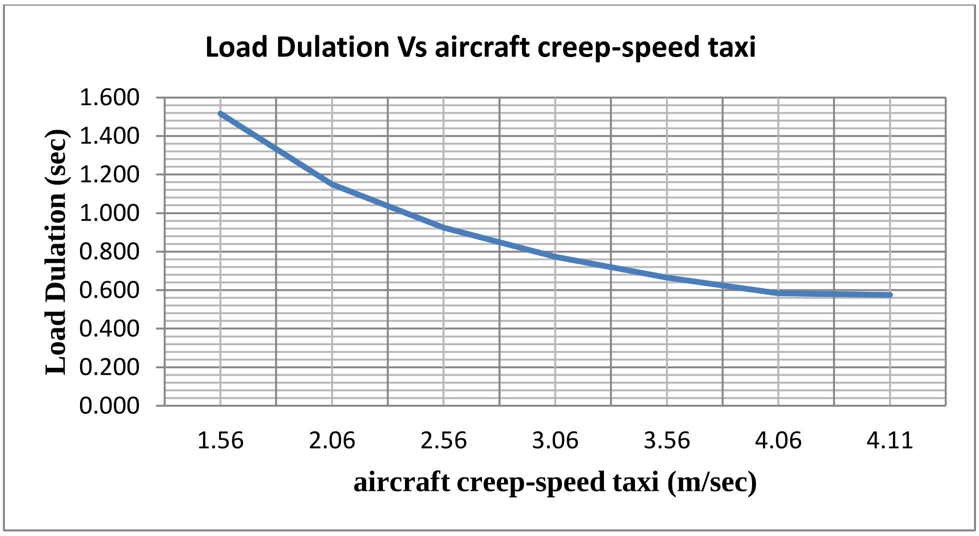

Figure 5-4 Graph for aircraft Creep-Speed Taxi and Load Duration

b. If a = 19.72cm (0.1972m) in radius and low-speed taxi at 27.8 (***7.72m/s***) to 55.6 km/h(***15.44m/s***) (15 to 30 knots),

- If a = 19.72cm (0.1972m) in radius and S=***7.72m/s***

$$d = \frac{12a}{s} \text{ , } \mathbf{d = \frac{12x0.1972m}{7.72m/s} = 0.3065sec}$$

- If a = 19.72cm (0.1972m) in radius and S=15.44m/s

$$d = \frac{12a}{s} \text{ , } \mathbf{d = \frac{12x0.1972m}{15.44m/s} = 0.153sec}$$

Table 5-5 aircraft low-speed taxi and Load Duration

aircraft Speed (m/sec)	7.72	8.72	9.72	10.72	11.72	12.72	13.72	14.72	15.44
Load Duration (Sec)	0.307	0.271	0.243	0.221	0.202	0.186	0.172	0.161	0.153

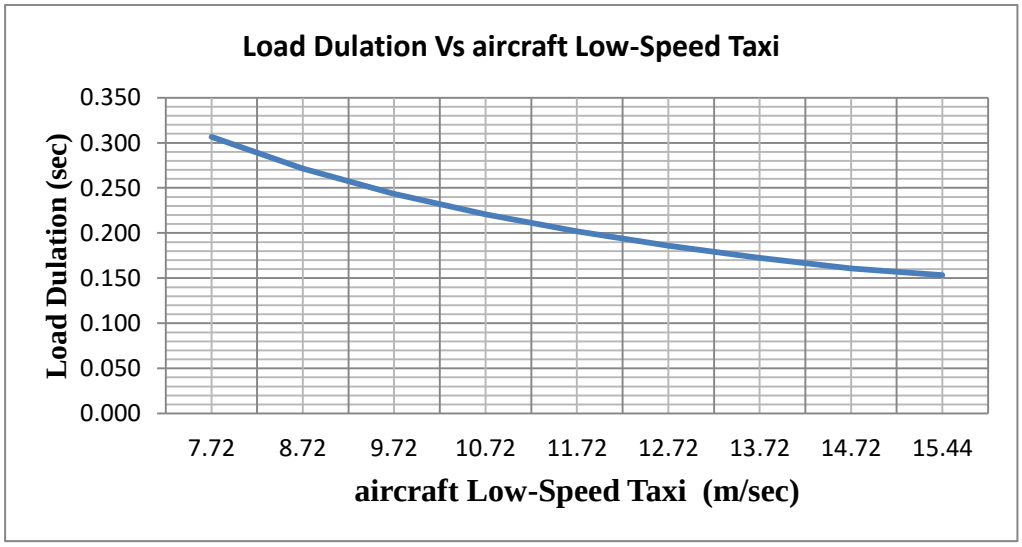

Figure 5-5 Graph aircraft Low-Speed Taxi and Load Duration

c. If a = 19.72cm (0.1972m) in radius and medium-speed taxi at 83.4(***23.17m/s***) to 148.2 km/h(***41.17m/s***) (45 to 80 knots),

✈If a = 19.72cm (0.1972m) in radius and S=***23.17m/s***

$$d = \frac{12a}{s} \quad , \mathbf{d} = \frac{\mathbf{12x0.1972m}}{\mathbf{23.17m/s}} = \mathbf{0.102sec}$$

✈If a = 19.72cm (0.1972m) in radius and S=41.17m/s

$$d = \frac{12a}{s} \quad , \mathbf{d} = \frac{\mathbf{12x0.1972m}}{\mathbf{41.17m/s}} = \mathbf{0.0575sec}$$

Table 5-6 aircraft Medium-Speed Taxi and Load Duration

aircraft Speed (m/sec)	23.17	25.17	27.17	29.17	31.17	33.17	35.17	38.17	41.17
Load Duration (Sec)	0.102	0.094	0.087	0.081	0.076	0.071	0.067	0.062	0.057

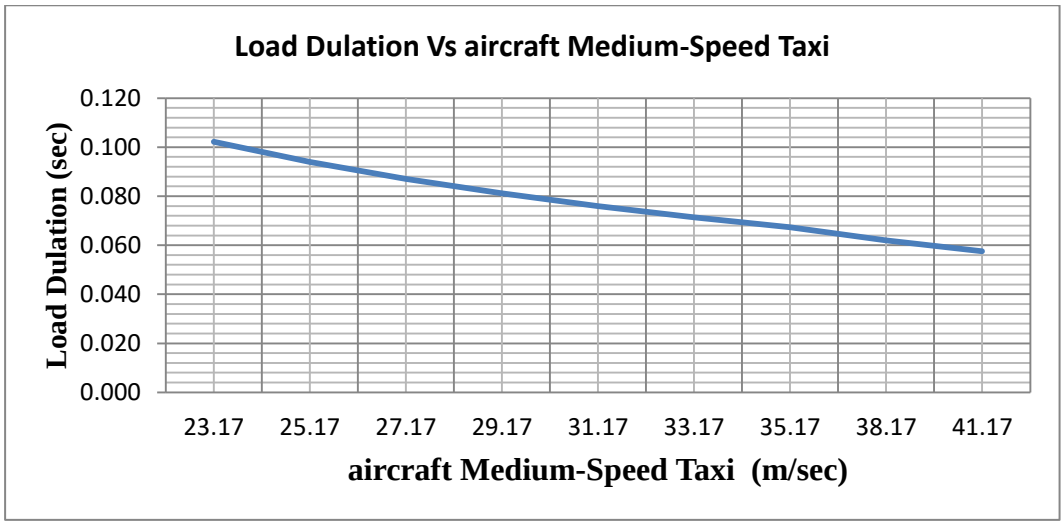

Figure 5-6 Graph aircraft Medium-Speed Taxi and Load Duration

d. If a = 19.72cm (0.1972m) in radius and high-speed taxi at 157.5(***43.75m/s***) to 240.9 km/h (***66.97m/s***) (85 to 130 knots),

✈If a = 19.72cm (0.1972m) in radius and S=***43.75m/s***

$$d = \frac{12a}{s} \quad , \mathbf{d} = \frac{\mathbf{12x0.1972m}}{\mathbf{43.75m/s}} = \mathbf{0.054sec}$$

✈If a = 19.72cm (0.1972m) in radius and S=66.97m/s

$$d = \frac{12a}{s} \quad , \mathbf{d} = \frac{\mathbf{12x0.1972m}}{\mathbf{66.97m/s}} = \mathbf{0.0353sec}$$

Table 5-7 aircraft High-Speed Taxi and Load Duration

aircraft Speed (m/sec)	43.75	46.75	49.75	52.75	55.75	58.75	61.75	64.75	66.97
Load Duration (Sec)	0.054	0.051	0.048	0.045	0.042	0.040	0.038	0.037	0.035

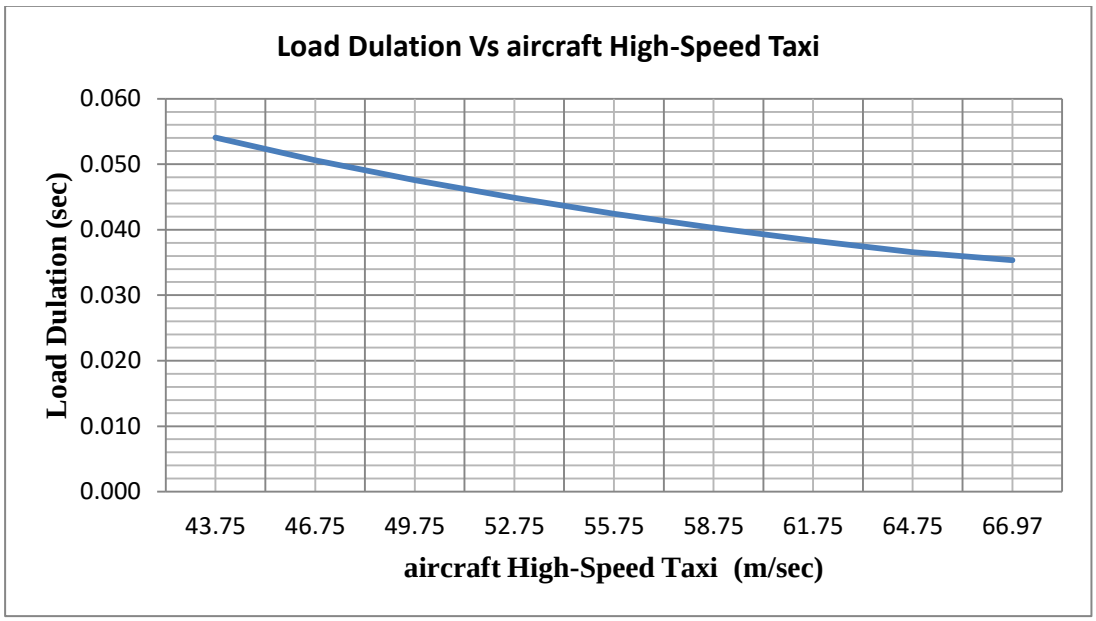

Table 5-8 Graph for aircraft High-Speed Taxi and Load Duration

e. If a = 19.72cm (0.1972m) in radius and high-speed braking at 240.9(***66.67m/s***) to 83.4 km/h (***23.17m/s***) (130 to 45 knots),

➔If a = 19.72cm (0.1972m) in radius and S=***66.67m/s***

$$d = \frac{12a}{s} \text{ , } \mathbf{d = \frac{12x0.1972m}{66.67m/s} = 0.035sec}$$

➔If a = 19.72cm (0.1972m) in radius and S=23.17m/s

$$d = \frac{12a}{s} \text{ , } \mathbf{d = \frac{12x0.1972m}{23.17m/s} = 0.1sec}$$

Table 5-9 aircraft High-Speed Braking and Load Duration

aircraft Speed (m/sec)	23.17	29.17	35.17	41.17	47.17	53.17	59.17	65.17	66.67
Load Duration	0.102	0.081	0.067	0.057	0.050	0.045	0.040	0.036	0.035

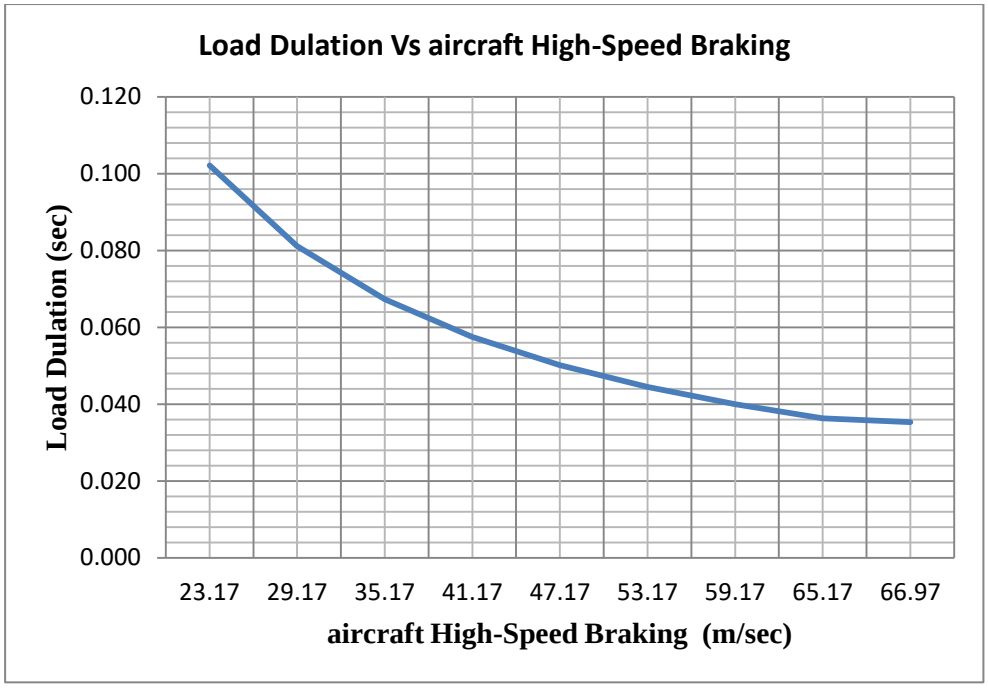

Figure 5-7 Graph for aircraft High-Speed Braking and Load Duration

f. If a = 19.72cm (0.1972m) in radius and takeoff rotation at ***43.75m/s*** to ***66.92m/s***,

➔ If a = 19.72cm (0.1972m) in radius and S=***43.75m/s***

$$d = \frac{12a}{s} \text{ , } \mathbf{d = \frac{12x0.1972m}{43.75m/s} = 0.054sec}$$

➔ If a = 19.72cm (0.1972m) in radius and S=66.92m/s

$$d = \frac{12a}{s} \text{ , } \mathbf{d = \frac{12x0.1972m}{66.92m/s} = 0.035sec}$$

Table 5-10 aircraft Takeoff Rotation Speed and Load Duration

aircraft Speed (m/sec)	43.750	46.250	48.750	51.250	53.750	56.250	58.750	61.250	63.750	66.250	66.720
Load Duration (Sec)	0.054	0.051	0.049	0.046	0.044	0.042	0.040	0.039	0.037	0.036	0.035

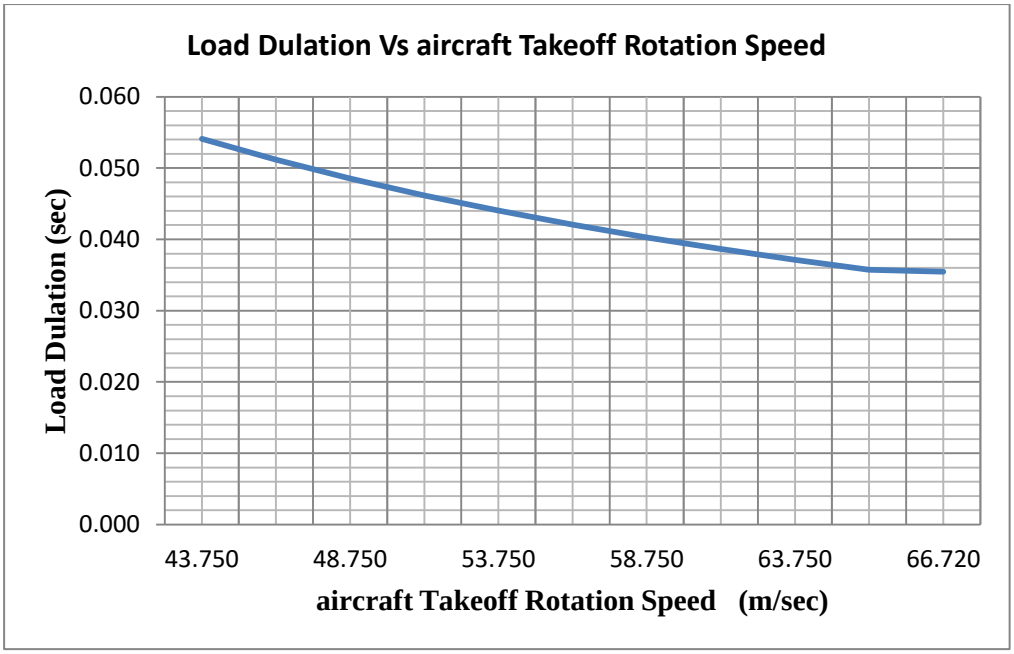

Figure 5-8 Graph for aircraft Takeoff Rotation Speed and Load Duration

g. If a = 19.72cm (0.1972m) in radius and Turning at 7.4(***12.15m/s***) to 55.6 km/h (***15.44m/s***) (4 to 30 knots).

➢ If a = 19.72cm (0.1972m) in radius and S=***12.15m/s***

$$d = \frac{12a}{s} \text{ , } \mathbf{d = \frac{12x0.1972m}{12.15m/s} = 0.195sec}$$

➢ If a = 19.72cm (0.1972m) in radius and S=15.44m/s

$$d = \frac{12a}{s} \text{ , } \mathbf{d = \frac{12x0.1972m}{15.44m/s} = 0.153sec}$$

Table 5-11 aircraft Turning Speed and Load Duration

aircraft Speed (m/sec)	12.150	12.650	13.150	13.650	14.150	14.650	15.150	15.440
Load Duration (Sec)	0.195	0.187	0.180	0.173	0.167	0.162	0.156	0.153

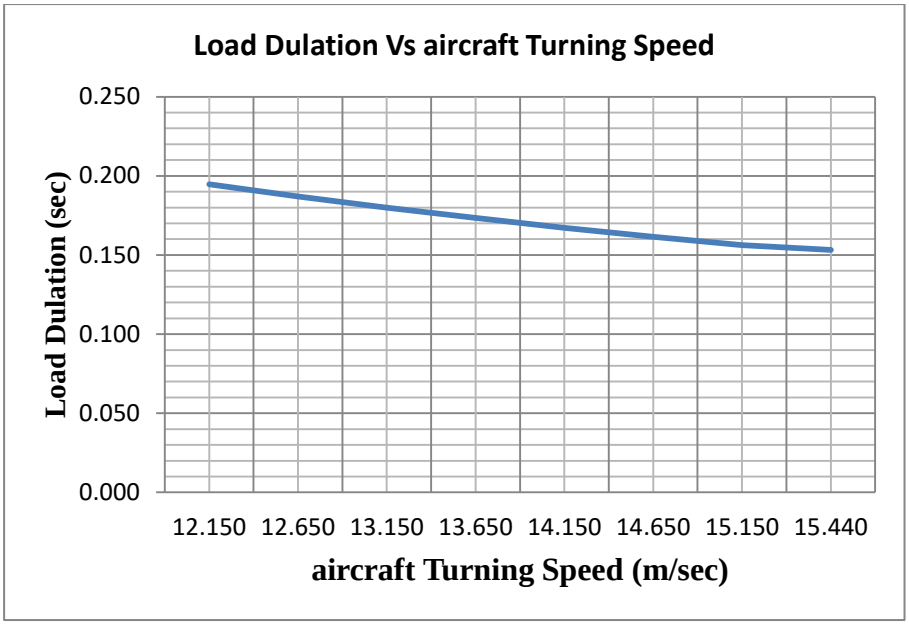

Figure 5-9 Graph of aircraft Turning Speed and Load Duration

Assuming that the half-space has Poisson ratio 0.5 and is subjected to a circular load with contact radius 197.2mm and contact pressure 200psi (1380kPa(1.38N/mm^2), as shown in Figure 2.39, determine the maximum surface time of T=0.1 s by deflection after a loading the collocation method

The first term is independent of time and therefore remains the same regardless of whether the load is moving. From Eqs.2.11, the second term ($\boldsymbol{e^{-10t}}$) with T=0.1 and d=0.1s (it is different for different aircraft speed) for 64 km/h should be changed to 0.5xπ^2 x 0.72 (1+e$^{-0.5}$)/ (π^2+0.25) =14.3mm, so maximum deflection=0 .72-0.564=3.96mm

5.2.2. The Response under Airport Flexible Pavement $(\boldsymbol{v = 0.45})$

5.2.2.1 The Response (Deflection) Under Static Load

It can be expressed as a Dirichlet series, From "Pavement Analysis and Design – Huang Book" (page 62) Eq.2.8

$$w_o = \frac{2(1-v^2)qa}{E} \text{.....5.2}$$

Most of the time the assumption for the following parameter is taken for different condition: - for flexible pavement v = 0.45 .

$$w_o = \frac{2(1-v^2)qa}{E} = \frac{2(1-0.5^2)qa}{E} = \frac{2(1-0.25)qa}{E} = \frac{1.5qa}{E}$$

$$w_o = \frac{1.5qa}{E} = 1.5qa\ D(t)$$

$$\mathrm{D(t)} = 0.001(1 - e^{-10t})$$

By substituting the D(t) in above equation, then w_o become as follow

$$w_o = 1.5qa\ [0.001(1 - e^{-10t})]$$

For q=200psi and a=197.2mm (7.764inch), D (t) can be determined by the following

$$w_o = 1.5x200psi\ x\ 7.764inch[0.001(1 - e^{-10t})]$$

$$w_o = 2.3292(1 - e^{-10t})$$

Therefor the surface deflection under static load for t=0.1sec is

$$w_o = 2.3292\left(1 - e^{-10(0.1)}\right)$$

$$\underline{w_o = 1.47inch = 37.39mm}$$

5.2.2.2 The Response (Deflection) Under Moving (Dynamic) Load

It can be obtained by Boltzmann's superposition principle:

$$R = \frac{q\pi^2}{2}\sum_{i=1}^{n} C_i \frac{1 + \exp(-d/2T_i)}{\pi^2 + (d/2T_i)^2}$$

$$R = \frac{1}{2}x\ \pi^2 x2.3292x\left(\frac{1 + \exp(-d/2T_i)}{\pi^2 + (d/2T_i)^2}\right)$$

$$R = 11.48249016x\left(\frac{1 + \exp(-d/2T_i)}{\pi^2 + (d/2T_i)^2}\right)$$

For this case we have T=0.1, but d values are different for different aircraft speed

a. If a = 19.72cm (0.1972m) in radius and creep-speed taxi at 5.6(*1.56m/s*) to 14.8 km/h(*4.11m/s*) (3 to 8 knots),

   ✈ If T=0.1 and d=1.56sec

$$R = 11.48249016x\left(\frac{1 + \exp(-d/2T_i)}{\pi^2 + (d/2T_i)^2}\right)$$

$$R = 11.48249016x\left(\frac{1+\exp(-1.56/2(0.1))}{\pi^2+(1.56/2(0.1))^2}\right)$$

$$R = 1.163inch = 29.545mm$$

➔If T=0.1 and d= $\mathbf{0.102sec}$

$$R = 11.48249016x\left(\frac{1+\exp(-d/2T_i)}{\pi^2+(d/2T_i)^2}\right)$$

$$R = 11.48249016x\left(\frac{1+\exp(-\mathbf{0.102}/2(0.1))}{\pi^2+(\mathbf{0.102}/2(0.1))^2}\right)$$

$$R = 1.698inch = 43.13mm$$

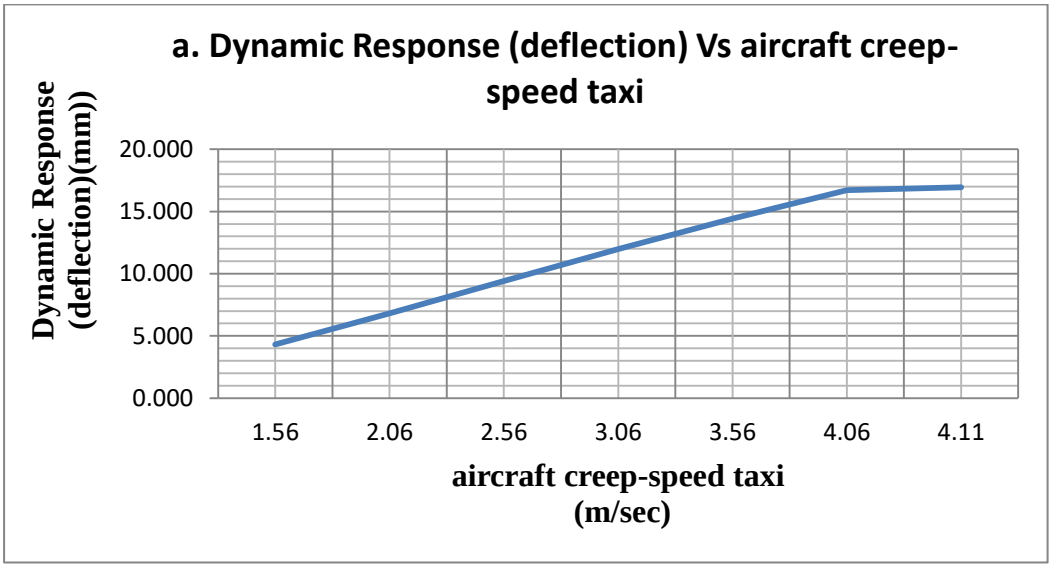

Figure 5-10 Graph for Dynamic Response (Deflection) Vs Creep-Speed Taxi

b. If a = 19.72cm (0.1972m) in radius and low-speed taxi at 27.8 (*7.72m/s*) to 55.6 km/h(*15.44m/s*) (15 to 30 knots),

➔If T=0.1 and d=0.306sec

$$R = 11.48249016x\left(\frac{1+\exp(-d/2T_i)}{\pi^2+(d/2T_i)^2}\right)$$

$$R = 11.48249016x\left(\frac{1+\exp(-0.306/2(0.1))}{\pi^2+(0.306/2(0.1))^2}\right)$$

$$R = 1.415inch = 35.95mm$$

➔If T=0.1 and d=0.153sec

$$R = 11.48249016x\left(\frac{1+\exp(-d/2T_i)}{\pi^2+(d/2T_i)^2}\right)$$

$$R = 11.48249016x\left(\frac{1+\exp(-0.153/2(0.1))}{\pi^2+(0.153/2(0.1))^2}\right)$$

$$R = 1.609inch = 40.868mm$$

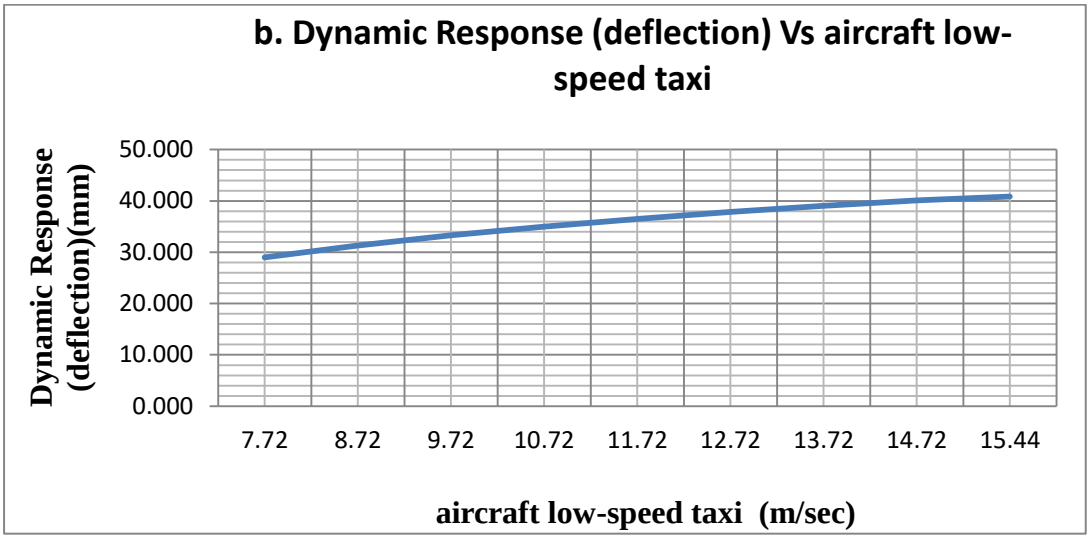

Figure 5-11 Graph for Dynamic Response (Deflection) Vs aircraft Low-Speed Taxi

c. If a = 19.72cm (0.1972m) in radius and medium-speed taxi at 83.4(***23.17m/s***) to 148.2 km/h(***41.17m/s***) (45 to 80 knots),

- If T=0.1 and d=0.306sec

$$R = 11.48249016x\left(\frac{1+\exp(-d/2T_i)}{\pi^2+(d/2T_i)^2}\right)$$

$$R = 11.48249016x\left(\frac{1+\exp(-0.306/2(0.1))}{\pi^2+(0.306/2(0.1))^2}\right)$$

$$R = 1.814inch = 46.067mm$$

- If T=0.1 and d= $\mathbf{0.0575sec}$

$$R = 11.48249016x\left(\frac{1+\exp(-d/2T_i)}{\pi^2+(d/2T_i)^2}\right)$$

$$R = 11.48249016x\left(\frac{1+\exp(-\mathbf{0.0575}/2(0.1))}{\pi^2+(\mathbf{0.0575}/2(0.1))^2}\right)$$

$$R = 2inch = 51.28mm$$

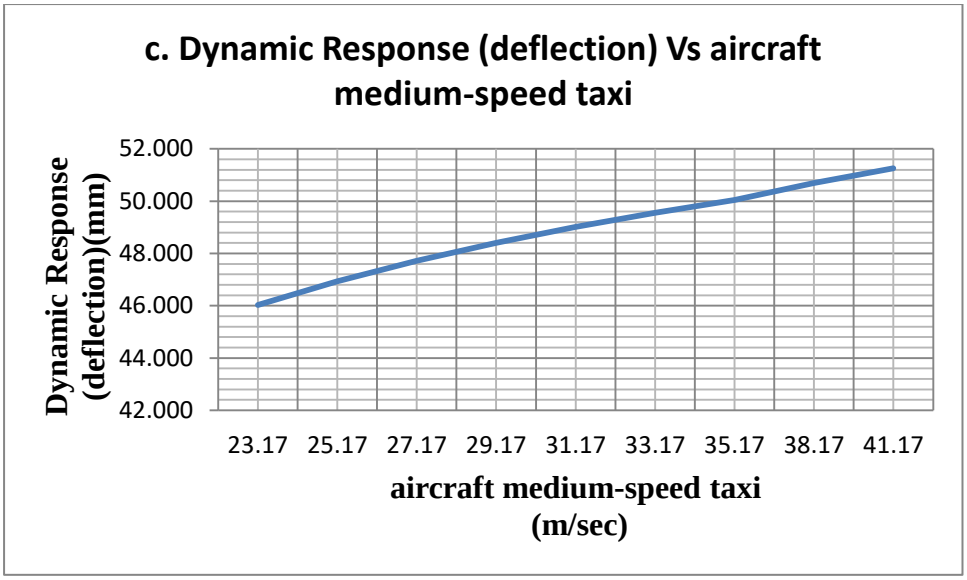

Figure 5-12 : Graph for Dynamic Response (Deflection) Vs aircraft Medium-Speed Taxi

d. If a = 19.72cm (0.1972m) in radius and high-speed taxi at 157.5(***43.75m/s***) to 240.9 km/h (***66.97m/s***) (85 to 130 knots),

➔If T=0.1 and d=$\mathbf{0.054sec}$

$$R = 11.48249016x\left(\frac{1+\exp(-d/2T_i)}{\pi^2+(d/2T_i)^2}\right)$$

$$R = 11.48249016x\left(\frac{1+\exp(-\mathbf{d}/2(0.1))}{\pi^2+(d/2(0.1))^2}\right)$$

$$R = 2.03inch = 51.63mm$$

➔If T=0.1 and d= 0.0353sec

$$R = 11.48249016x\left(\frac{1+\exp(-d/2T_i)}{\pi^2+(d/2T_i)^2}\right)$$

$$R = 11.48249016x\left(\frac{1+\exp(-0.0353/2(0.1))}{\pi^2+(0.0353/2(0.1))^2}\right)$$

$$R = 2.134inch = 54.20mm$$

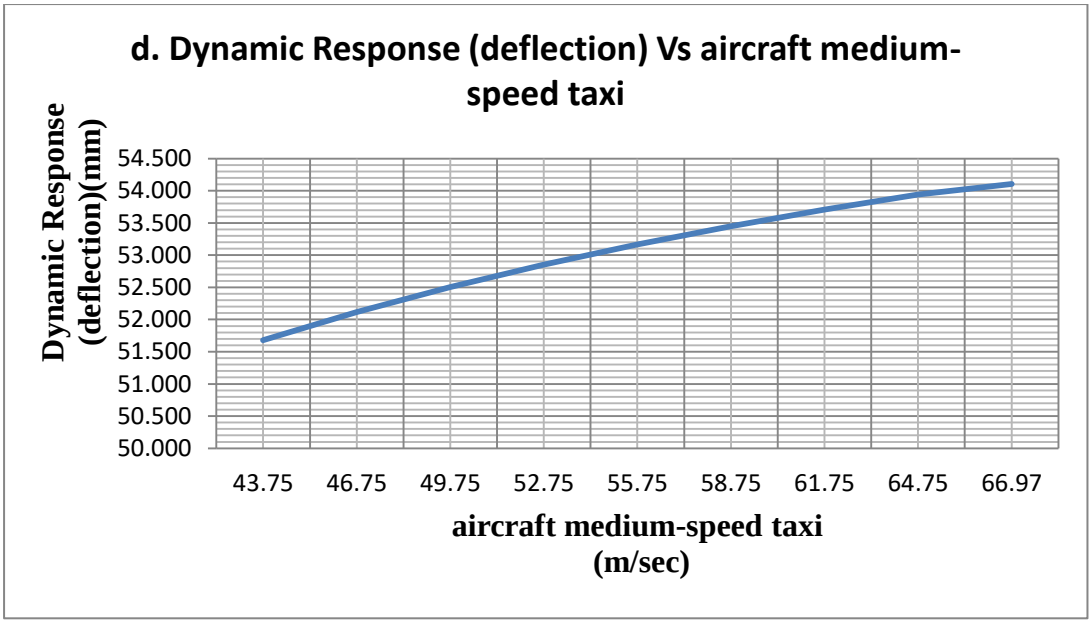

Figure 5-13: Graph for Dynamic Response (Deflection) Vs aircraft Medium-Speed Taxi

e. If a = 19.72cm (0.1972m) in radius and high-speed braking at 240.9(***66.67m/s***) to 83.4 km/h (***23.17m/s***) (130 to 45 knots),

- If T=0.1 and d=$\mathbf{0.035sec}$

$$R = 11.48249016x\left(\frac{1+\exp(-d/2T_i)}{\pi^2+(d/2T_i)^2}\right)$$

$$R = 11.48249016x\left(\frac{1+\exp(-\mathbf{0.035}/2(0.1))}{\pi^2+(\mathbf{0.035}/2(0.1))^2}\right)$$

$$R = 2.133inch = 54.18mm$$

- If T=0.1 and d= 0.1sec

$$R = 11.48249016x\left(\frac{1+\exp(-d/2T_i)}{\pi^2+(d/2T_i)^2}\right)$$

$$R = 11.48249016x\left(\frac{1+\exp(-0.1/2(0.1))}{\pi^2+(0.1/2(0.1))^2}\right)$$

$$R = 1.823inch = 46.31mm$$

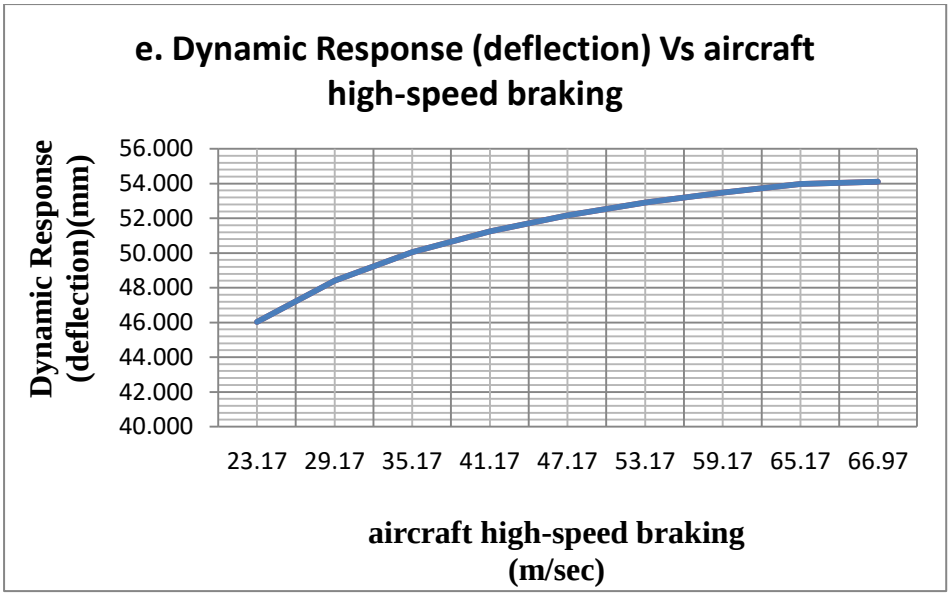

Figure 5-14: Dynamic Response (Deflection) Vs aircraft High-Speed Braking

f. If a = 19.72cm (0.1972m) in radius and takeoff rotation at 157.5 (***43.75m/s***) to 240.9 km/h (***66.92m/s***) (85 to 130 knots),

✈ If T=0.1 and d=$\mathbf{0.054sec}$

$$R = 11.48249016x\left(\frac{1+\exp(-d/2T_i)}{\pi^2+(d/2T_i)^2}\right)$$

$$R = 11.48249016x\left(\frac{1+\exp(-\mathbf{0.054}/2(0.1))}{\pi^2+(\mathbf{0.054}/2(0.1))^2}\right)$$

$$R = 2.036inch = 51.72mm$$

✈ If T=0.1 and d=$\mathbf{0.035sec}$

$$R = 11.48249016x\left(\frac{1+\exp(-d/2T_i)}{\pi^2+(d/2T_i)^2}\right)$$

$$R = 11.48249016x\left(\frac{1+\exp(-\mathbf{0.035}/2(0.1))}{\pi^2+(\mathbf{0.035}/2(0.1))^2}\right)$$

$$R = 2.133inch = 54.18mm$$

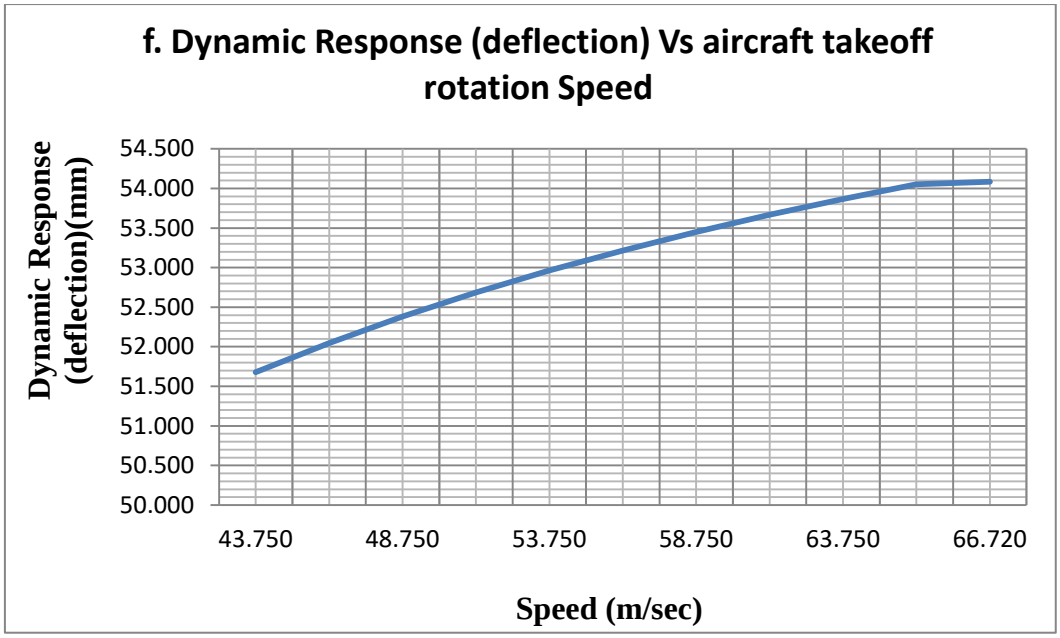

Figure 5-15: Graph for Dynamic Response (Deflection) Vs aircraft Takeoff Rotation Speed

g. If a = 19.72cm (0.1972m) in radius and Turning at 7.4(***12.15m/s***) to 55.6 km/h (***15.44m/s***) (4 to 30 knots).

➢ If T=0.1 and d=$\mathbf{0.195sec}$

$$R = 11.48249016x\left(\frac{1+\exp(-d/2T_i)}{\pi^2+(d/2T_i)^2}\right)$$

$$R = 11.48249016x\left(\frac{1+\exp(-\mathbf{0.195}/2(0.1))}{\pi^2+(\mathbf{0.195}/2(0.1))^2}\right)$$

$$R = 1.46inch = 37.12mm$$

➢ If T=0.1 and d=$\mathbf{0.153sec}$

$$R = 11.48249016x\left(\frac{1+\exp(-d/2T_i)}{\pi^2+(d/2T_i)^2}\right)$$

$$R = 11.48249016x\left(\frac{1+\exp(-\mathbf{0.153}/2(0.1))}{\pi^2+(\mathbf{0.153}/2(0.1))^2}\right)$$

$$R = 1.609inch = 40.87mm$$

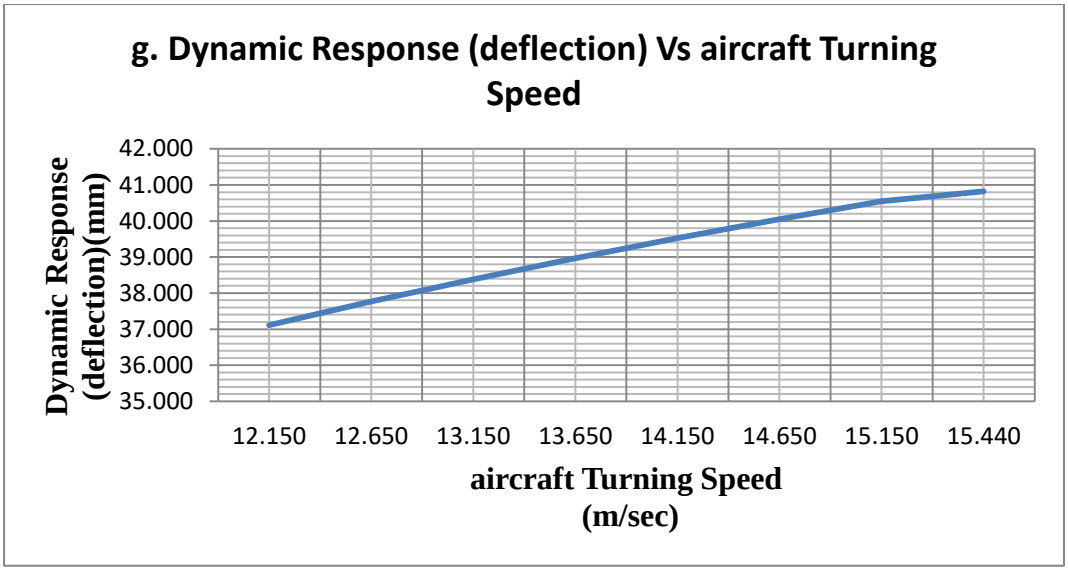

Figure 5-16 Graph for Dynamic Response (Deflection) Vs aircraft Turning Speed

5.2.2.3 Maximum Response or Deflection

Maximum response or Deflection can be determined by the following concept, i.e. the difference between the response under static load$R_{static\ load}$ and the response under the moving (dynamic) load ($R_{moving\ load}$). Mathematically represented as follow

$$\mathbf{R_{maximum\ deflection}} = [\mathbf{0.001x1.5xqa}] - R_{moving\ load}$$

a. If a = 19.72cm (0.1972m) in radius and creep-speed taxi at 5.6(**1.56m/s**) to 14.8 km/h(**4.11m/s**) (3 to 8 knots),

✈ If T=0.1 and d=1.56sec, $R_{moving\ load} = 1.163inch = 29.545mm.$

$$R_{maximum\ deflection} = [0.001x1.5xqa] - R_{moving\ load}$$

$$R_{maximum\ deflection} = [0.001x1.5x200psi\ x\ 7.75inch] - 1.163inch$$

$$R_{maximum\ deflection} = 1.162inch = 29.5148mm$$

✈ If T=0.1 and d=0.13sec, $R_{moving\ load} = 1.698inch = 43.13mm.$

$$R_{maximum\ deflection} = [0.001x1.5xqa] - R_{moving\ load}$$

$$R_{maximum\ deflection} = [0.001x1.5x200psi\ x\ 7.75inch] - 1.698inch$$

$$R_{maximum\ deflection} = 0.6312inch = 16.032mm$$

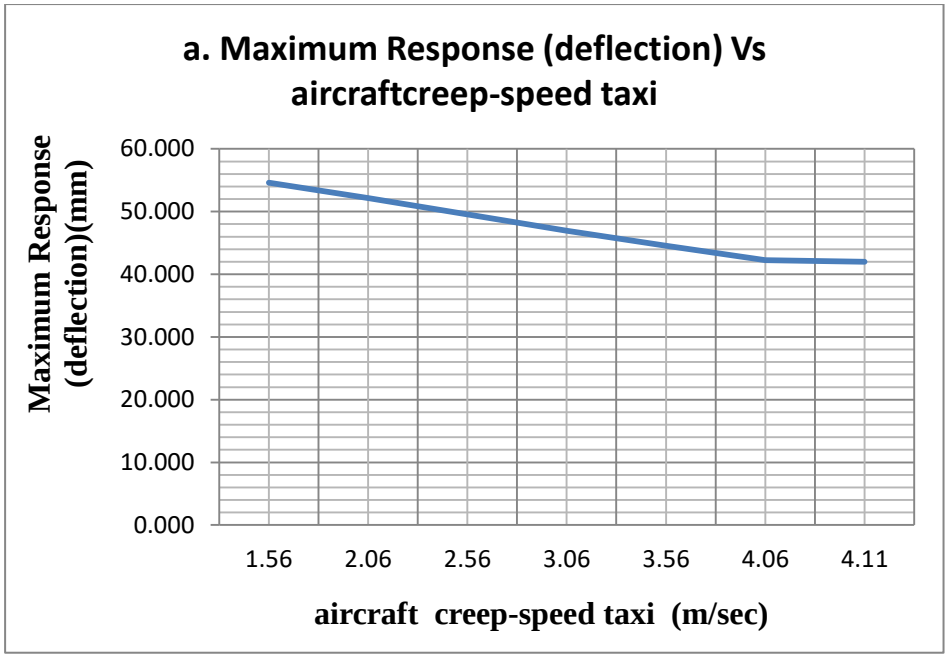

Figure 5-17: Graph for Maximum Response (Deflection) Vs aircraft Creep-Speed Taxi

b. If a = 19.72cm (0.1972m) in radius and low-speed taxi at 27.8 (*7.72m/s*) to 55.6 km/h(*15.44m/s*) (15 to 30 knots),

- If T=0.1 and d=0.306sec, $R_{moving\ load} = 1.415inch = 35.95mm.$

$$R_{maximum\ deflection} = [0.001x1.5xqa] - R_{moving\ load}$$

$$R_{maximum\ deflection} = [0.001x1.5x200psi\ x\ 7.75inch] - 1.415inch$$

$$R_{maximum\ deflection} = (2.325 - 1.415)inch$$

$$R_{maximum\ deflection} = 0.91inch = 23.114mm$$

- If T=0.1 and d=0.153sec, $R_{moving\ load} = 1.609inch = 40.868mm.$

$$R_{maximum\ deflection} = [0.001x1.5xqa] - R_{moving\ load}$$

$$R_{maximum\ deflection} = [0.001x1.5x200psi\ x\ 7.75inch] - 1.609inch$$

$$R_{maximum\ deflection} = (2.325 - 1.609)inch$$

$$R_{maximum\ deflection} = 0.716inch = 18.186mm$$

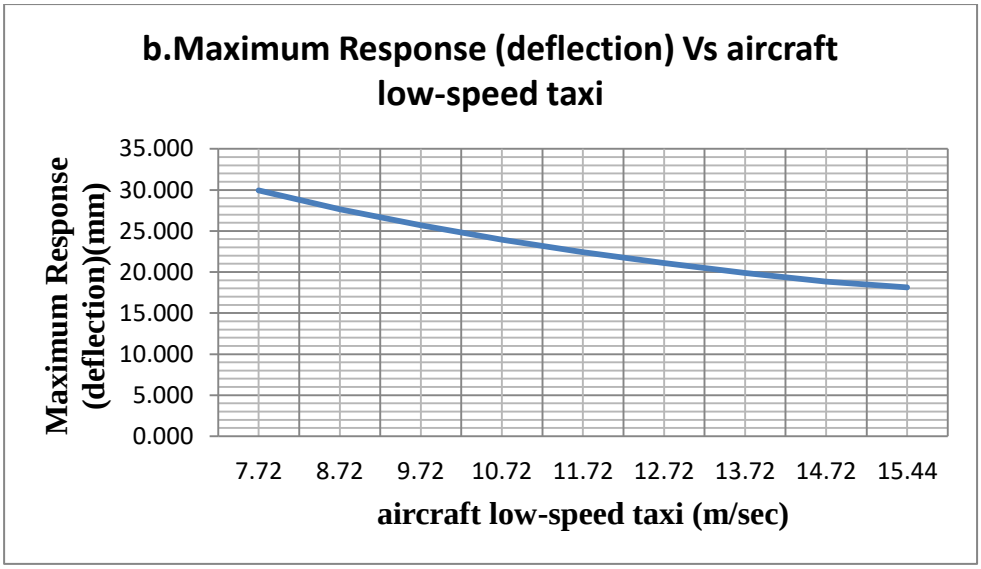

Figure 5-18: Maximum Response (Deflection) Vs aircraft Low-Speed Taxi

c. If a = 19.72cm (0.1972m) in radius and medium-speed taxi at 83.4(***23.17m/s***) to 148.2 km/h(***41.17m/s***) (45 to 80 knots),

- If T=0.1 and d=0.306sec, $R_{moving\ load} = 1.814inch = 46.067mm.$

$$R_{maximum\ deflection} = [0.001x1.5xqa] - R_{moving\ load}$$

$$R_{maximum\ deflection} = [0.001x1.5x200psi\ x\ 7.75inch] - 1.814inch$$

$$R_{maximum\ deflection} = (2.325 - 1.814)inch$$

$$R_{maximum\ deflection} = 0.511inch = 12.979mm$$

- If T=0.1 and d=0.0575sec, $R_{moving\ load} = 2.0inch = 51.28mm.$

$$R_{maximum\ deflection} = [0.001x1.5xqa] - R_{moving\ load}$$

$$R_{maximum\ deflection} = [0.001x1.5x200psi\ x\ 7.75inch] - 2.0inch$$

$$R_{maximum\ deflection} = (2.325 - 2.0)inch$$

$$R_{maximum\ deflection} = 0.325inch = 8.255mm$$

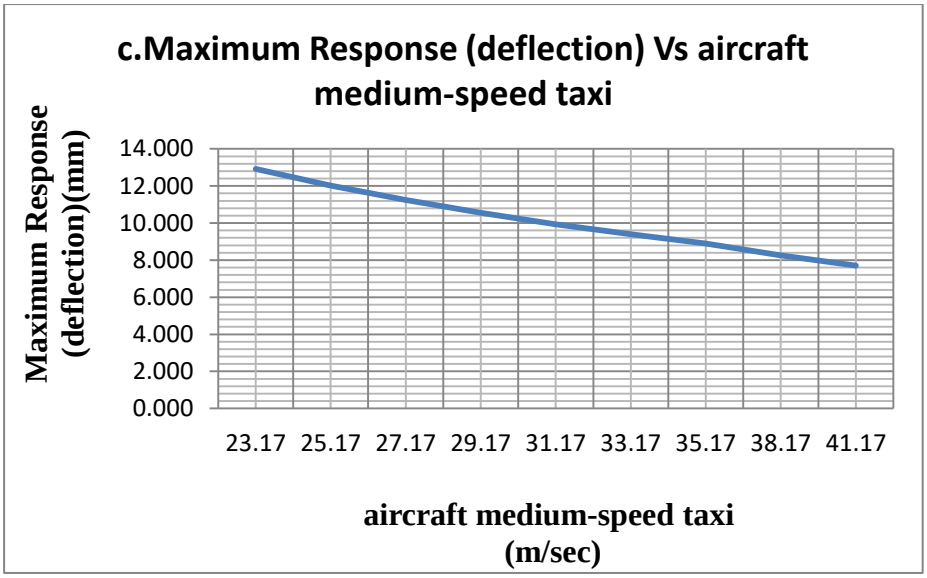

Figure 5-19: Graph for Maximum Response (deflection) Vs aircraft medium-speed taxi

d. If a = 19.72cm (0.1972m) in radius and high-speed taxi at 157.5(***43.75m/s***) to 240.9 km/h (***66.97m/s***) (85 to 130 knots),

- If T=0.1 and d=0.054sec, $R_{moving\ load} = 2.03inch = 51.63mm.$

$$R_{maximum\ deflection} = [0.001x1.5xqa] - R_{moving\ load}$$

$$R_{maximum\ deflection} = [0.001x1.5x200psi\ x\ 7.75inch] - 2.03inch$$

$$R_{maximum\ deflection} = (2.325 - 2.03)inch$$

$$R_{maximum\ deflection} = 0.295inch = 7.493mm$$

- If T=0.1 and d=0.0575sec, $R_{moving\ load} = 2.0inch = 51.28mm.$

$$R_{maximum\ deflection} = [0.001x1.5xqa] - R_{moving\ load}$$

$$R_{maximum\ deflection} = [0.001x1.5x200psi\ x\ 7.75inch] - 2.0inch$$

$$R_{maximum\ deflection} = (2.325 - 2.0)inch$$

$$R_{maximum\ deflection} = 0.295inch = 7.493mm$$

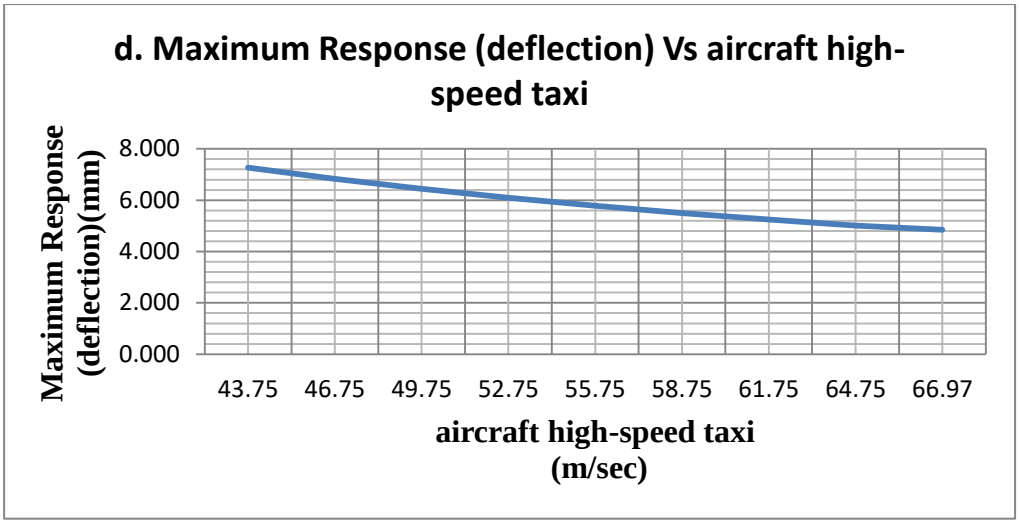

Figure 5-20: Graph for Maximum Response (Deflection) Vs aircraft High-Speed Taxi

e. If a = 19.72cm (0.1972m) in radius and high-speed braking at 240.9(***66.67m/s***) to 83.4 km/h (***23.17m/s***) (130 to 45 knots),

- If T=0.1 and d=0.035sec, $R_{moving\ load} = 2.133inch = 54.18mm.$

$$R_{maximum\ deflection} = [0.001x1.5xqa] - R_{moving\ load}$$

$$R_{maximum\ deflection} = [0.001x1.5x200psi\ x\ 7.75inch] - 2.133inch$$

$$R_{maximum\ deflection} = (2.325 - 2.133)inch$$

$$R_{maximum\ deflection} = 0.195inch = 4.8768mm$$

- If T=0.1 and d=0.1sec, $R_{moving\ load} = 1.823inch = 46.31mm.$

$$R_{maximum\ deflection} = [0.001x1.5xqa] - R_{moving\ load}$$

$$R_{maximum\ deflection} = [0.001x1.5x200psi\ x\ 7.75inch] - 1.823inch$$

$$R_{maximum\ deflection} = (2.325 - 1.823)inch$$

$$R_{maximum\ deflection} = 0.502inch = 12.75mm$$

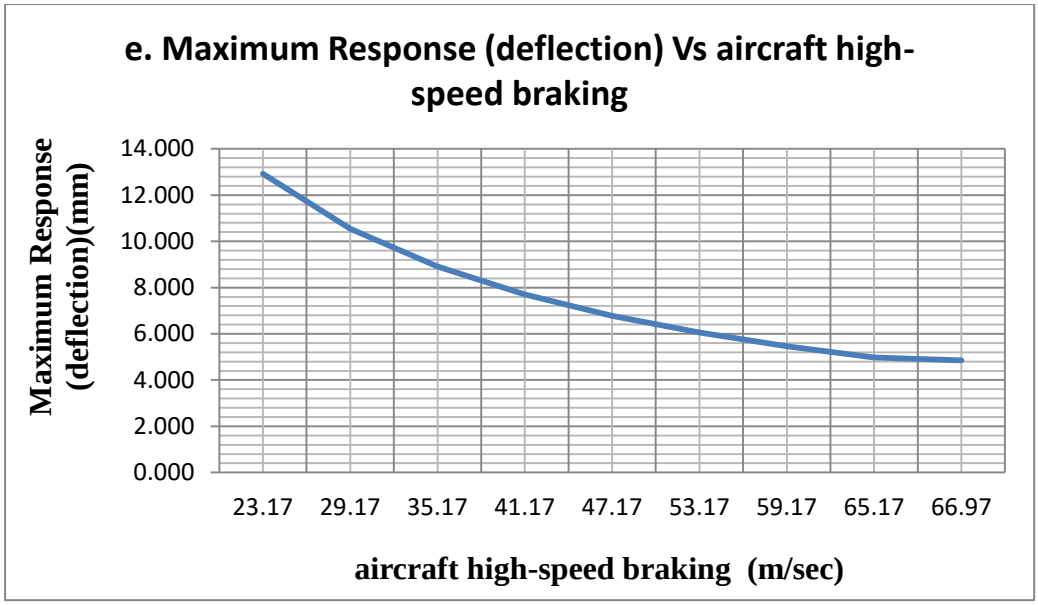

Figure 5-21: Graph for Maximum Response (Deflection) Vs aircraft High-Speed Braking

f. If a = 19.72cm (0.1972m) in radius and takeoff rotation at 157.5 (***43.75m/s***) to 240.9 km/h (***66.92m/s***) (85 to 130 knots),

- If T=0.1 and d=0.054sec, $R_{moving\ load} = 2.036inch = 51.72mm.$

$$R_{maximum\ deflection} = [0.001x1.5xqa] - R_{moving\ load}$$

$$R_{maximum\ deflection} = [0.001x1.5x200psi\ x\ 7.75inch] - 2.203inch$$

$$R_{maximum\ deflection} = (2.325 - 2.203)inch$$

$$R_{maximum\ deflection} = 0.122inch = 3.0988mm$$

- If T=0.1 and d=0.035sec, $R_{moving\ load} = 2.133inch = 54.18mm.$

$$R_{maximum\ deflection} = [0.001x1.5xqa] - R_{moving\ load}$$

$$R_{maximum\ deflection} = [0.001x1.5x200psi\ x\ 7.75inch] - 2.133inch$$

$$R_{maximum\ deflection} = (2.325 - 2.133)inch$$

$$R_{maximum\ deflection} = 0.192inch = 4.8768mm$$

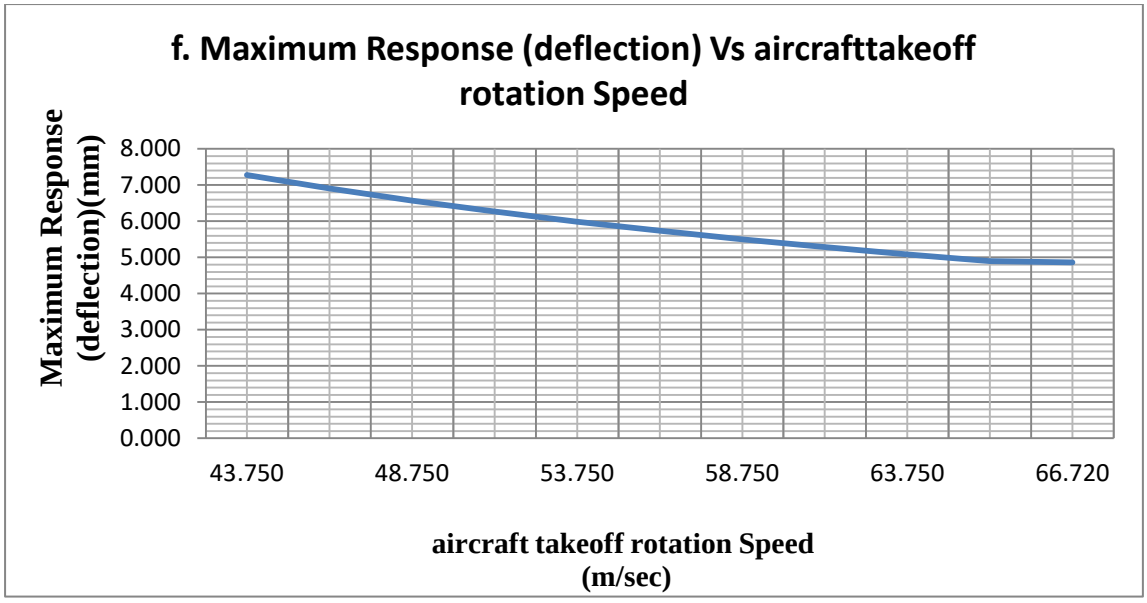

Figure 5-22: Maximum Response (Deflection) Vs aircraft Takeoff Rotation Speed

g. If a = 19.72cm (0.1972m) in radius and Turning at 7.4(***12.15m/s***) to 55.6 km/h (***15.44m/s***) (4 to 30 knots).

- If T=0.1 and d=0.195sec, $R_{moving\ load} = 1.46inch = 37.12mm.$

$$R_{maximum\ deflection} = [0.001x1.5xqa] - R_{moving\ load}$$

$$R_{maximum\ deflection} = [0.001x1.5x200psi\ x\ 7.75inch] - 1.46inch$$

$$R_{maximum\ deflection} = (2.325 - 1.46)inch$$

$$R_{maximum\ deflection} = 0.865inch = 21.971mm$$

- If T=0.1 and d=0.153sec, $R_{moving\ load} = 1.609inch = 40.87mm.$

$$R_{maximum\ deflection} = [0.001x1.5xqa] - R_{moving\ load}$$

$$R_{maximum\ deflection} = [0.001x1.5x200psi\ x\ 7.75inch] - 1.609inch$$

$$R_{maximum\ deflection} = (2.325 - 1.609)inch$$

$$R_{maximum\ deflection} = 0.716inch = 18.186mm$$

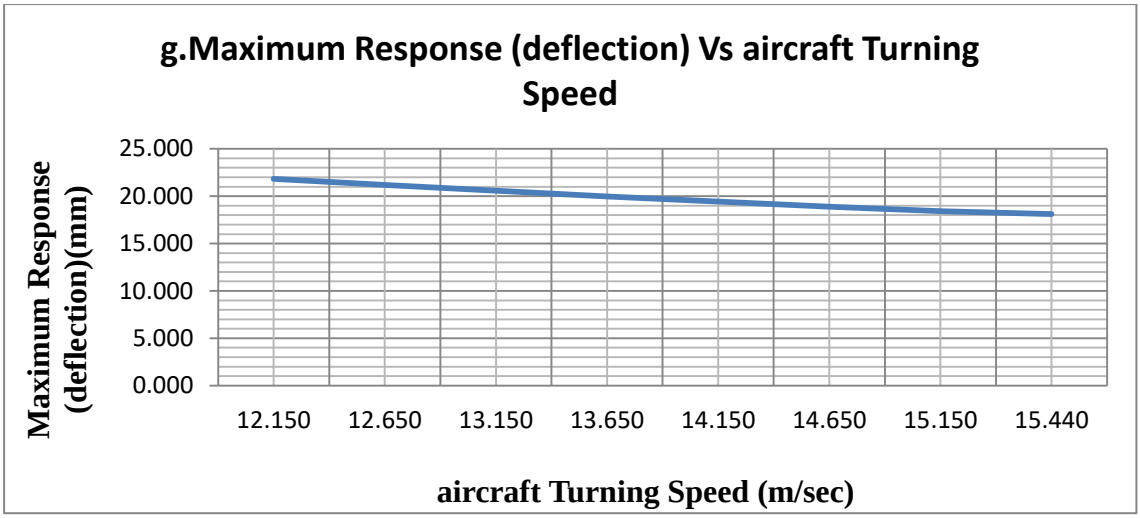

Figure 5-23: Graph for Maximum Response (deflection) Vs aircraft Turning Speed

5.2.2.4 The Impact Factor under Static and Dynamic Load

Yadav and Shukla (2012) model showed that the dynamic deflection increases with an increase in vertical velocity and contact pressure. Yadav and Shukla (2012) model showed the impact factor, which is defined as the ratio of the dynamic deflection to static deflection, also increases with an increase in vertical velocity for a given value of the contact pressure. They found that irrespective of contact pressure values, the impact factor for zero vertical velocity is 2 under elastic runway pavement conditions.

$$\text{IMPACT FACTOR} = \frac{\text{dynamic deflection}}{\text{stastic deflection}}$$

a. If a = 19.72cm (0.1972m) in radius and creep-speed taxi at 5.6(*1.56m/s*) to 14.8 km/h(*4.11m/s*) (3 to 8 knots),

✈ If T=0.1 and d=1.56sec

$$R = 1.163inch = 29.545mm$$

$$\underline{w_o = 1.47inch = 37.39mm}$$

$$\text{IMPACT FACTOR} = \frac{\text{dynamic deflection}}{\text{ststic deflection}} = \frac{R}{W_o}$$

$$\text{IMPACT FACTOR} = \frac{29.545mm}{37.39mm} = 0.790$$

➔If T=0.1 and d= **0.102sec**

$$R = 1.698inch = 43.13mm$$

$$\underline{w_o = 1.47inch = 37.39mm}$$

$$\text{IMPACT FACTOR} = \frac{\text{dynamic deflection}}{\text{ststic deflection}} = \frac{R}{W_o}$$

$$\text{IMPACT FACTOR} = \frac{43.13mm}{37.39mm} = 1.1535$$

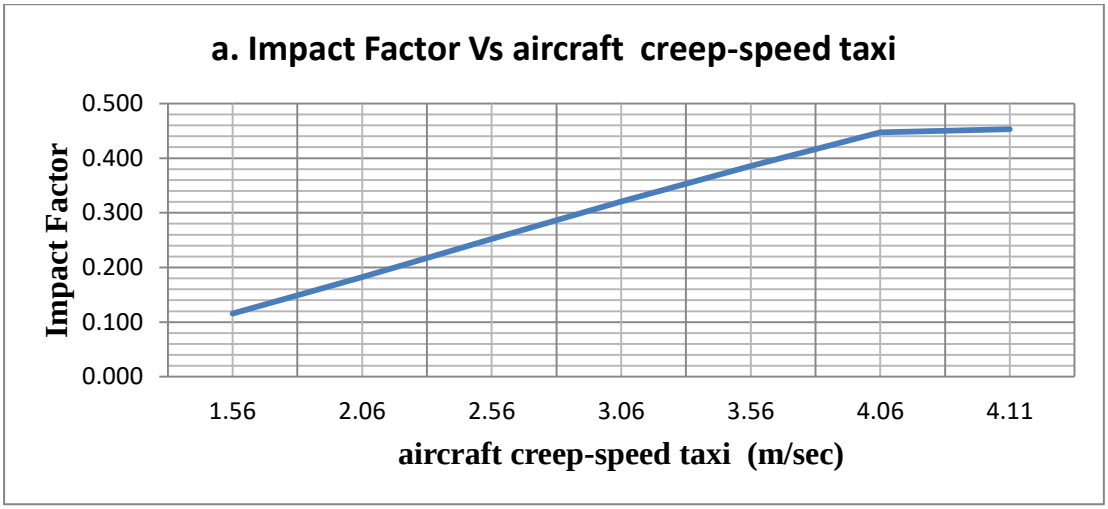

Figure 5-24: Graph for Impact Factor Vs aircraft Creep-Speed Taxi

b. If a = 19.72cm (0.1972m) in radius and low-speed taxi at 27.8 (*7.72m/s*) to 55.6 km/h(*15.44m/s*) (15 to 30 knots),

➔If T=0.1 and d=0.306sec

$$R = 1.415inch = 35.95mm$$

$$\underline{w_o = 1.47inch = 37.39mm}$$

$$\text{IMPACT FACTOR} = \frac{\text{dynamic deflection}}{\text{ststic deflection}} = \frac{R}{W_o}$$

$$\text{IMPACT FACTOR} = \frac{35.95mm}{37.39mm} = 0.962$$

➔If T=0.1 and d=0.153sec

$$R = 1.609inch = 40.868mm$$

$$\underline{w_o = 1.47inch = 37.39mm}$$

$$\text{IMPACT FACTOR} = \frac{\text{dynamic deflection}}{\text{ststic deflection}} = \frac{R}{W_o}$$

$$\text{IMPACT FACTOR} = \frac{40.868mm}{37.39mm} = 1.093$$

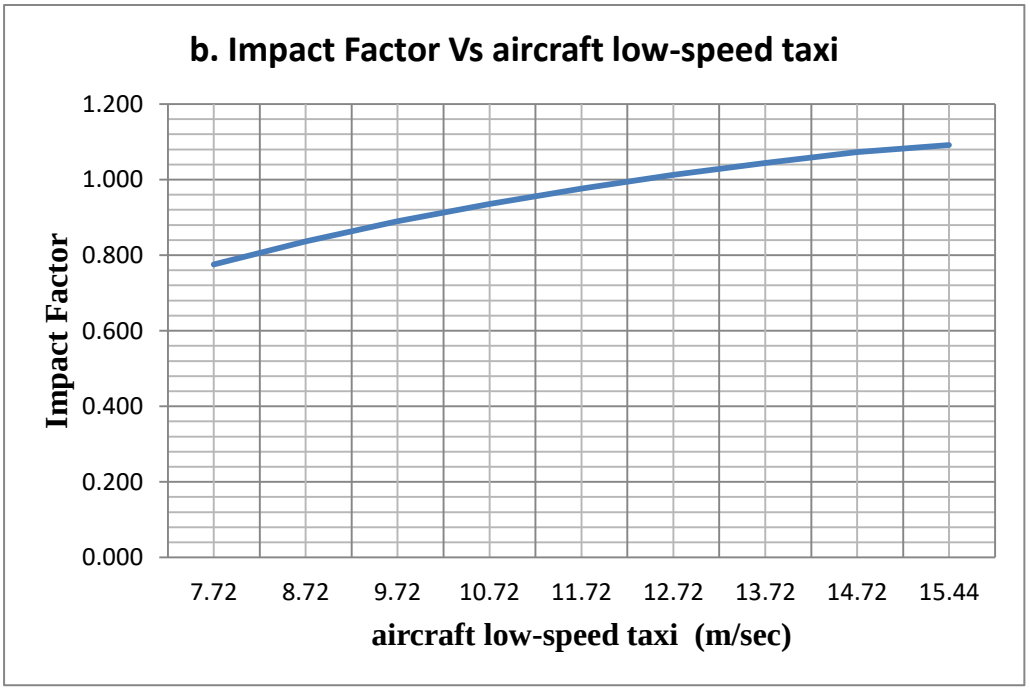

Figure 5-25: Graph for Impact Factor Vs aircraft Low-Speed Taxi

c. If a = 19.72cm (0.1972m) in radius and medium-speed taxi at 83.4(***23.17m/s***) to 148.2 km/h(***41.17m/s***) (45 to 80 knots),

✈If T=0.1 and d=0.306sec

$$R = 1.814inch = 46.067mm$$

$$\underline{w_o = 1.47inch = 37.39mm}$$

$$\text{IMPACT FACTOR} = \frac{\text{dynamic deflection}}{\text{ststic deflection}} = \frac{R}{W_o}$$

$$\text{IMPACT FACTOR} = \frac{46.067mm}{37.39mm} = 1.232$$

✈If T=0.1 and d= $\mathbf{0.0575sec}$

$$R = 2inch = 51.28mm$$

$$\underline{w_o = 1.47inch = 37.39mm}$$

$$\text{IMPACT FACTOR} = \frac{\text{dynamic deflection}}{\text{ststic deflection}} = \frac{R}{W_o}$$

$$\text{IMPACT FACTOR} = \frac{51.28mm}{37.39mm} = 1.372$$

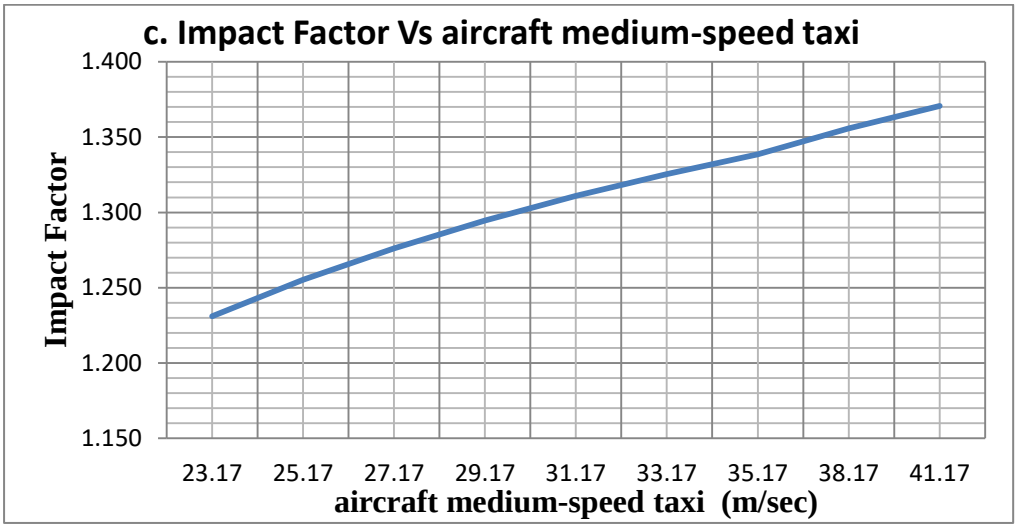

Figure 5-26: Graph for Impact Factor Vs aircraft Medium-Speed Taxi

d. If a = 19.72cm (0.1972m) in radius and high-speed taxi at 157.5(***43.75m/s***) to 240.9 km/h (***66.97m/s***) (85 to 130 knots),

✈If T=0.1 and d=$\mathbf{0.054sec}$

$$R = 2.03inch = 51.63mm$$

$$\underline{w_o = 1.47inch = 37.39mm}$$

$$\text{IMPACT FACTOR} = \frac{\text{dynamic deflection}}{\text{ststic deflection}} = \frac{R}{W_o}$$

$$\text{IMPACT FACTOR} = \frac{51.63mm}{37.39mm} = 1.381$$

✈If T=0.1 and d= 0.0353sec

$$R = 2.134inch = 54.20mm$$

$$\underline{w_o = 1.47inch = 37.39mm}$$

$$\text{IMPACT FACTOR} = \frac{\text{dynamic deflection}}{\text{ststic deflection}} = \frac{R}{W_o}$$

$$\text{IMPACT FACTOR} = \frac{54.20mm}{37.39mm} = 1.450$$

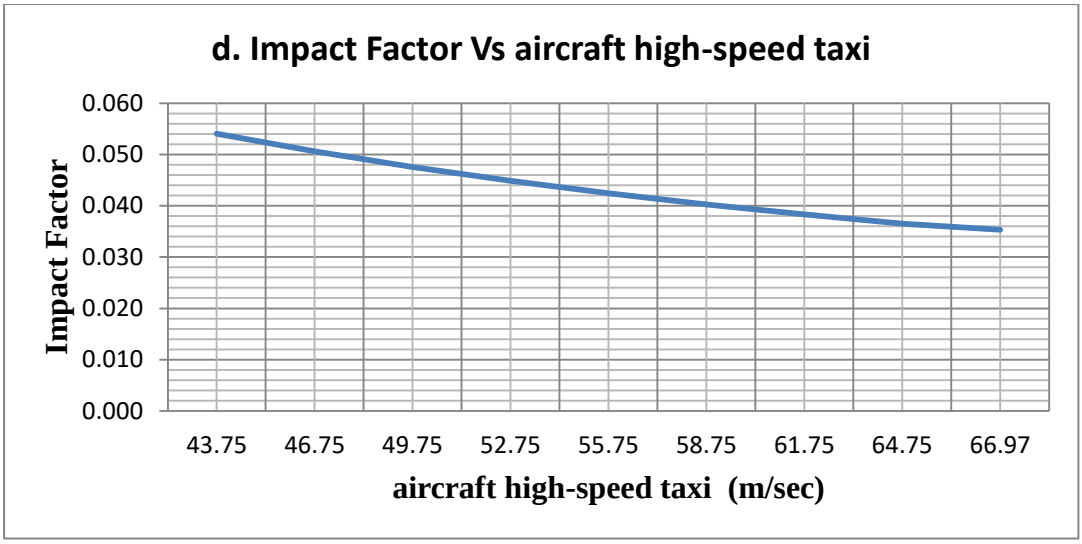

Figure 5-27: Graph for Impact Factor Vs aircraft High-Speed Taxi

e. If a = 19.72cm (0.1972m) in radius and high-speed braking at 240.9(***66.67m/s***) to 83.4 km/h (***23.17m/s***) (130 to 45 knots),

✈If T=0.1 and d=$\mathbf{0.035sec}$

$$R = 2.133inch = 54.18mm$$

$$\underline{w_o = 1.47inch = 37.39mm}$$

$$\text{IMPACT FACTOR} = \frac{\text{dynamic deflection}}{\text{ststic deflection}} = \frac{R}{W_o}$$

$$\text{IMPACT FACTOR} = \frac{54.18mm}{37.39mm} = 1.450$$

✈If T=0.1 and d= 0.1sec

$$R = 1.823inch = 46.31mm$$

$$\underline{w_o = 1.47inch = 37.39mm}$$

$$\text{IMPACT FACTOR} = \frac{\text{dynamic deflection}}{\text{ststic deflection}} = \frac{R}{W_o}$$

$$\text{IMPACT FACTOR} = \frac{46.31mm}{37.39mm} = 1.238$$

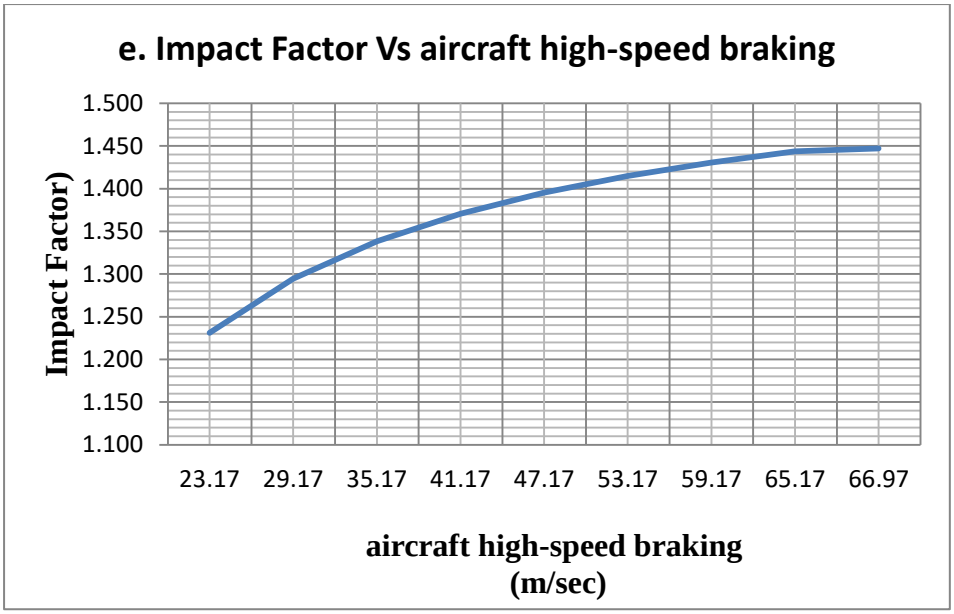

Figure 5-28: Graph for Impact Factor Vs aircraft high-speed braking

f. If a = 19.72cm (0.1972m) in radius and takeoff rotation at 157.5 (***43.75m/s***) to 240.9 km/h (***66.92m/s***) (85 to 130 knots),

✈If T=0.1 and d=$\mathbf{0.054sec}$

$$R = 2.036inch = 51.72mm$$

$$\underline{w_o = 1.47inch = 37.39mm}$$

$$\text{IMPACT FACTOR} = \frac{\text{dynamic deflection}}{\text{ststic deflection}} = \frac{R}{W_o}$$

$$\text{IMPACT FACTOR} = \frac{51.72mm}{37.39mm} = 1.383$$

✈If T=0.1 and d=$\mathbf{0.035sec}$

$$R = 2.133inch = 54.18mm$$

$$\underline{w_o = 1.47inch = 37.39mm}$$

$$\text{IMPACT FACTOR} = \frac{\text{dynamic deflection}}{\text{ststic deflection}} = \frac{R}{W_o}$$

$$\text{IMPACT FACTOR} = \frac{54.18mm}{37.39mm} = 1.450$$

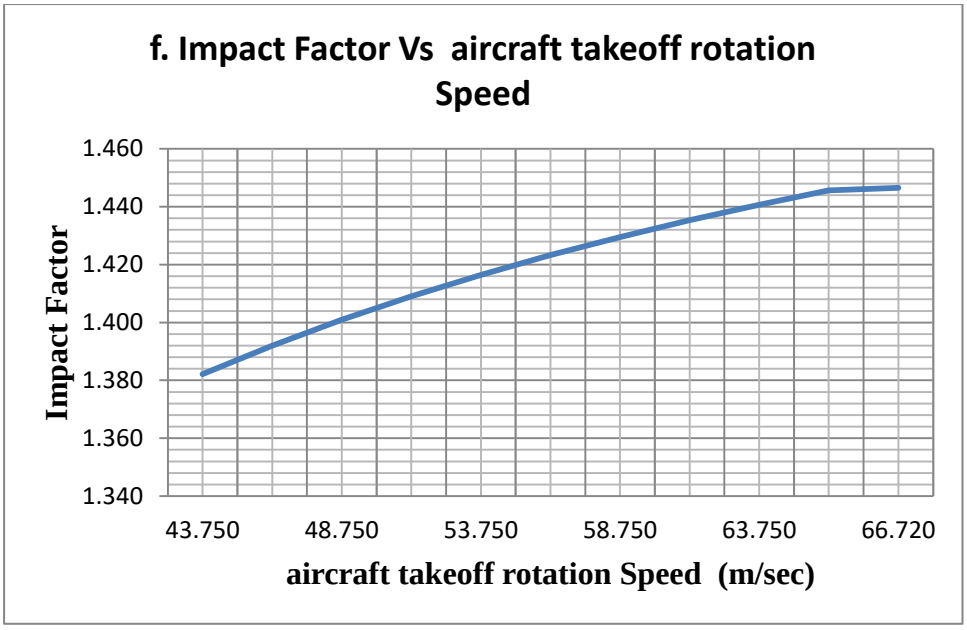

Figure 5-29: Graph Impact Factor Vs aircraft Takeoff Rotation Speed

g. If a = 19.72cm (0.1972m) in radius and Turning at 7.4(***12.15m/s***) to 55.6 km/h (***15.44m/s***) (4 to 30 knots).

✈If T=0.1 and d=$\mathbf{0.195sec}$

$$R = 1.46inch = 37.12mm$$

$$\underline{w_o = 1.47inch = 37.39mm}$$

$$\text{IMPACT FACTOR} = \frac{\text{dynamic deflection}}{\text{ststic deflection}} = \frac{R}{W_o}$$

$$\text{IMPACT FACTOR} = \frac{37.12mm}{37.39mm} = 0.993$$

✈If T=0.1 and d=$\mathbf{0.153sec}$

$$R = 1.609inch = 40.87mm$$

$$\underline{w_o = 1.47inch = 37.39mm}$$

$$\text{IMPACT FACTOR} = \frac{\text{dynamic deflection}}{\text{ststic deflection}} = \frac{R}{W_o}$$

$$\text{IMPACT FACTOR} = \frac{40.87mm}{37.39mm} = 1.0930$$

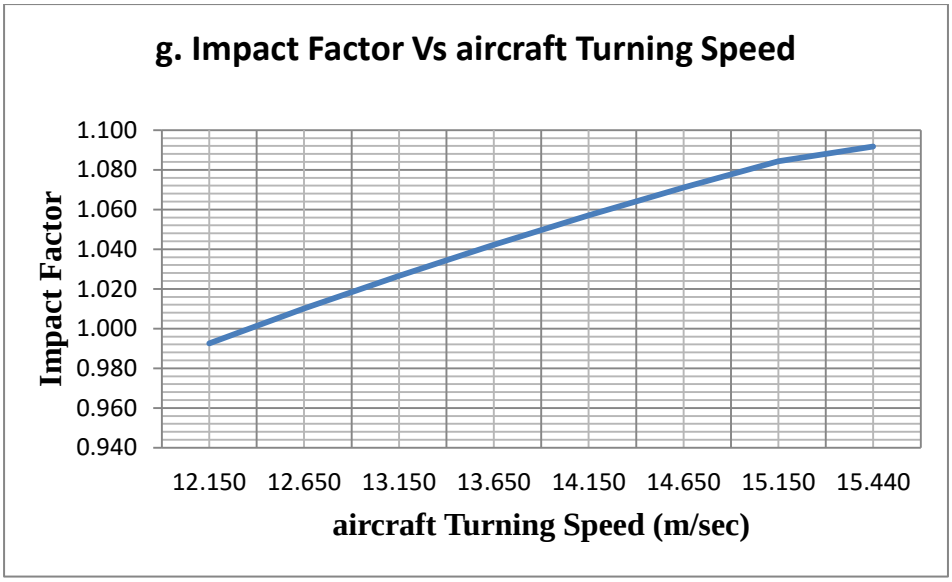

Figure 5-30: Graph for Impact Factor Vs aircraft Turning Speed

Table 5-12 the Response under Airport Flexible Pavement ($v = 0.45$)

Cases	aircraft Speed (m/sec)	Load Duration (Sec)	Static Response (deflection)(mm)	Dynamic Response (deflection)(mm)	Maximum Response (deflection) (mm)	Impact Factor
a	1.56	1.560	37.390	29.545	29.514	0.790
	4.11	0.102	37.390	43.130	16.032	1.153
b	7.72	0.306	37.390	35.950	23.114	0.962
	15.44	0.153	37.390	40.868	18.186	1.093
c	23.17	0.306	37.390	46.067	12.979	1.232
	41.17	0.057	37.390	51.280	8.255	1.372
d	43.75	0.054	37.390	51.630	7.493	1.381
	66.97	0.035	37.390	54.200	7.493	1.450
e	66.97	0.035	37.390	54.180	4.877	1.450
	23.17	0.100	37.390	46.310	12.750	1.238
f	43.75	0.054	37.390	51.720	3.099	1.383
	66.92	0.035	37.390	54.180	4.877	1.450
g	12.15	0.195	37.390	37.12	21.971	0.993
	15.44	0.153	37.390	40.87	18.186	1.093

5.2.2.5 Determination of Resilient Modulus (E-Value) and Foundation Modulus (k-Value) for flexible Pavement Subgrade.

The subgrade is assumed to be infinite in thickness and is characterized by either a modulus or CBR value. Subgrade modulus values for flexible pavement design can be determined in a number of ways. The procedure that will be applicable in most cases is to use available CBR values and substitute in the relationship:

$$E = 1500 \times CBR, \text{ (}E\text{ in psi)}$$

This method will provide designs compatible with the previous FAA design procedure based on the CBR equation. Although FAARFIELD requires input of the material elastic modulus, direct input of CBR values is also acceptable.

By default, FAARFIELD computes only the vertical subgrade strain for flexible pavement thickness design. However, the user has the option of enabling the asphalt strain computation by deselecting the "No AC CDF" checkbox in the FAARFIELD options screen. In most cases the thickness design is governed by the subgrade strain criterion. The user has the option of performing the asphalt strain check for the final design, and it is good engineering practice to do so

For this example, the B767-200 gives the maximum required compaction values from table 2-11.Using table 2-11 for non-cohesive soils and applying linear interpolation, obtain the following compaction requirements as shown in table 2-13.

Table 5-13 COMPACTION REQUIREMENTS

100%	95%	90%
0-21	21-37	37-52

Comparison of the tabulations show that for this example in-place density is satisfactory at a depth of 0.97m, being 90 percent within the required 90 percent zone. It will be necessary to compact an additional 0.03m at 95 percent. Therefore, compact the top 0.53m of subgrade at 100 percent density and the 21 to 38 inches at 95 percent density.

Subgrade soils are usually rather variable and the selection of a design CBR value requires some judgment. The design CBR value should be equal to or less than 85 percent of all the 27 AC 150/5320-6E 9/30/2009 subgrade CBR values. This corresponds to a design value of one

standard deviation below the mean. In some cases subgrade soils that are significantly different in strength occur in different layers. In these instances several designs should be examined to determine the most economical pavement section. It may be more economical to remove and replace a weak layer than to design for it. On the other hand, circumstances may be such that designing for the weakest layer is more economical. Local conditions will dictate which approach should be used.

The subgrade is assumed to be infinite in thickness and is characterized by either a modulus or CBR value. Subgrade modulus values for flexible pavement design can be determined in a number of ways. The procedure that will be applicable in most cases is to use available CBR values and substitute in the relationship: $E = 1500 \times CBR$, (E in psi) this method will provide designs compatible with the previous FAA design procedure based on the CBR equation. Although FAARFIELD requires input of the material elastic modulus, direct input of CBR values is also acceptable.

The use of the FAARFIELD, assume a flexible pavement is to be designed for the aircraft traffic mix in table 2-6. The subgrade CBR is 8(E=12,000psi), 25(E=12,000psi), 29(E=12,000psi) and 33.3(E=12,000psi). Since the traffic mix includes jet aircrafts weighing 45,359 kg or more, an asphalt stabilized base will be used. The pavement layer thicknesses obtained from the design software FAARFIELD are listed in Annex III.

For the flexible pavement part there were five cases depending on the CBR-Value. Such as

- Case–One (1) - CBR Value =8%
- Case–Two (2) - CBR Value =15%
- Case–Three (3) - CBR Value =25%
- Case–Four (4) - CBR Value =29%
- Case–Five (5) - CBR Value =33.3%

The design Aircraft for Addis Ababa bole international Airport was Boeing 777-300Er which Rides on 27x7.75 R15 Rubber

CASE–ONE (1)- CBR VALUE =8%

Table 5-14 Additional aircraft Information for Design (For CBR-8)

SUBGRADE CDF				
No.	Name	CDF Contribution	CDF Max for aircraft	P/C Ratio
1	A320-100	0.00	0.00	1.21
2	A340-600 opt	0.09	0.09	0.59
3	A340-600 opt Belly	0.00	0.04	0.58
4	A380-800	0.01	0.01	0.42
5	B737-800	0.00	0.00	1.22
6	B747-400B Combi	0.01	0.01	0.57
7	B747-400ER Passenger	0.01	0.01	0.57
8	B757-300	0.00	0.00	0.72
9	B767-400 ER	0.04	0.05	0.60
10	B777-300 ER	0.81	0.82	0.40
11	B787-8 (Preliminary)	0.03	0.03	0.58

Table 5-14 shows that the pavement thickness design in this case is controlled primarily by the B777-300 ER, which contributes 81 percent of the CDF.

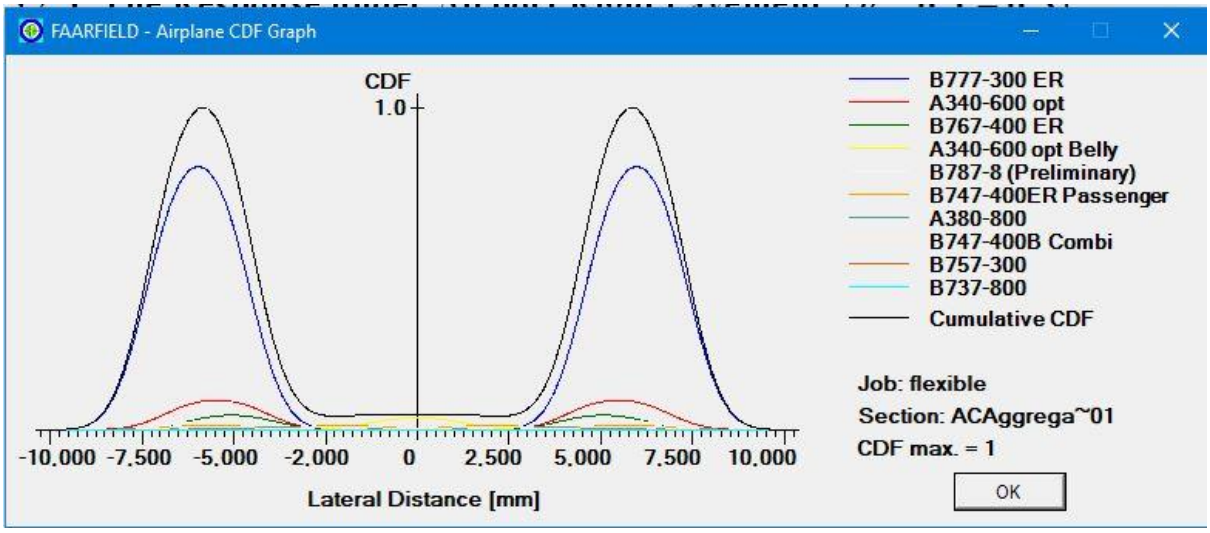

Figure 5-31 CDF Graph for CBR-8 Subgrade

CASE–ONE (2)- CBR VALUE =15%

Table 5-15 Additional aircraft Information for Design (For CBR-15%)

SUBGRADE CDF				
No.	Name	CDF Contribution	CDF Max for aircraft	P/C Ratio
1	A320-100	0.00	0.00	1.46
2	A340-600 opt	0.18	0.18	0.81
3	A340-600 opt Belly	0.00	0.05	0.84
4	A380-800	0.01	0.01	0.58
5	B737-800	0.00	0.00	1.39
6	B747-400B Combi	0.01	0.01	0.73
7	B747-400ER Passenger	0.01	0.01	0.75
8	B757-300	0.00	0.00	0.73
9	B767-400 ER	0.02	0.02	0.76
10	B777-300 ER	0.13	0.13	0.55
11	B787-8 (Preliminary)	0.02	0.02	0.80

Table 5-15 shows that the pavement thickness design in this example is controlled primarily by the A340-600 opt, which contributes 18 percent of the CDF.

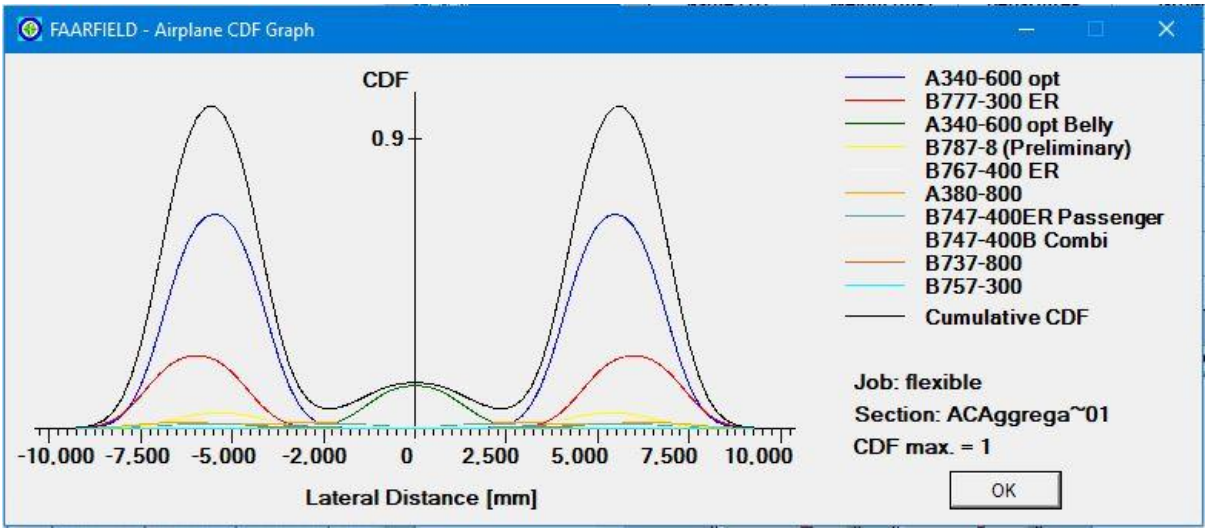

Figure 5-32 CDF Graph for CBR-15 Subgrade

CASE–Three (3)- CBR VALUE =25%

Table 5-16: Additional aircraft Information for Design (For CBR-25%)

SUBGRADE CDF				
No.	Name	CDF Contribution	CDF Max for aircraft	P/C Ratio
1	A320-100	0.00	0.00	1.46
2	A340-600 opt	0.00	0.00	0.81
3	A340-600 opt Belly	0.00	0.00	0.84
4	A380-800	0.00	0.00	0.58
5	B737-800	0.00	0.00	1.39
6	B747-400B Combi	0.00	0.00	0.73
7	B747-400ER Passenger	0.00	0.00	0.75
8	B757-300	0.00	0.00	0.73
9	B767-400 ER	0.00	0.00	0.76
10	B777-300 ER	0.00	0.00	0.55
11	B787-8 (Preliminary)	0.00	0.00	0.80

Table 5-16 shows that the pavement thickness design in this case is not controlled by any aircraft, which All contributes 0 percent of the CDF.

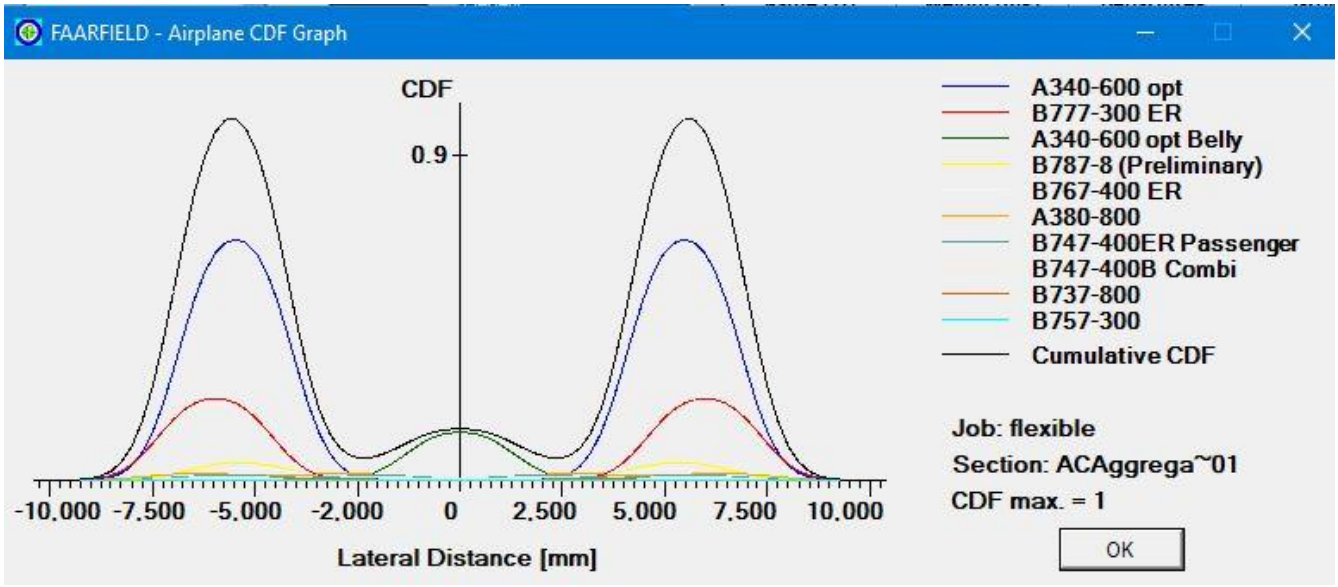

Figure 5-33 CDF graph for CBR-25 subgrade

CASE–Four (4)- CBR VALUE =29%

Table 5-17: Additional aircraft Information for Design (For CBR-29%)

SUBGRADE CDF				
No.	Name	CDF Contribution	CDF Max for aircraft	P/C Ratio
1	A320-100	0.00	0.00	1.46
2	A340-600 opt	0.00	0.00	0.81
3	A340-600 opt Belly	0.00	0.00	0.84
4	A380-800	0.00	0.00	0.58
5	B737-800	0.00	0.00	1.39
6	B747-400B Combi	0.00	0.00	0.73
7	B747-400ER Passenger	0.00	0.00	0.75
8	B757-300	0.00	0.00	0.73
9	B767-400 ER	0.00	0.00	0.76
10	B777-300 ER	0.00	0.00	0.55
11	B787-8 (Preliminary)	0.00	0.00	0.80

Table 5-17 shows that the pavement thickness design in this case is not controlled by any Aircraft, which All contributes 0 percent of the CDF.

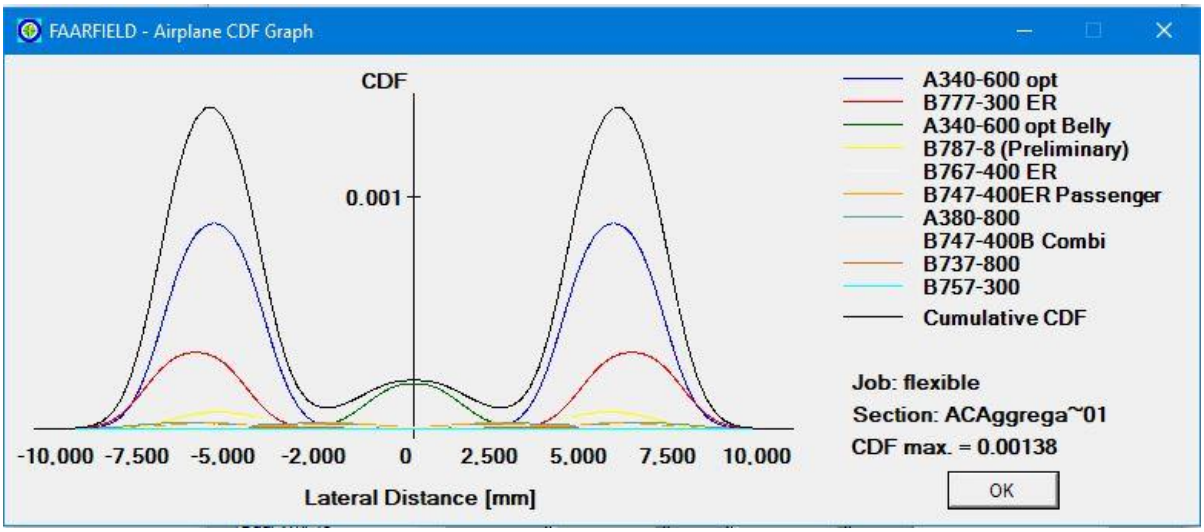

Figure 5-34: CDF Graph for CBR-29 Subgrade

CASE–Five (5)- CBR VALUE =33.3%

Table 5-18: Additional aircraft Information for Design (For CBR-33.3%)

SUBGRADE CDF				
No.	Name	CDF Contribution	CDF Max for aircraft	P/C Ratio
1	A320-100	0.00	0.00	1.46
2	A340-600 opt	0.00	0.00	0.81
3	A340-600 opt Belly	0.00	0.00	0.84
4	A380-800	0.00	0.00	0.58
5	B737-800	0.00	0.00	1.39
6	B747-400B Combi	0.00	0.00	0.73
7	B747-400ER Passenger	0.00	0.00	0.75
8	B757-300	0.00	0.00	0.73
9	B767-400 ER	0.00	0.00	0.76
10	B777-300 ER	0.00	0.00	0.55
11	B787-8 (Preliminary)	0.00	0.00	0.80

Table 5-18 shows that the pavement thickness design in this case is not controlled by any Aircraft, which All contributes 0 percent of the CDF.

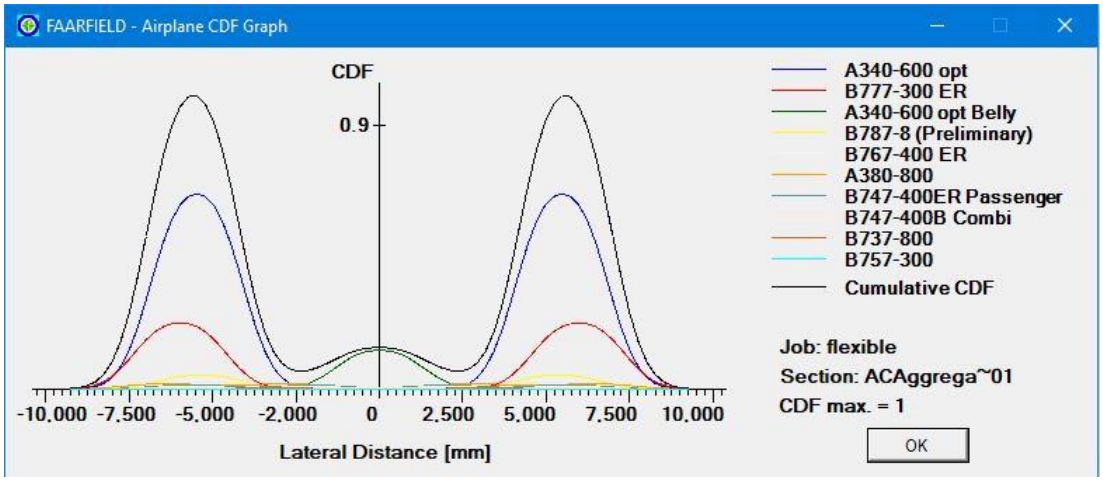

Figure 5-35: CDF Graph for CBR-33.3 Subgrade

Table 5-19 CBR Value and Subgrade CDF Value for Different aircraft Category

Subgrade CBR value	8	15	25	29	33.3
Subgrade CDF value (A320-100)	0	0	0	0	0
Subgrade CDF value(A340-600 opt)	9	18	0	0	0
Subgrade CDF value(A340-600 opt Belly)	0	0	0	0	0
Subgrade CDF value(A380-800)	1	1	0	0	0
Subgrade CDF value(B737-800)	0	0	0	0	0
Subgrade CDF value(B747-400B Combi)	1	1	0	0	0
Subgrade CDF value(B747-400ER Passenger)	1	1	0	0	0
Subgrade CDF value (B757-300)	0	0	0	0	0
Subgrade CDF value(B767-400 ER)	4	2	0	0	0
Subgrade CDF value(B777-300 ER)	81	13	0	0	0
Subgrade CDF value(B787-8 (Preliminary))	3	2	0	0	0

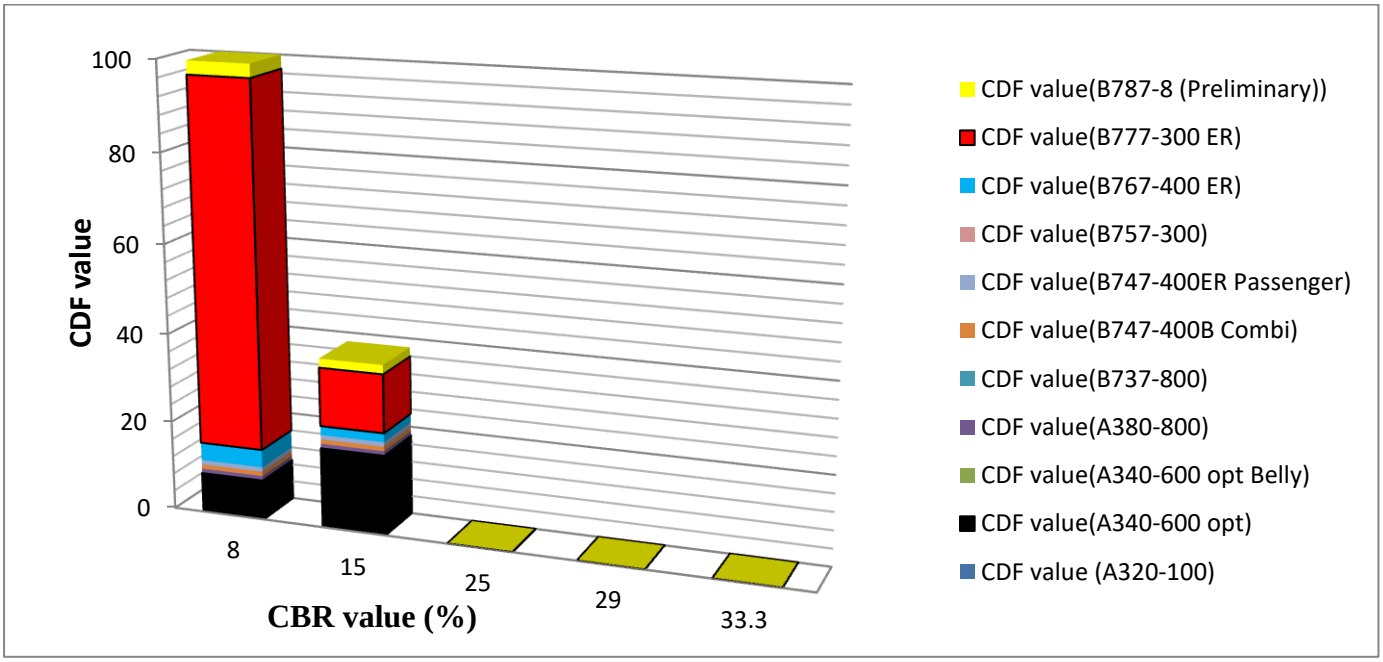

Figure 5-36: Graph of CBR Value and Subgrade CDF Value for Different aircraft Category

CHAPTER SIX

CONCLUSION AND RECOMMENDATION

6.1 CONCLUSION

- From analysis of load duration, load duration and aircraft speed have inverse relation.
- For flexible pavement part the response (Deflection) under static load is constant and depends on the poison ratio (v), load (q) and contact radius (a).
- The impact factor increase with the increase of speed and with decrease of load duration
- This all show that load duration and maximum deflection (response) have inverse relation with the Aircraft speed, and also dynamic deflection (response) and impact factor have direct relation with the Aircraft speed.
- From Analysis of subgrade response under flexible pavement:
    - For CBR Value =8% ,the B777-300Er contribute 81 percent of subgrade CDF and the pavement design in this case is controlled primarily by the B777-300ER ,which contributed 81percent of the subgrade CDF
    - For CBR Value =15% ,the pavement design in this case is controlled primarily by the A340-600 opt ,which contributed 18 percent of the subgrade CDF
    - For CBR Value ≥ 25%, the pavement design in this case is not controlled Aircraft, because they contributed 0 percent of the subgrade CDF. That means for subgrade which have CBR value 25 and above does not have any effect on the subgrade.
    - Subgrade CDF value decreases with increase in CBR value and finally it becomes zero.
    - This show that for Flexible pavement structure Subgrade CDF-value, k-value and natural frequency are tend to Zero with time is tend to infinity.

6.2 RECOMMENDATION

- New compaction techniques were recommended to increase the strength of airport asphalt pavement structure.
- During the operation of Aircraft, the speed of Aircraft should not increase beyond design value. This is because dynamic response (deflection) and impact factor have direct relation with the Aircraft speed.
- To control subgrade response under flexible pavement using CBR–value which gives Subgrade CDF value of zero is the best. Because beyond then Subgrade CDF value constant i.e. zero.

REFERENCES

AASHO Road Test (1962).Report7, American Association of State High Officials, Washington, D.C.

AASHTO (2002) Standard method of test for resilient modulus of subgrade soils and untreated base/subbase materials,

AASHTO designation 307, standard specifications for transportation materials and methods of sampling and testing, part ii tests

Al-Qadi I, Xie W, Elseifi MA (2008) Frequency determination from vehicular loading time pulse to predict appropriate complex modulus in MEPDG Jason Asphalt Paving Technol AAPT, Vol. 77

Barksdale RD, Itani SY (1989). Influence of aggregate shape on base behavior, transportation research record 1227, Transportation Research Board, National Research Council, Washington, D.C.

Cardone F, Cerni G, Virgil A, Camilli S (2011). Characterization of permanent deformation behavior of unbound granular materials under repeated triaxial loading. J. Constr. Build. Mater

Cebon D (1988). Theoretical road damage due to dynamic type forces of heavy vehicles, Part1: Dynamic Analysis of Vehicles and Road Surfaces [J], in: Proceedings of the Institution of Mechanical Engineers, Part C: Mech. Eng. Sci. 202(C2).

Craig, R., 2004. *Craig's Soil Mechanics.* New York, USA: CRC Press.

Divine O (1998) Dynamic Interaction between vehicles and infrastructure experiment: Technical Report, Organization for Economic Co-operation and Development, Road Transport Research, Scientific Expert Group, Paris.

Drumm, E. C. Boateng-Poku Y and Pierce, T. J. (1990) "Estimation of Subgrade Resilient Modulus from Standard Tests" Journal of Geotechnical Engineering, ASCE, Vol. 116, No. 5, pp.774-789

Dongré R, Myers L, D'Angelo J, Paugh C, Gudimettla J (2005). Field Evaluation of Witczak and Hirsh Models for Predicting Dynamic Modulus of Hot-Mix Asphalt, Journal of The Association of Asphalt Paving Technologists, AAPT, Vol. 74.

Daehyeon Kim, and Nayyar Zia Siddiki, **FHWA/IN/JTRP-2005/23**

Elliott, R.P. and Thornton, S.I.(1988) "Resilient Modulus and AASHTO Pavement Design" Transportation Research Record, 1196, TRB, National Research Council, Washington, D.C., pp. 116-124.

Gillespie TD (1992) Truck factors affecting dynamic loads and road damage [C], University of Cambridge Queens' College, and Cambridge, UK.

Giroud JP, Han J (2004). Design method for geogrid-reinforced unpaved roads. I. Development of design method, II. Calibration and Applications J. Geotechnical Geo-environmental Eng. Am. Soc. Civil Eng. Vol. 130, ASCE

Huang YH (2004). Pavement analysis and design Pearson prentice Hall, Second edition, Pearson Education, Inc. Upper saddle River New Jersey

Hill, R., 1998. The mathematical theory of plasticity s.loxford university press

Jegede G (2000). Effect of soil properties on pavement failures along the F209 highway at Ado-Ekiti, south-western Nigeria, J. Constr. Build Mater P.14

Loulizi A, Al-Qadi I, Lahouar S, Freeman TE (2002), Measurement of Vertical Compressive Stress Pulse in Flexible Pavements: Representation for Dynamic Loading Tests, Transportation Research Board of the National Academies, Washington, D.C. Vol. 1816.

Lu S, Xueju D (1996). Dynamic load caused by vehicle–pavement interactions. J. Southeast Univ. 26(5) (Natural Science Edition)

Lytton RL, Uzan J, Fernando EG, Roque R, Hiltunen D, Stoffels SM (1993) Development and validation of performance prediction models and specifications for asphalt binders and paving mixes, Transportation Research Board, Washington, D.C.

Ladd,C.C., Foote, R., Ishihara, K., Schlosser, F. and Poulos, H. G. (1977). "Stress Deformation and Strength Characteristics", Proc., of 9th International Conference on Soil Mechanics and Foundation Engineering, Tokyo, Vol. 2, pp. 421-494.

Monismith, C.L. Ogawa, N and Freeme, C.R. (1975) "Permanent Deformation Characteristics of Subgrade Soils Due to Repeated Loading", Transportation Research Record, 537, TRB, National Research Council, Washington, D.C., pp. 1-17.

Mulungye RM, Owende PMO, Mellon K (2007). Finite element modeling of flexible pavements on soft soil subgrades, J Mater Design 28

NCHRP 1-37A (2004). Guide for mechanistic-empirical design of new and rehabilitated pavement structures, Final Report, Project 1-37A, TRB, National Cooperative Highway Research Program, and Washington, D.C.

Poulos, H.G., 2015. Soil-structure interaction in tall Buildings foundation design Australia, The HKIE Geotechnical division annual seminar

Van Zyl NJW, Maree JH (1983). The behavior of high standard crushed stone base pavement during heavy vehicle simulator test. Civ. Eng. S. Africa P. 25.

Wright PH, Paquette RJ (1987). Highway Engineering, 5th ed., John Wiley, New York

Xu T, Huang X (2011). Investigation into causes of in-place rutting in asphalt pavement, J Constr. Build Mater P.28

Yong L, Shaopu Y, Shaohua L, Liqun C (2010). Numerical and experimental investigation on stochastic dynamic load of a heavy duty vehicle Appl Math Model P 34

Zakaria M, Leest G (1996). Rutting characteristics of unbound aggregate layers, Constr. Build Mater 10(3)

Zhou F, Fernando E, Scullion T (2010). Development, calibration, and validation of performance prediction models for the Texas M-E flexible pavement design system. Texas Transportation Institute, the Texas A&M University System College Station.

ANNEX

Annex I

SITE LOCATION AND INFORMATION

Site Location on Google Earth Map

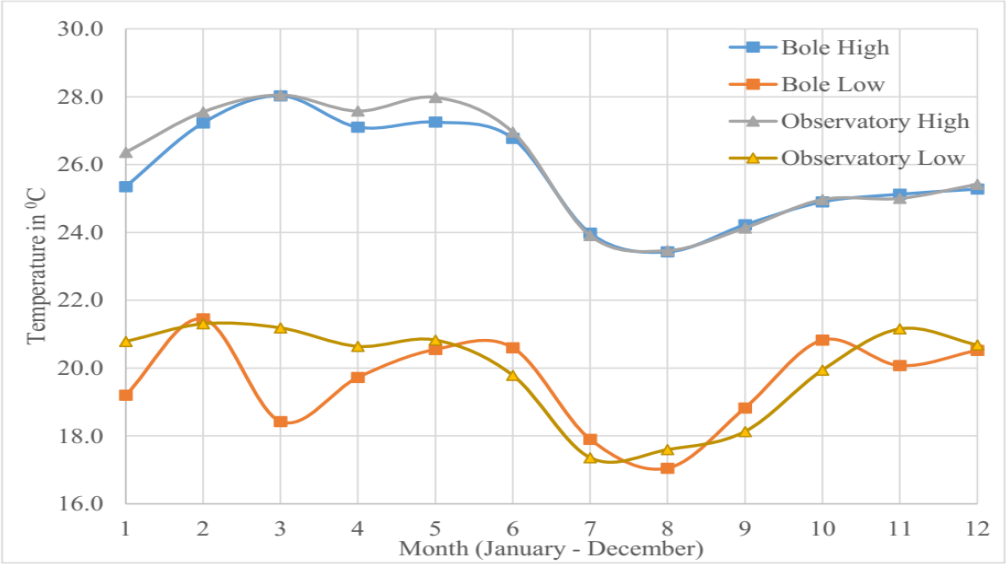

Average High and Low Temperature of Bole and Observatory Gauging Stations (Ethiopian Meteorological Agency, , 2015)

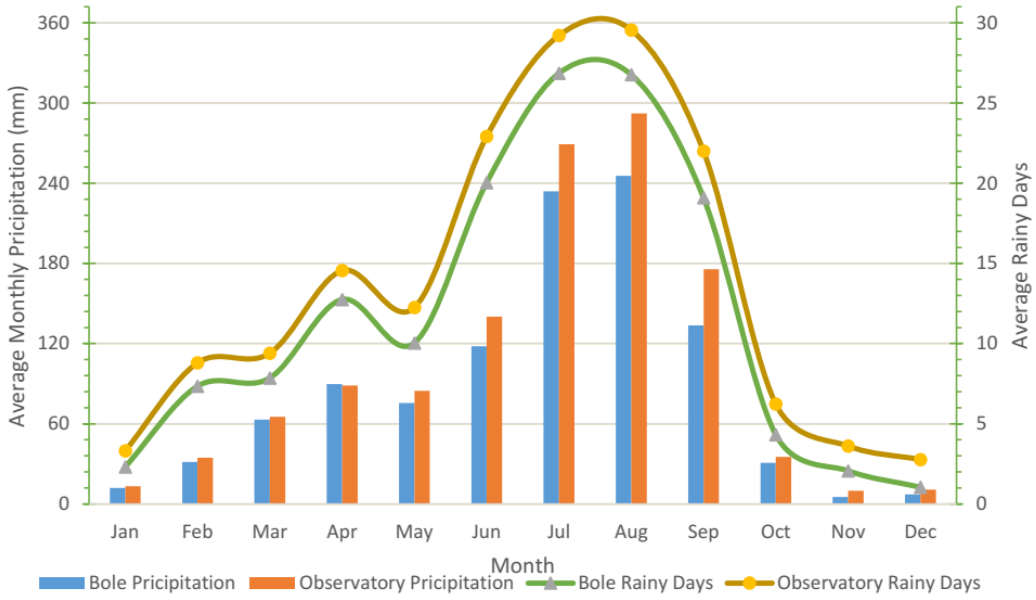

Average Monthly Rainfall Depth and Rainy Days of Bole and Observation Stations (Ethiopian Meteorological Agency, , 2015)

Annex II

LABORATORY TEST RESULT

Addis Ababa Bole International Airport Terminal Expantion Project

Contractor : China Communications Construction Co. Ltd Consultant:Aéroports de paris Ingénierie(ADPI, FRANCE)

Report of Soil for Embankment Fill

Sample No		Lab Ref No	AABIA-171002-02_1
Sample Declaration	Stone and clay	Type of Material	Backfill
Digging Depth		Location/Source	Kilinto/T2 Parking area
Test By (Organization)	AABIA Head Laboratory	Date Report	2017/10/19
Specification Used	AACRA		

CBR

No. of blows	10	30	65
No. of layers	5	5	5
Dry unit weight (g/cm^3)	1.76	1.83	1.91
CBR (%)	29	35	122
Absorptivity (g)	180	122	77
Swell (%)	1.24	0.97	0.63

Moisture Density Relations(Proctor)

Proctor Modifiy	1	2	3	4	5	OPM
Moisture content(%)	6.1	9.7	12.0	16.2	/	11.6
Dry density(g/cm^3)	1.84	1.87	1.90	1.82	/	1.90

Sieve Analysis

Sieve Size (mm)	50	37.5	20	5	2	1.18	0.425	0.3	0.075	Soil Sort
Percentage passing(%)	86.7	79.7	47.7	23.4	18.2	17.0	15.1	14.6	13.2	Coarse-Grained

Plasticity Index

Limit of Liquid (%)	/	Limit of Plasticity (%)	/
Plastic Index (%)	/	Free Swell Ratio (%)	/

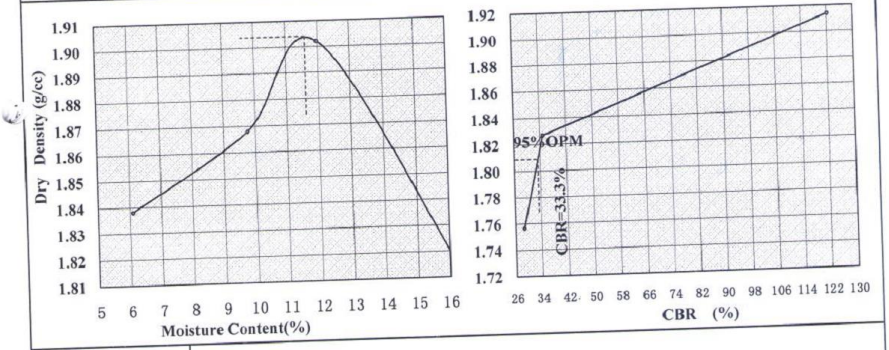

Remarks:	
Conclusion	All the indicators meet the technical requirements of Backfill
Idea of the Material Engineer(Consultant)	Upon examination，the material can be used for every region of subgrade

Submit by: Contractor's representative Checked by: Material Engineer(Contractor) Witness by: Consultant's representative Supervisor: Material Engineer(Consultant)

Addis Ababa Bole International Airport Terminal Expantion Project

ontractor: China Communications Construction Co. Ltd. **Consultant: Aéroports de paris Ingénierie(ADPI, FRANCI**

Record of Sieve Analysis Test of Soil

Sample No		Lab Ref No	AABIA-171002-02-2
Sample declaration	Stone and clay	Material Source/ Location	Kilinto/T2 Parking area
Method Used	AACRA	Material Type	Backfill
Digging Depth		Date test	2017/10/14
Total Weight of soil befor wash (g)		9050	
Weight of soil(>2mm)(g)	7447	Percentage of soil(>2mm)	82.3
Wt of soil(<2mm and >0.075mm)(g)	678	Percentage of soil(<2mm and >0.075mm)	7.5
Wt of soil(<0.075mm)(g)	925	Percentage of soil(<0.075mm)	10.2

Rough Sieving Analysis(>2mm)					Fine Sieving Analysis(<2mm)				
Sieve size	Weight Lefe in sieve	accumulative of Weight Retained	Weight Passing	Percentage passing	Sieve size	Weight Lefe in sieve	Accumulative of Weight Retained	Weight Passing	Percentage passing
(mm)	(g)	(g)	(g)	(%)	(mm)	(g)	(g)	(g)	(%)
50	0	0	9050	100.0	2.00	757	7447	1603	17.7
37.5	2500	2500	6550	72.4	1.18	178	7625	1425	15.7
20	1223	3723	5327	58.9	0.425	248	7873	1177	13.0
5	2967	6690	2360	26.1	0.3	111	7984	1066	11.8
2	757	7447	1603	17.7	0.075	141	8125	925	10.2

Conclusion: Coarse-Grained

Nonuniformity Coefficient $C_u = \frac{D_{60}}{D_{10}} = \frac{/}{/} = /$

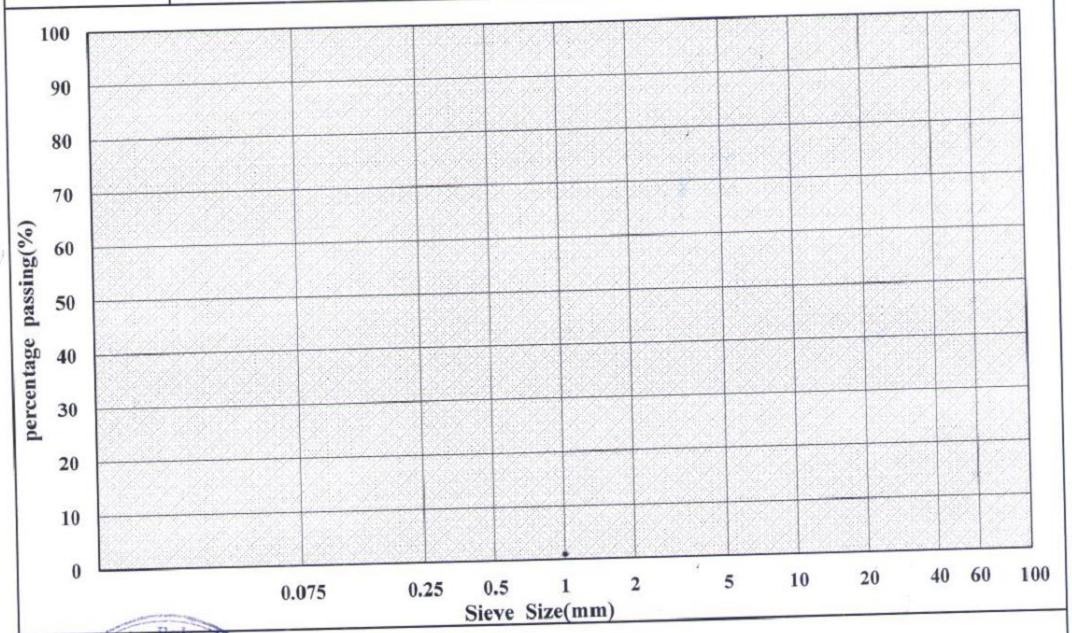

Remarks:

Submit by: Contractor's representative | Checked by: Material Engineer(Contractor) | Witness by: Consultant's representative | Supervisor: Material Engineer(Consultant)

Addis Ababa Bole International Airport Terminal Expantion Project

Contractor: China Communications Construction Co. Ltd. Consultant:Aéroports de paris Ingénierie(ADPI, FRANCE)

Moisture Density Relations Of The Soil

Sample No		Lab Ref.No	AABIA-171002-02-3
Sample declaration	Stone and clay	Type of Material	Backfill
Location/Source	Kilinto/T2 Parking area	Max-sized	19mm
Blows/layer	56	No.of layers	5
Rammer Wt	4.5KG	Digging depth	
Method used	AACRA	Date test	2017/10/14

Water added (g)	150		300		450		600					
1)Weight mold+sample(g)	9073		9285		9454		9412					
2)Weight of mold(g)	4939.0		4939.0		4939.0		4939.0					
3)Weight of sample(g)	4134.0		4346.0		4515.0		4473.0					
4)Volume(cm)^3	2120		2120		2120		2120					
5)Wet density (g/cm^3)	1.95		2.05		2.13		2.11					
Tare No	G3	G4	G1	G2	6	7	A1	A2				
6)Weight of tare(g)	53	53	53	53	56	56	56	56				
7)Weight tare+sample(g)	262.0	262.0	312.0	312.0	290.0	290.0	300.0	300.0				
8)Weight tare+dry sample(g)	250.0	250.0	289.0	289.0	265.0	265.0	266.0	266.0				
9)Weight of water(g)	12.0	12.0	23.0	23.0	25.0	25.0	34.0	34.0				
10)Weight of dry sample(g)	197.0	197.0	236.0	236.0	209.0	209.0	210.0	210.0				
11)Moisture content(%)	6.09	6.09	9.75	9.75	11.96	11.96	16.19	16.19				
12)Average water content(%	6.1		9.7		12.0		16.2					
13)Dry density(g/cm^3)	1.84		1.87		1.90		1.82					

Optimal water content OMC(%)
11.6
Max.dry density (g/cm^3)
1.90
Remarks:

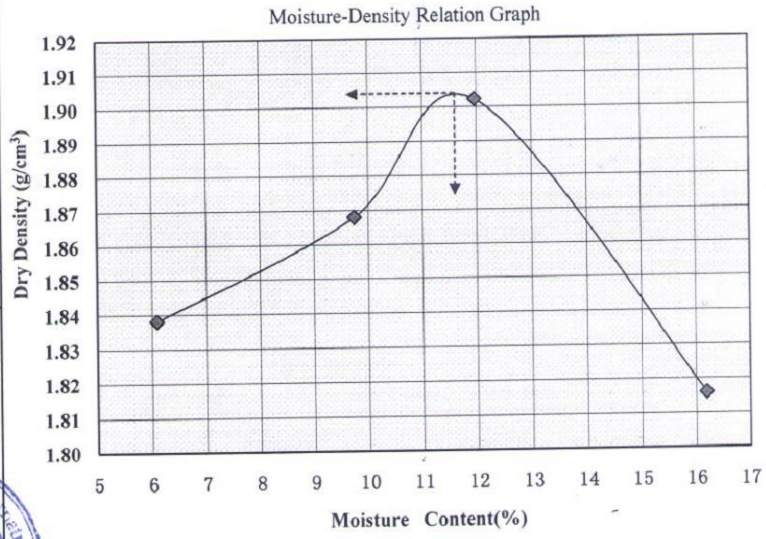

Submit by: Checked by: Witness by: Supervisor:

Addis Ababa Bole International Airport Terminal Expantion Project

Contractor : China Communications Construction Co. Ltd. **Consultant:Aéroports de paris Ingénierie(ADPI, FRANCE)**

California Bearing Ratio

Sample No		Lab Ref No	AABIA-171002-02-4	Sample declaration	Stone and clay
Max-sized	19mm	Type of material	Backfill	Location/source	Kilinto/T2 Parking area
Digging Depth(m)		Method Used	AACRA	Date test	2017/10/15

Moisture Content And Dry Density (Before soaking)									
Mould No.		F1		F2		F3			
No. of layers		5		5		5			
No.of blows per layer		10		10		10			
Wt.of wet sample+mould (g)		10239		10239		10239			
Wt.of mould (g)		6009		6009		6009			
Wt.of wet sample (g)		4230		4230		4230			
Volume of mould (cc)		2084		2084		2084			
Wet unit weight (g/cc)		2.03		2.03		2.03			
Can No.		B-1	B-2	B-3	B-4	B-5	B-6		
Wt.wet sample + can (g)		300	288	300	288	300	288		
Wt.of can (g)		50	54	50	54	50	54		
Wt.dry sample +can (g)		275	249	275	249	275	249		
Wt.of water (g)		25	39	25	39	25	39		
Wt.dry sample (g)		225	195	225	195	225	195		
Moisture content(%)		11.1	20.0	11.1	20.0	11.1	20.0		
Average moisture content		15.6		15.6		15.6			
Dry density (g/cc)		1.76		1.76		1.76			
Average dry density (g/cc)		1.76							
Wt.of sample+mould (After soaking)(g)		10419		10419		10419			
Wt.of absorbed water (g)		180		180		180			
Average wt.of absorbed water (g)		180							

SWELL DATA

Initial height of sample = 120mm

Day of month	Elapse time (day)	Mould 1			Mould 2			mould 3		
		gauge reading	swell		gauge reading	swell		gauge reading	swell	
			mm	%		mm	%		mm	%
2017/10/15	0	0	0	0	0	0	0	0	0	0
2017/10/19	4	149.0	1.49	1.24	149.0	1.49	1.24	149.0	1.49	1.24
Average Swell (%)		1.24								

CBR DATA

Max. Dry Density(g/cc)	1.90	Optimal water content(%)	11.6
Calibration Coef of Proving ring(n/%mm)	100	Area of Penetration Post(cm^2)	19.635

Penetration (mm)	Std load (KPa)	mould (1)					mould (2)					mould (3)				
		Gauge readin	test load		corr.CBR		Gauge readin	test load		corr.CBR		Gauge readin	test load		corr.CBR	
			N	KPa	KPa	%		N	KPa	KPa	%		N	KPa	KPa	%
0.00		0	0	0			0	0	0			0	0	0		
0.64		23	2300	1171			23	2300	1171			23	2300	1171		
1.27		31	3100	1579			31	3100	1579			31	3100	1579		
1.91	7000	39	3900	1986	1986	28	39	3900	1986	1986	28	39	3900	1986	1986	28
2.54		50	5000	2546			50	5000	2546			50	5000	2546		
3.81	10500	59	5900	3005	3005	29	59	5900	3005	3005	29	59	5900	3005	3005	29
5.08		68	6800	3463			68	6800	3463			68	6800	3463		
7.62		84	8400	4278			84	8400	4278			84	8400	4278		

Conclusion: Penetration=2.5mm C_v= 0 (%) CBR= 28 (%)

Penetration=5.0mm C_v= 0 (%) CBR= 29 (%)

Submit by: Checked by: Witness by: Supervisor:

Contractor's representative Material Engineer(Contractor) Consultant's representative Material Engineer(Consultant)

Addis Ababa Bole International Airport Terminal Expantion Project

Contractor : China Communications Construction Co. Ltd. **Consultant:Aéroports de paris Ingénierie(ADPI, FRANCE)**

California Bearing Ratio

Sample No		Lab Ref No	AABIA-171002-02-5	Sample declaration	Stone and clay		
Max-sized (mm)	19mm	Type of material	Backfill	Location/source	Kilinto/T2 Parking area		
Digging Depth(m)		Method Used	AACRA	Date test	2017/10/15		

Moisture Content And Dry Density (Before soaking)											
	Mould No.	F4		F5		F6					
	No. of layers	5		5		5					
	No.of blows per layer	30		30		30					
	Wt.of wet sample+mould (g)	10831		10831		10831					
	Wt.of mould (g)	6476		6476		6476					
	Wt.of wet sample (g)	4355		4355		4355					
	Volume of mould (cc)	2084		2084		2084					
	Wet unit weight (g/cc)	2.09		2.09		2.09					
	Can No.	C-1	C-2	C-3	C-4	C-5	C-6				
	Wt.wet sample + can (g)	375	401	375	401	375	401				
	Wt.of can (g)	52	50	52	50	52	50				
	Wt.dry sample +can (g)	342	349	342	349	342	349				
	Wt.of water (g)	33	52	33	52	33	52				
	Wt.dry sample (g)	290	299	290	299	290	299				
	Moisture content(%)	11.4	17.4	11.4	17.4	11.4	17.4				
	Average moisture content	14.4		14.4		14.4					
	Dry density (g/cc)	1.83		1.83		1.83					
	Average dry density (g/cc)	1.83									
Wt.of sample+mould (After soaking)(g)		10953		10953		10953					
Wt.of absorbed water (g)		122		122		122					
Average wt.of absorbed water (g)		122									

SWELL DATA Initial height of sample = 120mm

Day of month	Elapse time (day)	Mould 1			Mould 2			mould 3		
		gauge reading	swell		gauge reading	swell		gauge reading	swell	
			mm	%		mm	%		mm	%
2017/10/15	0	0	0	0	0	0	0	0	0	0
2017/10/19	4	116	1	0.97	116	1	0.97	116	1	0.97
Average Swell (%)		0.97								

CBR DATA

Max. Dry Density(g/cc)	1.90	Optimal water content(%)	11.6
Calibration Coef of Proving ring(n/%mm)	100	Area of Penetration Post(cm^2)	19.635

Penetration (mm)	Std load (KPa)	mould (1)					mould (2)					mould (3)				
		Gauge readin	test load		corr.CBR		Gauge readin	test load		corr.CBR		Gauge readin	test load		corr.CBR	
			N	KPa	KPa	%		N	KPa	KPa	%		N	KPa	KPa	%
0.00		0	0	0			0	0	0			0	0	0		
0.64		30	3000	1528			30	3000	1528			30	3000	1528		
1.27		39	3900	1986			39	3900	1986			39	3900	1986		
1.91	7000	48	4800	2445	2445	35	48	4800	2445	2445	35	48	4800	2445	2445	35
2.54		61	6100	3107			61	6100	3107			61	6100	3107		
3.81	10500	69	6900	3514	3514	33	69	6900	3514	3514	33	69	6900	3514	3514	33
5.08		80	8000	4074			80	8000	4074			80	8000	4074		
7.62		89	8900	4533			89	8900	4533			89	8900	4533		
Conclusion		Penetration=2.5mm						C_V= 0 (%)					CBR= 35 (%)			
		Penetration=5.0mm						C_V= 0 (%)					CBR= 33 (%)			

Submit by: Contractor's representative Checked by: Material Engineer(Contractor) Witness by: Consultant's representative Supervisor: Material Engineer(Consultant)

Addis Ababa Bole International Airport Terminal Expantion Project

Contractor : China Communications Construction Co. Ltd. **Consultant:** Aéroports de paris Ingénierie(ADPI, FRANCE)

California Bearing Ratio

Sample No		Lab Ref No	AABIA-171002-02-6	Sample declaration	Stone and clay
Max-sized (mm)	19mm	Type of material	Backfill	Location/source	Kilinto/T2 Parking area
Digging Depth(m)		Method Used	AACRA	Date test	2017/10/15

Moisture Content And Dry Density (Before soaking)									
	Mould No.	F7		F8		F9			
	No. of layers	5		5		5			
	No.of blows per layer	65		65		65			
	Wt.of wet sample+mould (g)	10700		10700		10700			
	Wt.of mould (g)	6199		6199		6199			
	Wt.of wet sample (g)	4501		4501		4501			
	Volume of mould (cc)	2084		2084		2084			
	Wet unit weight (g/cc)	2.16		2.16		2.16			
	Can No.	D-1	D-2	D-3	D-4	D-5	D-6		
	Wt.wet sample + can (g)	350	328	350	328	350	328		
	Wt.of can (g)	55	58	55	58	55	58		
	Wt.dry sample +can (g)	320	294	320	294	320	294		
	Wt.of water (g)	30.0	34.0	30.0	34.0	30.0	34.0		
	Wt.dry sample (g)	265.0	236.0	265.0	236.0	265.0	236.0		
	Moisture content(%)	11.3	14.4	11.3	14.4	11.3	14.4		
	Average moisture content	12.9		12.9		12.9			
	Dry density (g/cc)	1.91		1.91		1.91			
	Average dry density (g/cc)	1.91							
Wt.of sample+mould (After soaking)(g)		10777		10777		10777			
Wt.of absorbed water (g)		77		77		77			
Average wt.of absorbed water (g)		77							

SWELL DATA Initial height of sample = 120mm

Day of month	Elapse time (day)	Mould 1			Mould 2			mould 3		
		gauge reading	swell		gauge reading	swell		gauge reading	swell	
			mm	%		mm	%		mm	%
2017/10/15	0	0	0	0	0	0	0	0	0	0
2017/10/19	4	75.0	0.75	0.63	75.0	0.75	0.63	75.0	0.75	0.63
Average Swell (%)		0.63								

CBR DATA

Max. Dry Density(g/cc)	1.90	Optimal water content(%)	11.6
Calibration Coef of Proving ring(n/%mm)	280	Area of Penetration Post(cm^2)	19.635

Penetration (mm)	Std load (KPa)	mould (1)					mould (2)					mould (3)				
		Gauge readin	test load		corr.CBR		Gauge readin	test load		corr.CBR		Gauge readin	test load		corr.CBR	
			N	KPa	KPa	%		N	KPa	KPa	%		N	KPa	KPa	%
0.00		0	0	0			0	0	0			0	0	0		
0.64		39	10920	5561			39	#####	5561			39	#####	5561		
1.27		48	13440	6845			48	#####	6845			48	#####	6845		
1.91	7000	60	16800	8556	8556	122	60	#####	8556	8556	122	60	#####	8556	8556	122
2.54		73	20440	10410			73	#####	#####			73	#####	#####		
3.81	####	88	24640	12549	#####	120	88	#####	#####	#####	120	88	#####	#####	12549	120
5.08		97	27160	13832			97	#####	#####			97	#####	#####		
7.62		102	28560	14545			102	#####	#####			102	#####	#####		
Conclusion		Penetration=2.5mm					C_V= 0 (%)					CBR= 122 (%)				
		Penetration=5.0mm					C_V= 0 (%)					CBR= 120 (%)				

Submitted by: Checked by: Witness by: Supervisor:

Contractor's Representative Material Engineer(Contractor) Consultant's representative Material Engineer(Consultant)

Addis Ababa Bole International Airport Terminal Expantion Project

Contractor : China Communications Construction Co. Ltd. Consultant: Aéroports de paris Ingénierie(ADPI, FRAN

Penetration and Load Relation

Sample No		Lab Ref No	AABIA-171002-02-7	Sample declaration	Stone and clay
Digging Depth(m)		Type of material	Backfill	Location/Source	Cilinto/T2 Parking are
Max-sized (mm)	19mm	Method Used	AACRA	Date test	2017/10/19

Penetration and Load Relation

Penetration / No. of layers	0.00 (mm)	0.64 (mm)	1.27 (mm)	1.91 (mm)	2.54 (mm)	3.81 (mm)	5.08 (mm)	7.62 (mm)
10	0	1171	1579	1986	2546	3005	3463	4278
30	0	1528	1986	2445	3107	3514	4074	4533
65	0	5561	6845	8556	10410	12549	13832	14545

Remarks:

Submit by: Contractor's representative

Checked by: Material Engineer(Contractor)

Witness by: Consultant's representative

Supervisor: Material Engineer(Consultant)

Addis Ababa Bole International Airport Terminal Expantion Project

Contractor : China Communications Construction Co. Ltd. **Consultant:Aéroports de paris Ingénierie(ADPI, FRAN**

Three-Point C.B.R Curve

Sample No		Lab Ref No	AABIA-171002-02-8	Sample declaration	Stone and clay
Digging Depth(m)		Type of material	Backfill	Location/Source	Kilinto/T2 Parking are
Max-sized (mm)	19mm	Method Used	AACRA	Date test	2017/10/19

Blows/Layer	10/5	30/5	65/5
Soaked C.B.R (%)	29	35	122
Density(g/cm^3)	1.76	1.83	1.91

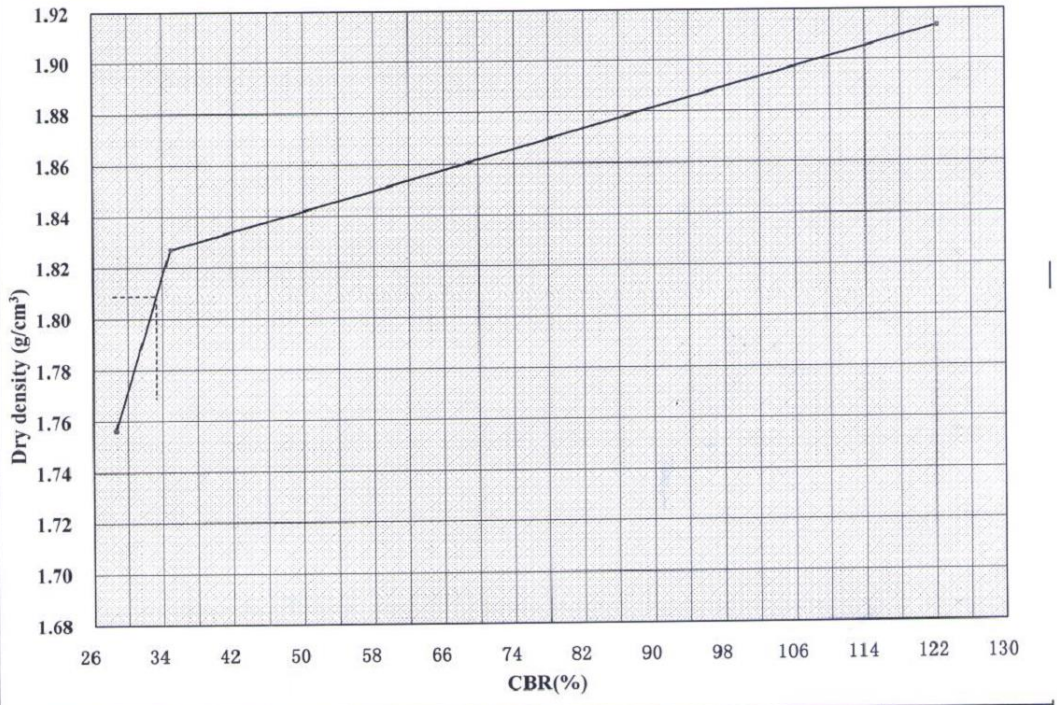

Maximum Dry Density(MDD) (g/cm^3)	1.90	Optimum Moisture Content(OMC) (%)	11.6
Compactness Requirment (%)	95	Targit Density (g/cm^3)	1.81
C.B.R. index value at Requirment Compactness (%)		33.3	
AACRA Specification required of CBR(%)		CBR at 95% MDD, more than 15.	

Remarks:

Submit by: Checked by: Witness by: Supervisor:

Contractor's representative Material Engineer(Laboratory) Consultant's representative Material Engineer(Consultant)

Table of Subgrade Compaction Requirements for Flexible Pavements

GEAR TYPE	GROSS WEIGHT(Lb)	NON-COHESIVE SOILS Depth of Compaction, inch				COHESIVE SOILS Depth of Compaction, inch			
		100%	**95%**	**90%**	**85%**	**100%**	**95%**	**90%**	**85%**
S	30,000	8	8-18	18-32	32-44	6	6-9	9-12	12-17
	50,000	10	10-24	24-36	36-48	6	6-9	9-16	16-20
	75,000	12	12-30	30-40	40-52	6	6-12	10-19	19-25
D (incls.2S)	50,000	12	12-28	28-38	38-50	6	6-10	10-17	17-22
	100,000	17	17-30	30-42	42-55	6	6-12	12-19	19-25
	150,000	19	19-32	32-46	46-60	7	6-14	14-21	21-28
	200,000	21	21-37	37-53	53-59	9	7-16	16-24	24-32
2D (incls. B757, B767,A-300, DC-10-10, L1011)	100,000	14	14-26	26-38	38-49	5	9-10	10-17	17-22
	200,000	17	17-30	30-43	43-56	5	6-12	12-18	18-26
	300,000	20	20-34	34-48	48-63	7	7-14	14-22	22-29
	400,000-600,000	23	23-41	41-59	59-76	9	9-18	18-27	27-36
2D/D1,2D/2D1(incls. MD11, A340,DC10-30/40)	500,000-600,000	23	23-41	41-59	59-76	9	9-18	18-27	27-36
2D/2D2 (incls. B747 series)	800,000	23	23-41	41-59	59-76	9	9-18	18-27	27-36
	975,000	24	24-44	44-62	62-78	10	10-20	20-28	20-28
3D (incls. B777 series)	550,000	20	20-36	36-52	52-67	6	6-14	14-21	14-21

	650,000	22	22-39	39-56	56-70	7	7-16	16-22	16-22
	750,000	24	24-42	42-57	57-71	8	8-17	17-23	17-23
2D/3D2 (incls. A380 series)	1,250,000	24	24-42	42-61	61-78	9	9-18	18-27	18-27
	1,350,000	25	25-44	44-64	64-81	10	10-20	20-29	20-27

Table of Densities for Subgrade

Depth Below Existing Grade	Depth Below Finished Grade	In-Place Density
1′ (0.3 m)	2″ (50 mm)	70%
2′ (0.6 m)	14″ (0.36 m)	84%
3′ (0.9 m)	26″ (0.66 m)	86%
4′ (1.2 m)	38″ (0.97 m)	90%
5′ (1.5 m)	50″ (1.27 m)	93%

Table of Compaction Requirements

100%	95%	90%
0-21	21-37	37-52

Table of specification of grain size analysis of ERA grading chart (ERA, 2013)

SIEVE SIZE (mm)	Mass Percent Passing			
	A	B	C	D
63	100			
50	90-100	100	100	
37.5			80-100	
25	51-80	55-85		100
20			60-100	
9.5		40-70		51-85
5			30-100	
4.75	35-70	30-60		35-65
2		20-51		25-51
1.18			17-75	
0.425		10-31		15-30
0.3			9-50	
0.075	5-15	5-15	5-25	5-15

Table of Record of Sieve Analysis Test of Soil

Sieve size	Weight left in sieve	Accumulative of weight retained	Weight passing	Percentage passing	Sieve size	Weight left in sieve	Accumulative of weight retained	Weight passing	Percentage passing
(mm)	(g)	(g)	(g)	(%)	(mm)	(g)	(g)	(g)	(%)
50	0	0	9050	100.0	2.00	757	7447	1603	17.7
37.5	2500	2500	6550	72.4	1.18	178	7625	1425	15.7
20	1223	3723	5327	58.9	0.425	248	7873	1177	13.0
5	2967	6690	2360	26.1	0.3	111	7984	1066	11.8
2	757	7447	1603	17.7	0.075	141	8125	925	10.2
Conclusion		Coarse-grained			Non uniformity Cu = $\frac{D_{60}}{D_{10}}$				

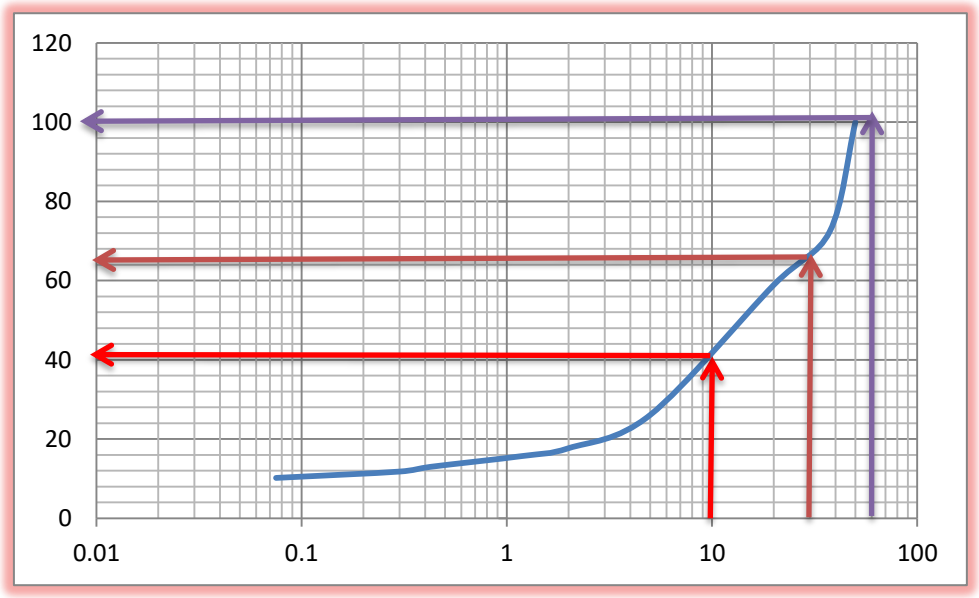

Figure of Graph Sieve Analysis Test of Soil

Table of Compaction test result of natural Soil

Water added(g)	150		300		450		600	
Weight mold + sample (g)	9073		9285		9454		9412	
Weight of mold(g)	4939.0		4939.0		4939.0		4939.0	
Weight of sample (g)	4134.0		4346.0		4515.0		4473.0	
volume (cm^3)	2120		2120		2120		2120	
(γ_t) =wet density(g/cm3)	1.95		2.05		2.13		2.11	
Tare No	G3	G4	G1	G2	6	7	A1	A2
weight of Tare(g)	53	53	53	53	56	56	56	56
weight tare +sample (g)	262.0	262.0	312.0	312.0	290.0	290.0	300.0	300.0
weight of tare +dry sample (g)	250.0	250.0	289.0	289.0	265.0	265.0	266.0	266.0
weight of water (g)	12.0	12.0	23.0	23.0	25.0	25.0	34.0	34.0
weight of dry sample(g)	197.0	197.0	236.0	236.0	209.0	209.0	210.0	210.0
Moisture content (%)	6.09	6.09	9.75	9.75	11.96	11.96	16.19	16.19
Average Moisture content (%)	6.09		9.75		11.96		16.19	
Dry density (g/cm3)=$\gamma_d = \frac{\gamma_t}{1+\left(\frac{\omega}{100}\right)}$	1.84		1.87		1.90		1.82	
Remarks :	Optimal water content OMC (%) =11.6				Max. dry density (g/cm3) =1.90			

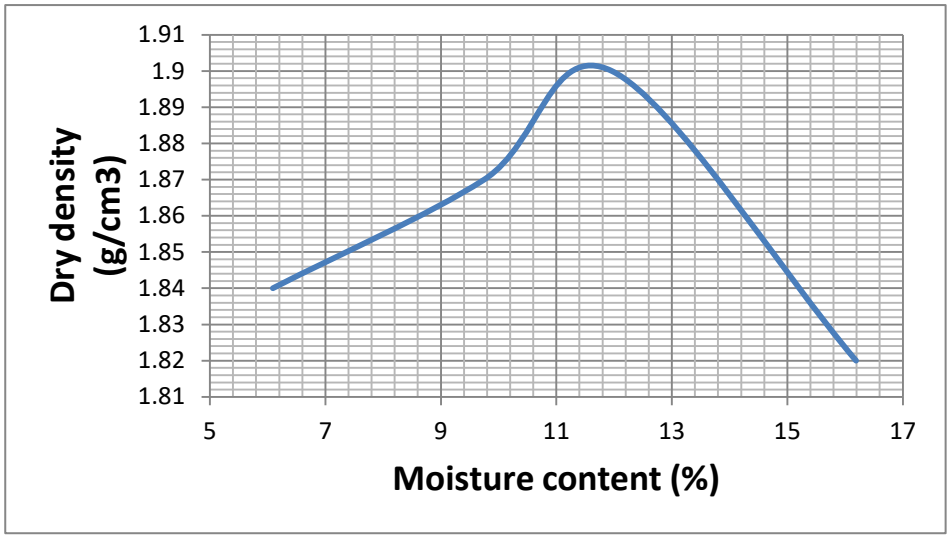

Figure of moisture – density relations by modified proctor test

Table of CBR and swell values at 95 % of MDD

Mold No	F4		F5		F6	
No. of layers	5		5		5	
No.of blows per layer	10		10		10	
Wt. of wet sample + mold (g)	10239		10239		10239	
Wt. of mold (g)	6009		6009		6009	
Wt. of wet sample (g)	4230		4230		4230	
Volume of mold (cc)	2084		2084		2084	
γ_t =Wet unit weight (g/cc)	2.03		2.03		2.03	
Can No.	B-1	B-2	B-3	B-4	B-5	B-6
Wt. wet sample +can (g)	300	288	300	288	300	288

Wt. of can (g)			50	54	50	54	50	54			
Wt. dry sample +can (g)			275	249	275	249	275	249			
Wt. of water (g)			25	39	25	39	25	39			
Wt. of dry sample (g)			225	195	225	195	225	195			
Moisture content (%)			11.1	20.0	11.1	20.0	11.1	20.0			
Average moisture content			15.6		15.6		15.6				
Dry density (g/cc)			1.76		1.76		1.76				
Average dry density (g/cc)			1.76								
Wt. of sample +mould (after soaking)(g)			10419		10419		10419				
Wt. of absorbed water (g)			180		180		180				
Average wt. of absorbed water (g)			180								
SWELL DATA Initial height of sample =120mm											
Date of month	Elapse time (day)	Mould 1			Mould 2			Mould 3			
		Gauge reading	swell		Gauge reading	swell		Gauge Reading	swell		
			mm	%		mm	%		mm	%	
2017/10/15	0	0	0	0	0	0	0	0	0	0	
2017/10/19	4	149.0	1.49	1.24	149.0	1.49	1.24	149.0	1.49	1.24	
Average Swell (%)	1.24										
CBR DATA											
Max. Dry Density (g/cc)		1.90	Optimal water content (%)		11.6						
Calibration coeff. of providing ring(n/%mm)		100	Area of penetration (cm2)		19.635						

Penetration (mm)	Std load (kpa)	Mould(1)					Mould(2)					Mould(3)				
		Gauge reading	Test load		Corr.CBR		Gauge reading	Test load				Gauge reading	Test load			
			N	KPa	KPa	%		N	KPa	KPa	%		N	KPa	KPa	%
0.00		0	0	0			0	0	0			0	0	0		
0.64		23	2300	1171			23	2300	1171			23	2300	1171		

1.27		31	3100	1579			31	3100	1579			31	3100	1579		
1.97	7000	39	3900	1986	1986	28	39	3900	1986	1986	28	39	3900	1986	1986	28
2.54		50	5000	2546			50	5000	2546			50	50000	2546		
3.81	10500	59	5900	3005	3005	29	59	5900	3005	3005	29	59	5900	3005	3005	29
5.08		68	6800	3463			68	6800	3463			68	6800	3463		
7.62		84	8400	4278			84	8400	4278			84	8400	4278		
Conclusion																

Penetration =2.54mm C_v =0 (%) CBR = 28(%)

Penetration =5.08mm C_v =0 (%) CBR = 29(%)

Table of California Bearing Ratio

	Mold No	F4		F5		F6	
	No. of layers	5		5		5	
	No.of blows per layer	30		30		30	
	Wt. of wet sample + mold (g)	10831		10831		10831	
	Wt. of mold (g)	6476		6476		6476	
	Wt. of wet sample (g)	4355		4355		4355	
	Volume of mold (cc)	2084		2084		2084	
	Wet unit weight (g/cc)	2.09		2.09		2.09	
	Can No.	C-1	C-2	C-3	C-4	C-5	C-6
	Wt. wet sample +can (g)	375	401	375	401	375	401
	Wt. of can (g)	52	50	52	50	52	50
	Wt. dry sample +can (g)	342	349	342	349	342	349
	Wt. of water (g)	33	52	33	52	33	52
	Wt. of dry sample (g)	290	299	290	299	290	299
	Moisture content (%)	11.4	17.4	11.4	17.4	11.4	17.4
	Average moisture content	14.4		14.4		14.4	
	Dry density (g/cc)	1.83		1.83		1.83	
	Average dry density (g/cc)	1.83					
Wt. of sample +mould (after soaking)(g)		10953		10953		10953	

Wt. of absorbed water (g)						122						122			122	
Average wt. of absorbed water (g)						122										
SWELL DATA **Initial height of sample =120mm**																
Date of month	Elapse time (day)	Mould 1				Mould 2						Mould 3				
		Gauge reading	swell			Gauge Reading	swell					Gauge Reading	swell			
			mm	%			mm	%					mm	%		
2017/10/15	0	0	0	0		0	0	0				0	0	0		
2017/10/19	4	116	1	0.97		116	1	0.97				116	1	0.97		
Average Swell(%)	0.97															
CBR DATA																
Max. Dry Density (g/cc)					1.90						Optimal water content (%)				11.6	
Calibration coef. of providing ring(n/ %mm)					100						Area of penetration (cm2)				19.635	
Penetration (mm)	Std Load (kpa)	Mould(1)					Mould (2)					Mould(3)				
		Gauge readin g	Test load		Corr.CBR		Gauge reading	Test load				Gauge reading	Test load			
			N	KPa	KPa	%		N	KPa	KPa	%		N	KPa	KPa	%
0.00		0	0	0			0	0	0			0	0			
0.64		30	3000	1528			30	3000	1528			30	3000	1528		
1.27		39	3900	1986			39	3900	1986			39	3900	1986		
1.97	7000	48	4800	2445	2445	35	48	4800	2445	2445	35	48	4800	2445	2445	35
2.54		61	6100	3107			61	6100	3107			61	6100	3107		
3.81	10500	69	6900	3514	3514	33	69	6900	3514	3514	33	69	6900	3514	3514	33
5.08		80	8000	4074			80	8000	4074			80	8000	4074		
7.62		89	8900	4533			89	8900	4533			89	8900	4533		
Conclusion		Penetration =2.54mm Cv =0 (%) CBR = 35(%)														
		Penetration =5.08mm Cv =0 (%) CBR = 33(%)														

Table of California Bearing Ratio

Sample No		Lab Ref No	AAIA-171002-02-04	Sample declaration	Stone and clay
Max-sized	19mm	Type of Material	Back fill	Location /source	Kilinto/T2 parking area
Digging depth (m)		Method used	AACRA	Date of test	2017/10/15

Mold No	F7		F8		F9	
No. of layers	5		5		5	
No.of blows per layer	65		65		65	
Wt. of wet sample + mold (g)	10700		10700		10700	
Wt. of mold (g)	6199		6199		6199	
Wt. of wet sample (g)	4501		4501		4501	
Volume of mold (cc)	2084		2084		2084	
Wet unit weight (g/cc)	2.16		2.16		2.16	
Can No.	D-1	D-2	D-3	D-4	D-5	D-6
Wt. wet sample +can (g)	350	328	350	328	350	328
Wt. of can (g)	55	58	55	58	55	58
Wt. dry sample +can (g)	320	294	320	294	320	294
Wt. of water (g)	30	34	30	34	30	34
Wt. of dry sample (g)	265	236	265	236	265	236
Moisture content (%)	11.3	14.4	11.3	14.4	11.3	14.4
Average moisture content	12.9		12.9		12.9	

Dry density (g/cc)			1.91			1.91			1.91		
Average dry density (g/cc)			1.91								
Wt. of sample +mould (after soaking)(g)			10777			10777			10777		
Wt. of absorbed water (g)			77			77			77		
Average wt. of absorbed water (g)			77								
SWELL DATA Initial height of sample =120mm											
Date of month	Elapse time (day)	Mould 1			Mould 2			Mould 3			
		Gauge reading	Swell		Gauge reading	swell		Gauge Reading	swell		
			mm	%		mm	%		mm	%	
2017/10/15	0	0	0	0	0	0	0	0	0	0	
2017/10/19	4	75	0.75	0.63	75	0.75	0.63	75	0.75	0.63	
Average Swell (%)	0.63										

CBR DATA

Max. Dry Density (g/cc)	1.90	Optimal water content (%)	11.6
Calibration coef. of providing ring(n/ %mm)	280	Area of penetration (cm2)	19.635

Penetration (mm)	Std load (kpa)	Mould(1)					Mould(2)					Mould(3)				
		Gauge reading	Test load		Corr.CBR		Gauge reading	Test load				Gauge reading	Test load			
			N	kPa	kPa	%		N	kPa	kPa	%		N	kPa	kPa	%

0.00		0	0	0			0	0	0			0	0	0		
0.64		39	10920	5561			39	10920	5561			39	10920	5561		
1.27		48	13440	6845			48	13440	6845			48	13440	6845		
1.97	7000	60	16800	8556	8556	122	60	16800	8556	8556	122	60	16800	8556	8556	122
2.54		73	20440	10410			73	20440	10410			73	20440	10410		
3.81	10500	88	24640	12549	12549	120	88	24640	12549	12549	120	88	24640	12549	12549	120
5.08		97	27160	13832			97	27160	13832			97	27160	13832		
7.62		102	28560	14545			102	28560	14545			102	28560	14545		
Conclusion		Penetration =2.54mm Cv =0 (%) CBR = 122(%)														
		Penetration =5.08mm Cv =0 (%) CBR = 120(%)														

Penetration and Loading Relation

Table ofPenetration and Loading Relation

Penetration No.of layer	0.00	0.64	1.27	1.91	2.54	3.81	5.08	7.62
	mm	mm	mm	mm	mm	mm	mm	mm
10	0	1171	1579	1986	2546	3005	3463	4278
30	0	1528	1986	2445	3107	3514	4074	4533
65	0	5561	6845	8556	10410	12549	13832	14545

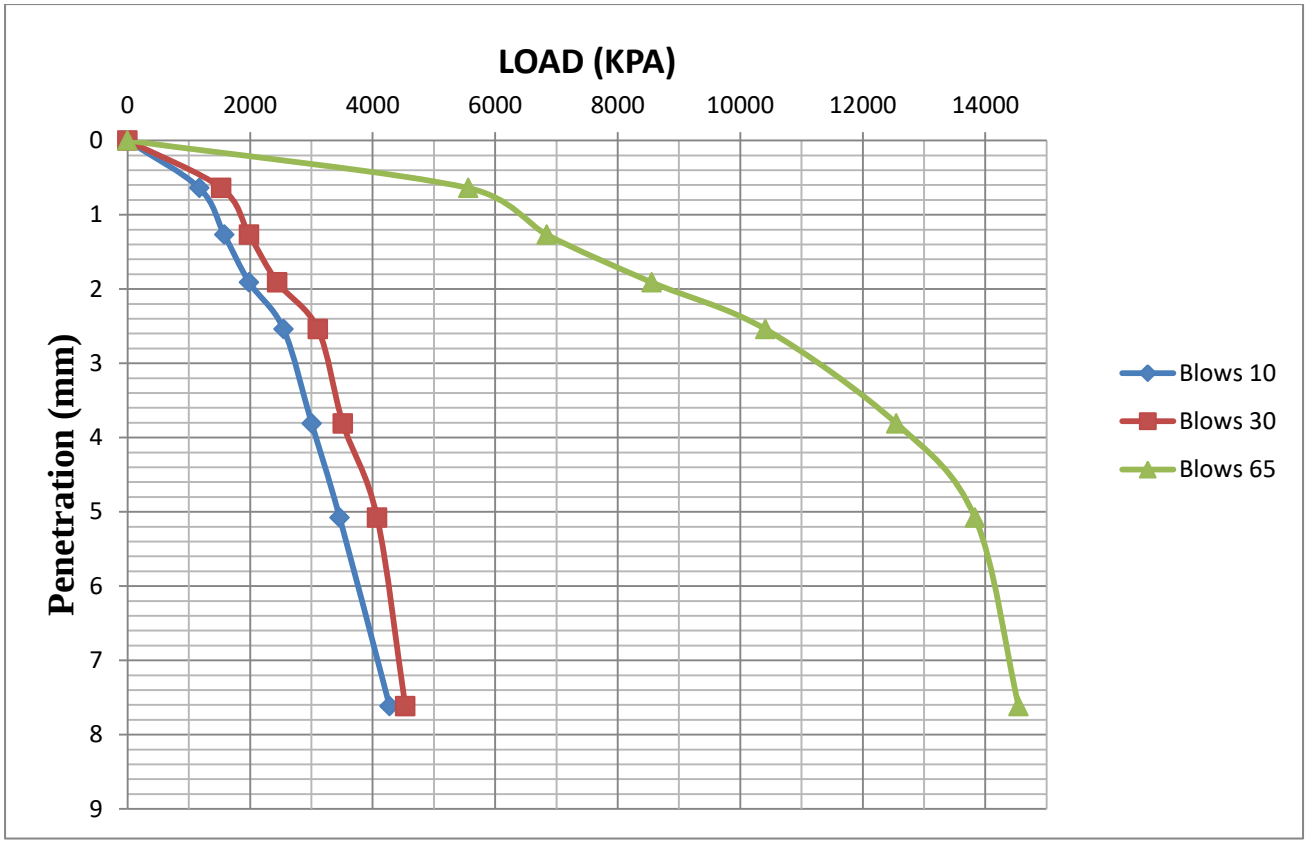

Figure of Penetration and Loading Relation

Table of Three-point C.B.R Curve

Blows/Layer	10/5	30/5	65/5
Soaked C.B.R (%)	29	35	122
Density (g/cm3)	1.76	1.83	1.91

Maximum Dry Density(MDD)(g/cm3)	1.90	Optimum moisture content (OMC) (%)	11.6
Compactness Requirement (%)	95	Target Density (g/cm3)	1.81
C.B.R. index value at requirement Compactness (%)		33.3	
AACRA Specification Required of CBR (%)		CBR at 95%MDD, more than 15	
Remarks:			

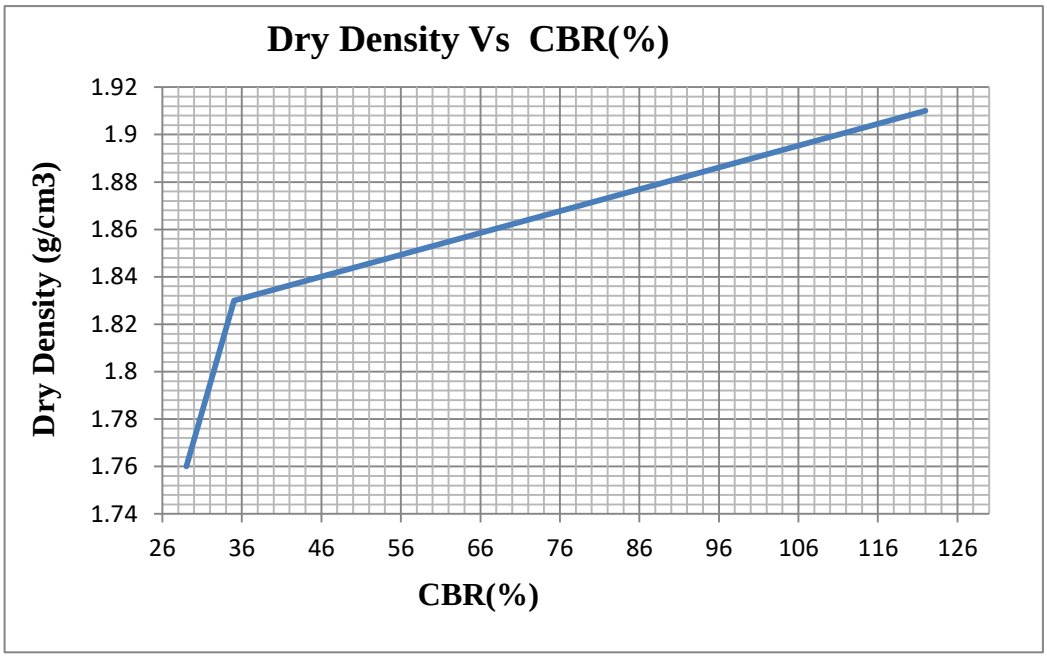

Figure of Graph of Dry Density- CBR (%)

CBR			
No. of blows	10	30	65
No. of layers	5	5	5
Dry unit weight (g/cm3)	1.76	1.83	1.91
CBR (%)	29	35	122
Absorptivity(g)	180	122	77
Swell (%)	1.24	0.97	0.63

Moisture Density Relations(Proctor)						
Proctor modify	1	2	3	4	5	OPM
Moisture content (%)	6.1	9.7	12.0	16.2	/	11.6
Dry density (g/cm3)	1.84	1.87	1.90	1.82	/	1.90

Sieve Analysis										
Sieve size (mm)	50	37.5	20	5	2	1.18	0.425	0.3	0.075	Soil sort
Percentage passing (%)	86.7	79.7	47.7	23.4	18.2	17.0	15.1	14.6	13.2	Course-Grained

Remarks:	

Conclusion	All the indicator meet the technical requirements of Backfill
Idea of the material Engineer consultant	Upon examination, the material can be used for every region of subgrade

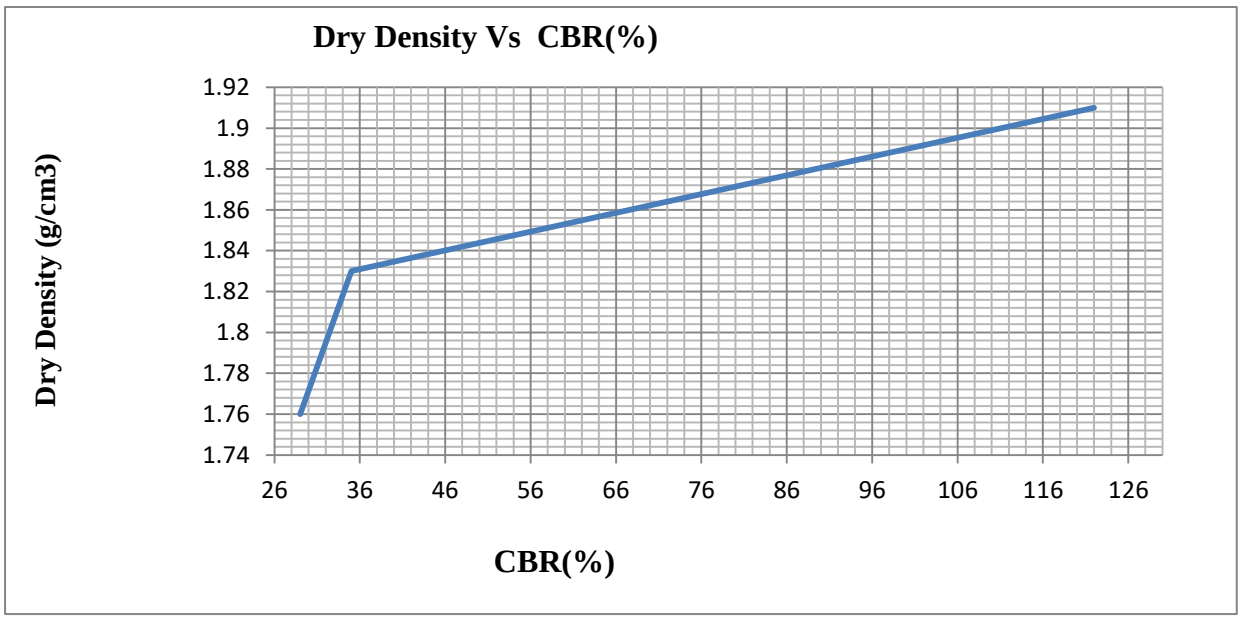

Figure of Graph of Dry Density - CBR (%)

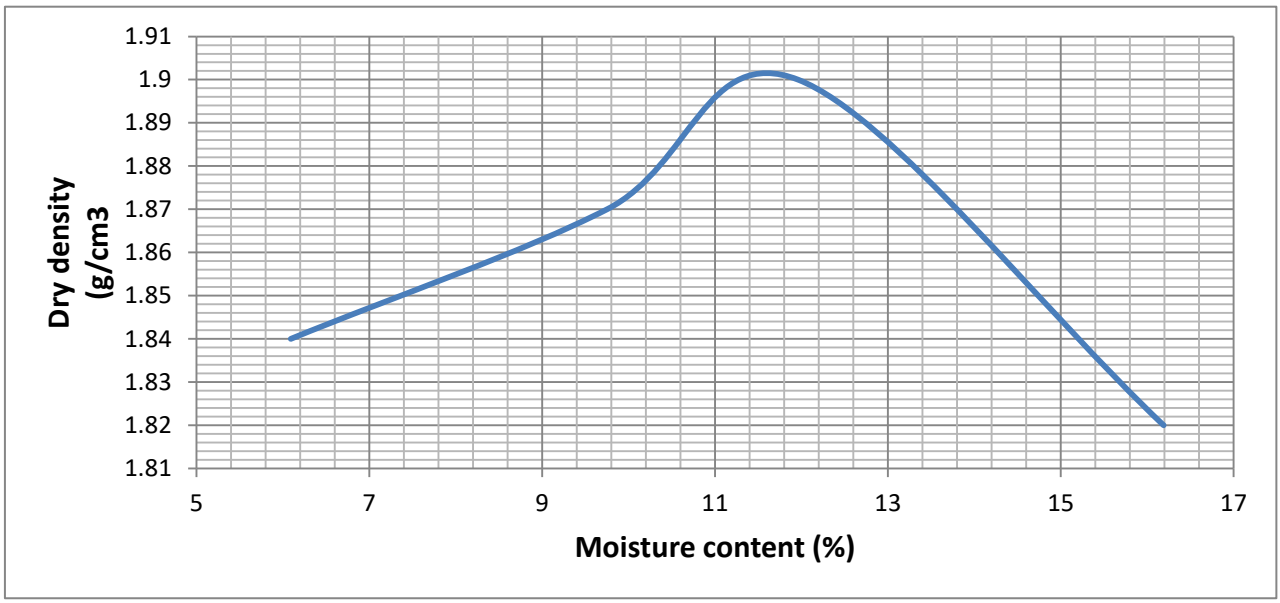

Figure of Moisture – Dry Density

Annex III

FAARFIELD SOFTWARE OUT PUT

Table of COMPACTION REQUIREMENTS

100%	95%	90%
0-21	21-37	37-52

Determination of Resilient Modulus (E_{SG}-Value) and Foundation Modulus (k-Value) for flexible Pavement Subgrade

CASE–ONE (1)- CBR VALUE =8%

The screenshot from the design software showing final thickness design is shown below:

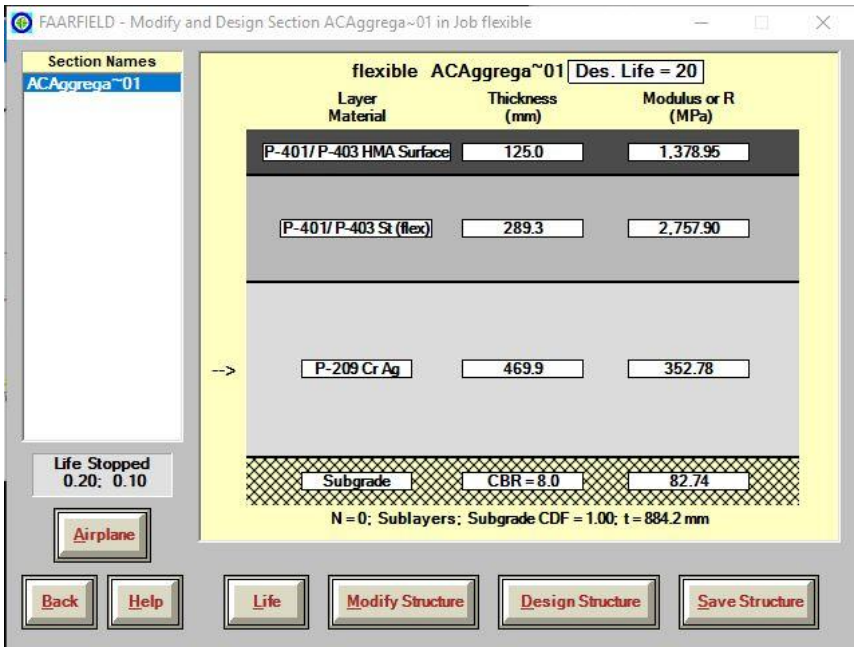

Figure of FAARFIELD Screenshot Showing Final Pavement Thickness Design

(For CBR-8)

Table of Additional Aircraft Information for Design (For CBR-8)

SUBGRADE CDF				
No.	Name	CDF Contribution	CDF Max for Aircraft	P/C Ratio
1	A320-100	0.00	0.00	1.21
2	A340-600 opt	0.09	0.09	0.59
3	A340-600 opt Belly	0.00	0.04	0.58
4	A380-800	0.01	0.01	0.42
5	B737-800	0.00	0.00	1.22
6	B747-400B Combi	0.01	0.01	0.57
7	B747-400ER Passenger	0.01	0.01	0.57
8	B757-300	0.00	0.00	0.72
9	B767-400 ER	0.04	0.05	0.60
10	B777-300 ER	0.81	0.82	0.40
11	B787-8 (Preliminary)	0.03	0.03	0.58

Above Table of Additional Aircraft Information for Design, shows that the pavement thickness designs in this case are controlled primarily by the B777-300 ER, which contributes 81 percent of the CDF.

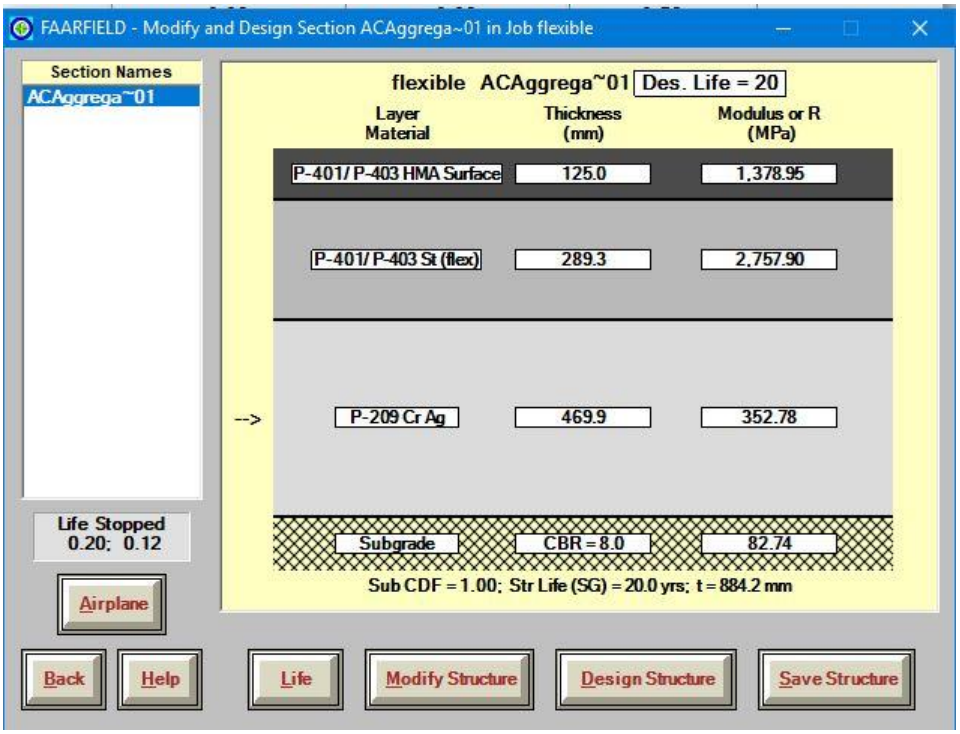

Figure of Analyzed data of Life for CBR 8 subgrade

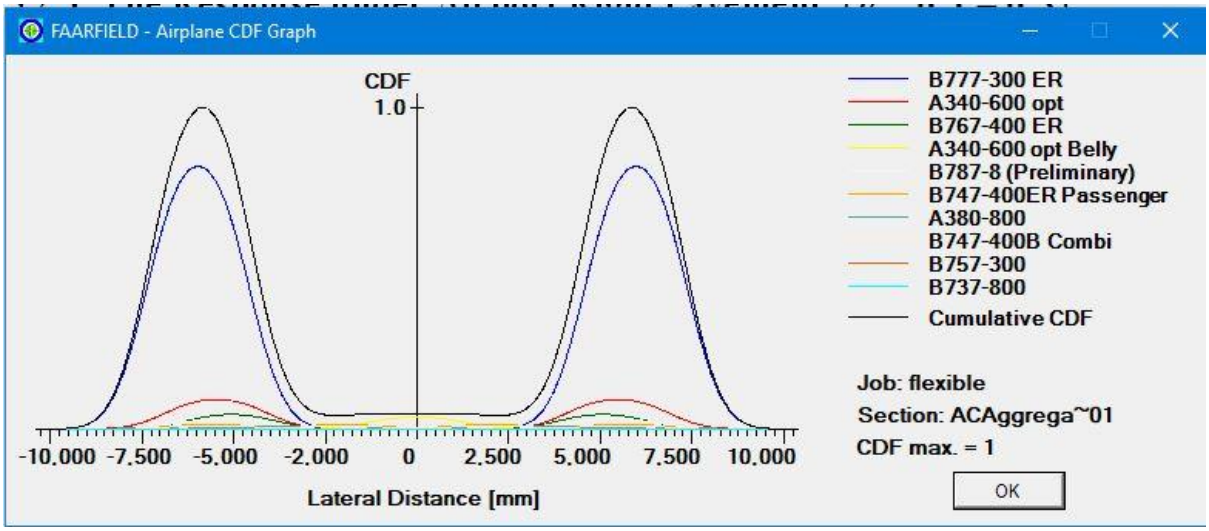

Figure of CDF Graph for CBR-8 Subgrade

CASE–ONE (2)- CBR VALUE =15%

The screenshot from the design software showing final thickness design is shown below:

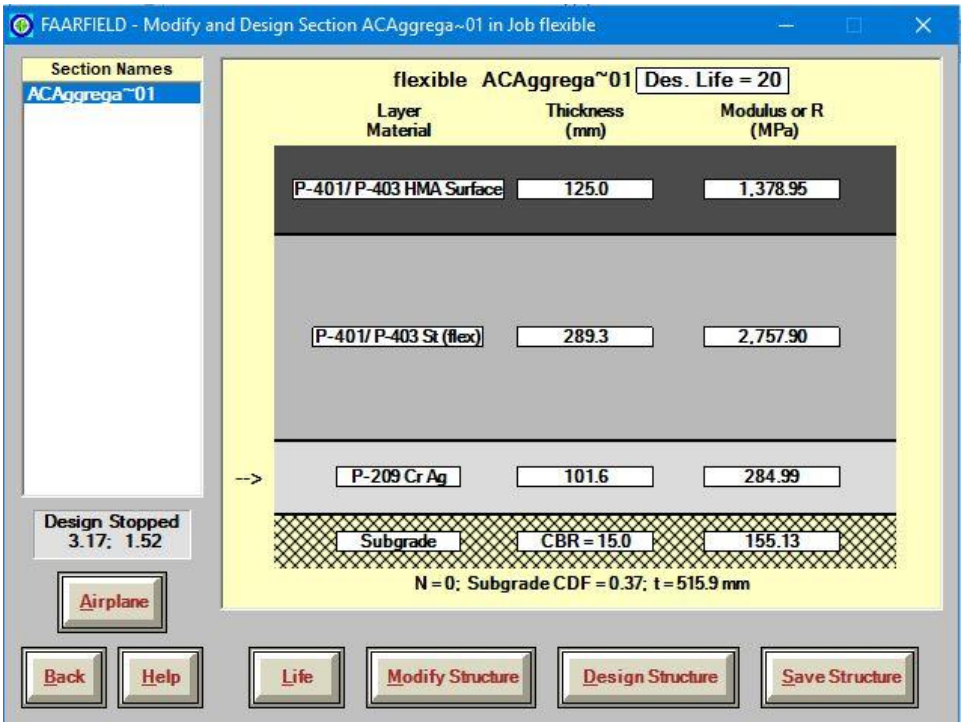

Figure of FAARFIELD Screenshot Showing Final Pavement Thickness Design (For CBR-15)

Table of Additional Aircraft Information for Design (For CBR-15%)

SUBGRADE CDF				
No.	Name	CDF Contribution	CDF Max for Aircraft	P/C Ratio
1	A320-100	0.00	0.00	1.46
2	A340-600 opt	0.18	0.18	0.81
3	A340-600 opt Belly	0.00	0.05	0.84
4	A380-800	0.01	0.01	0.58
5	B737-800	0.00	0.00	1.39
6	B747-400B Combi	0.01	0.01	0.73
7	B747-400ER Passenger	0.01	0.01	0.75
8	B757-300	0.00	0.00	0.73
9	B767-400 ER	0.02	0.02	0.76
10	B777-300 ER	0.13	0.13	0.55
11	B787-8 (Preliminary)	0.02	0.02	0.80

Table of Additional Aircraft Information for Design (For CBR-15%) shows that the pavement thickness design in this example is controlled primarily by the A340-600 opt, which contributes 18 percent of the CDF.

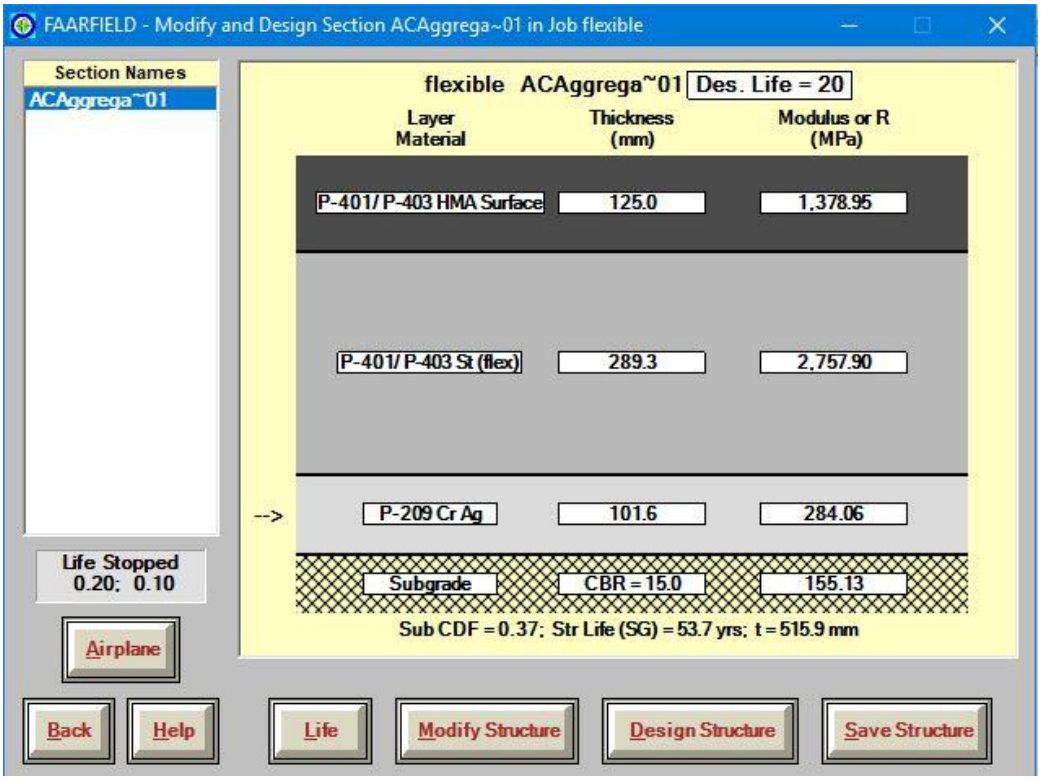

Figure of Analyzed data of Life for CBR 15 subgrade

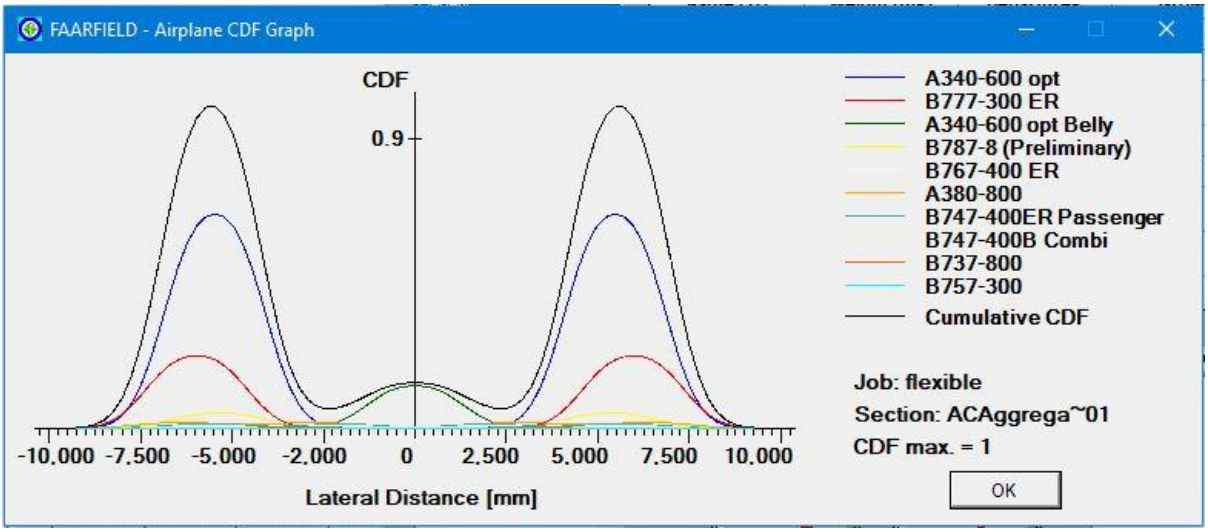

Figure of CDF Graph for CBR-15 Subgrade

CASE–Three (3)- CBR VALUE =25%

The screenshot from the design software showing final thickness design is shown below:

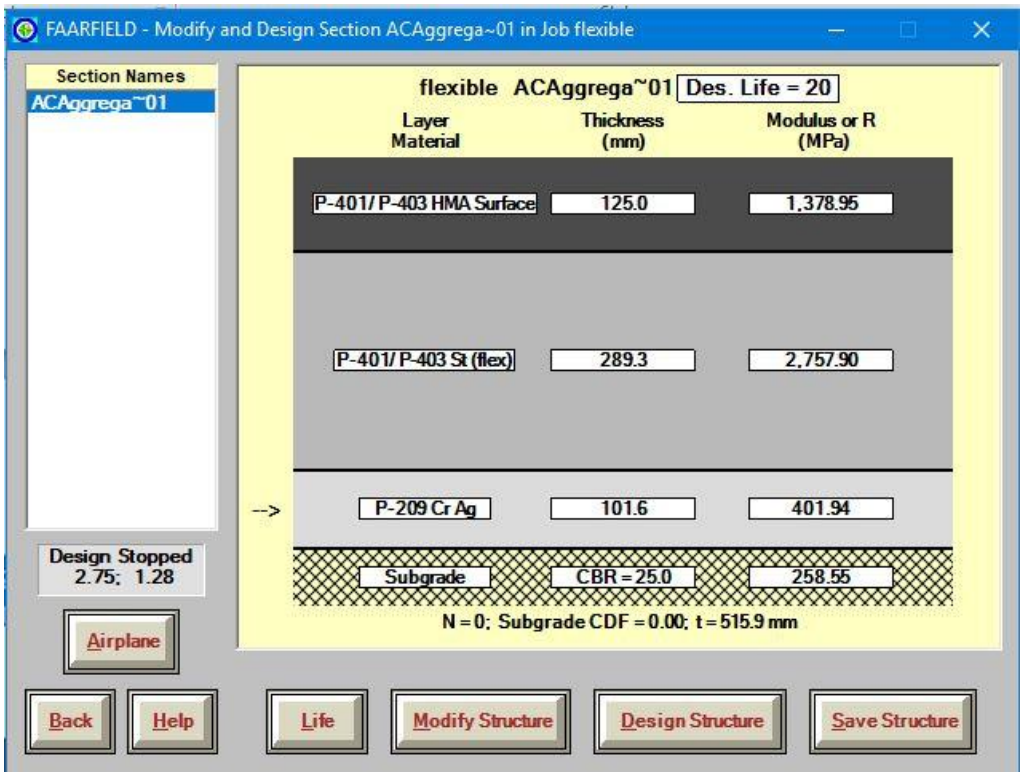

Figure of FAARFIELD Screenshot Showing Final Pavement Thickness Design (For CBR-25%)

Table of Additional Aircraft Information for Design (For CBR-25%)

SUBGRADE CDF				
No.	Name	CDF Contribution	CDF Max for Aircraft	P/C Ratio
1	A320-100	0.00	0.00	1.46
2	A340-600 opt	0.00	0.00	0.81
3	A340-600 opt Belly	0.00	0.00	0.84
4	A380-800	0.00	0.00	0.58
5	B737-800	0.00	0.00	1.39
6	B747-400B Combi	0.00	0.00	0.73
7	B747-400ER Passenger	0.00	0.00	0.75
8	B757-300	0.00	0.00	0.73
9	B767-400 ER	0.00	0.00	0.76
10	B777-300 ER	0.00	0.00	0.55
11	B787-8 (Preliminary)	0.00	0.00	0.80

Table of Additional Aircraft Information for Design (For CBR-25%) shows that the pavement thickness design in this case is not controlled by any Aircraft, which All contributes 0 percent of the CDF.

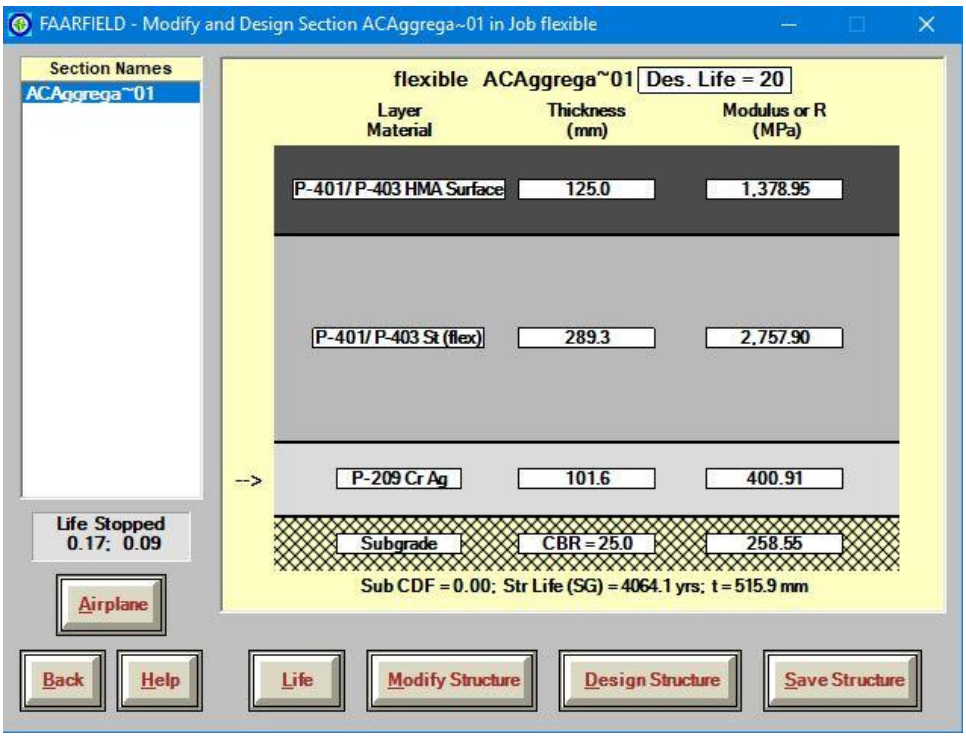

Figure of Analyzed Data of Life for CBR-25 Subgrade

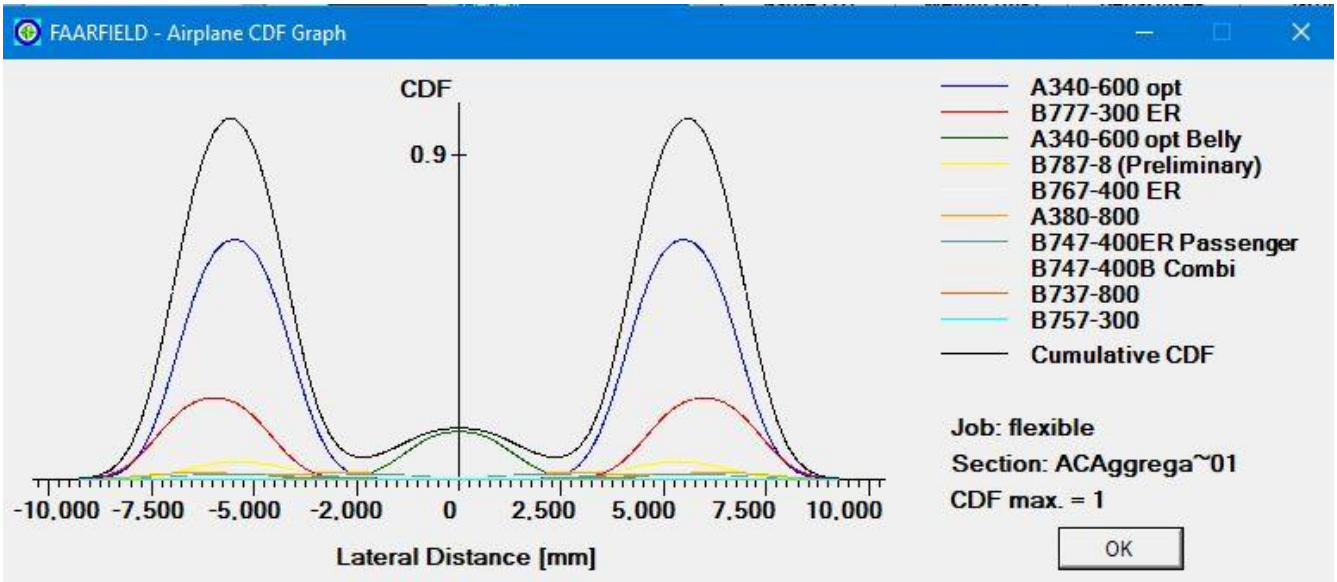

Figure of CDF graph for CBR-25 subgrade

CASE–Four (4)- CBR VALUE =29%

The screenshot from the design software showing final thickness design is shown below:

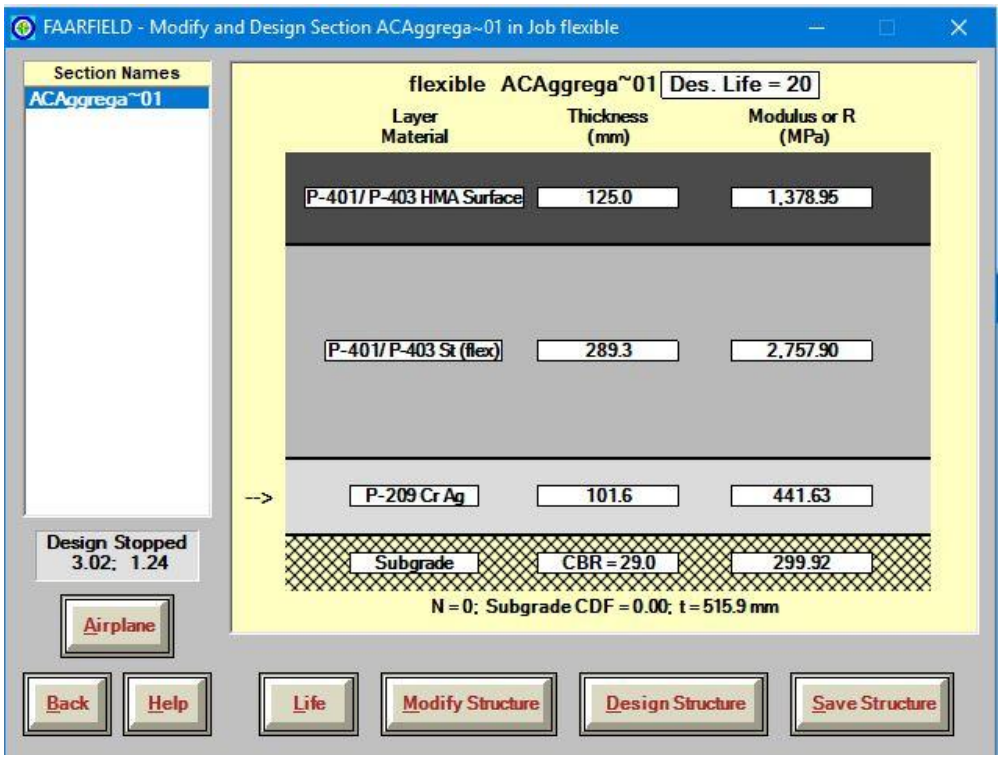

Figure of FAARFIELD screenshot showing final pavement thickness design (for CBR-29%)

Table of Additional Aircraft Information for Design (For CBR-29%)

SUBGRADE CDF				
No.	Name	CDF Contribution	CDF Max for Aircraft	P/C Ratio
1	A320-100	0.00	0.00	1.46
2	A340-600 opt	0.00	0.00	0.81
3	A340-600 opt Belly	0.00	0.00	0.84
4	A380-800	0.00	0.00	0.58
5	B737-800	0.00	0.00	1.39
6	B747-400B Combi	0.00	0.00	0.73
7	B747-400ER Passenger	0.00	0.00	0.75
8	B757-300	0.00	0.00	0.73
9	B767-400 ER	0.00	0.00	0.76
10	B777-300 ER	0.00	0.00	0.55
11	B787-8 (Preliminary)	0.00	0.00	0.80

Table of Additional Aircraft Information for Design (For CBR-29%) shows that the pavement thickness design in this case is not controlled by any Aircraft, which All contributes 0 percent of the CDF.

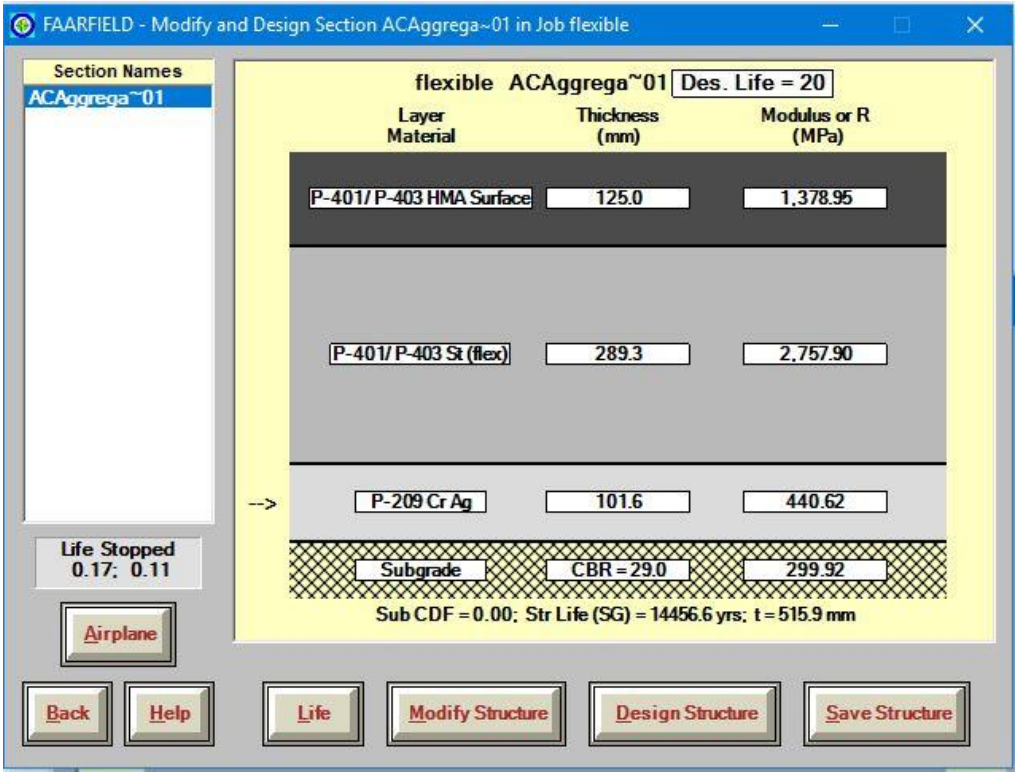

Figure of Analyzed Data of Life for CBR-29 Subgrade

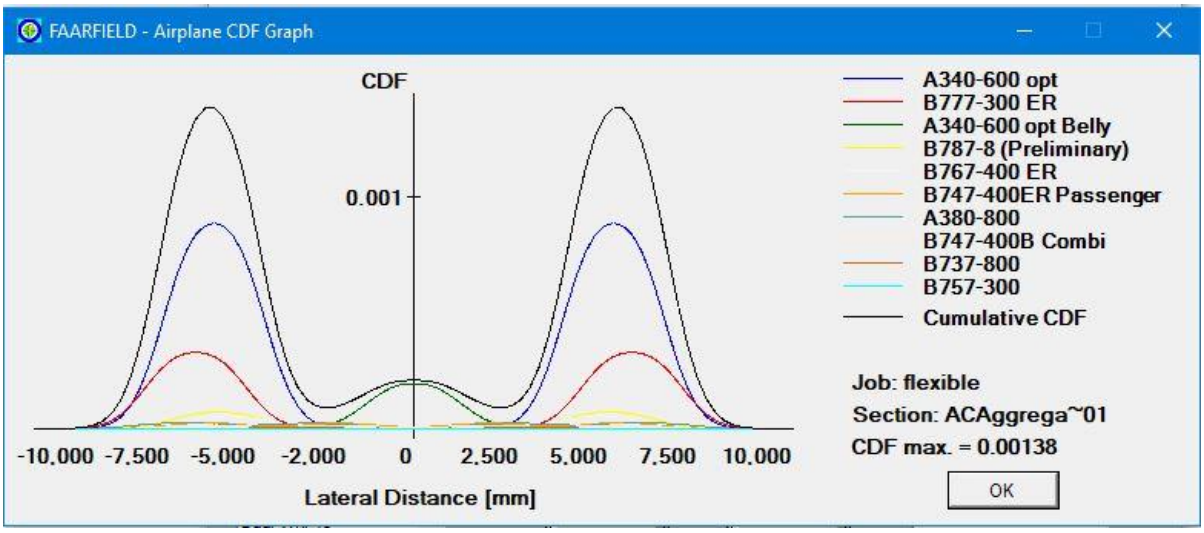

Figure of CDF Graph for CBR-29 Subgrade

CASE–Five (5)- CBR VALUE =33.3%

The screenshot from the design software showing final thickness design is shown below:

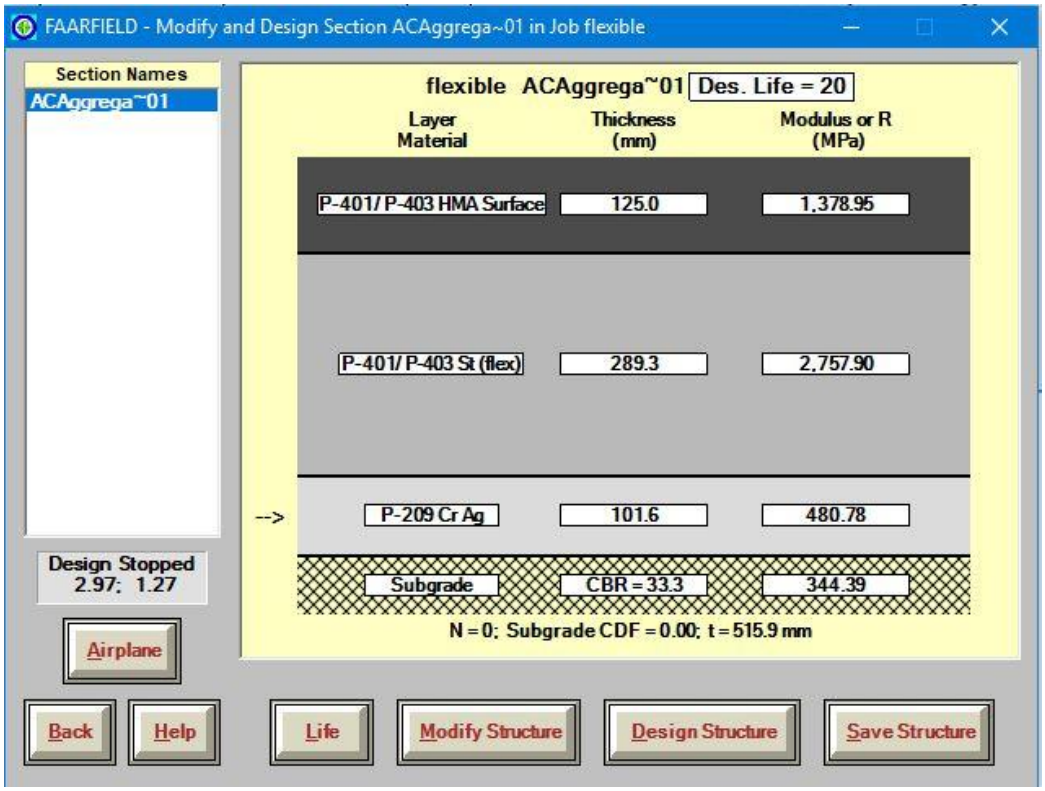

Figure of FAARFIELD Screenshot Showing Final Pavement Thickness Design (For CBR-33.3%)

Table of Additional Aircraft Information for Design (For CBR-33.3%)

SUBGRADE CDF				
No.	Name	CDF Contribution	CDF Max for Aircraft	P/C Ratio
1	A320-100	0.00	0.00	1.46
2	A340-600 opt	0.00	0.00	0.81
3	A340-600 opt Belly	0.00	0.00	0.84
4	A380-800	0.00	0.00	0.58
5	B737-800	0.00	0.00	1.39
6	B747-400B Combi	0.00	0.00	0.73
7	B747-400ER Passenger	0.00	0.00	0.75
8	B757-300	0.00	0.00	0.73
9	B767-400 ER	0.00	0.00	0.76
10	B777-300 ER	0.00	0.00	0.55
11	B787-8 (Preliminary)	0.00	0.00	0.80

Table of Additional Aircraft Information for Design (For CBR-33.3%) shows that the pavement thickness design in this case is not controlled by any Aircraft, which All contributes 0 percent of the CDF.

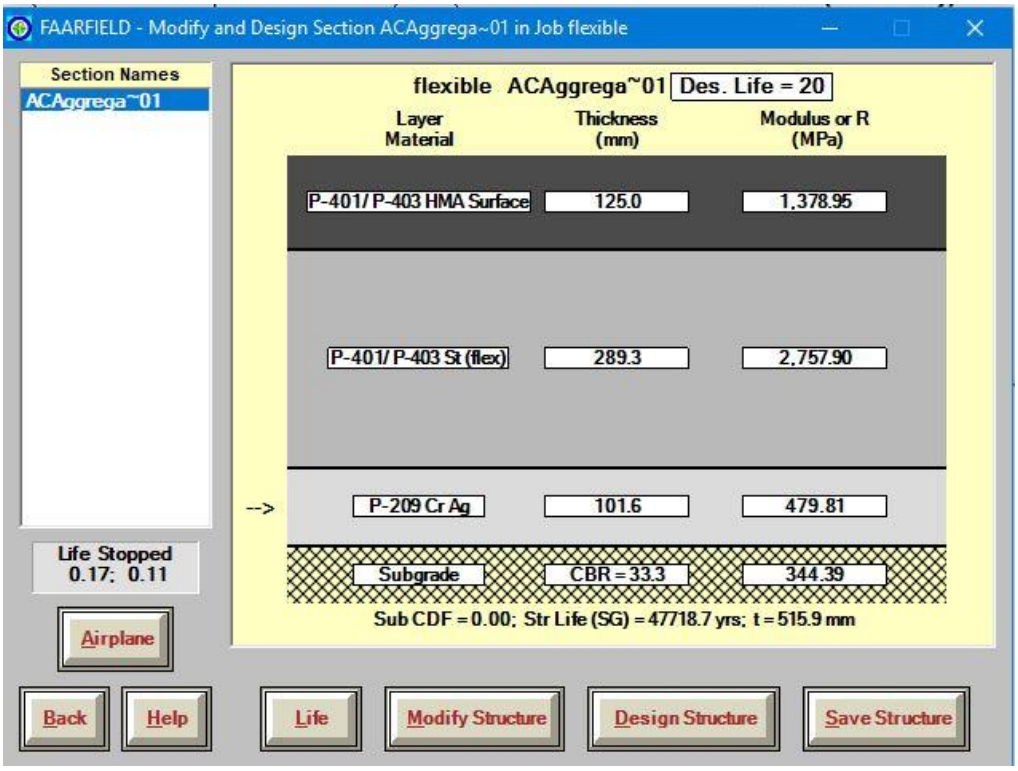

Figure of Analyzed Data of Life for CBR-33.3 Subgrade

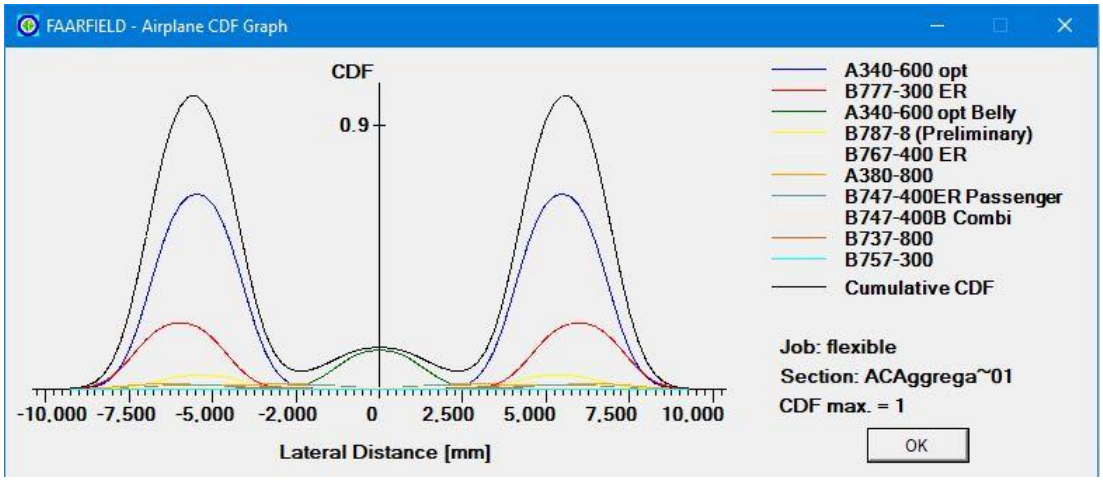

Figure of CDF Graph for CBR-33.3 Subgrade

Table of CBR Value and Subgrade CDF Value for Different Aircraft Category

Subgrade CBR value	8	15	25	29	33.3
Subgrade CDF value (A320-100)	0	0	0	0	0
Subgrade CDF value(A340-600 opt)	9	18	0	0	0
Subgrade CDF value(A340-600 opt Belly)	0	0	0	0	0
Subgrade CDF value(A380-800)	1	1	0	0	0
Subgrade CDF value(B737-800)	0	0	0	0	0
Subgrade CDF value(B747-400B Combi)	1	1	0	0	0
Subgrade CDF value(B747-400ER Passenger)	1	1	0	0	0
Subgrade CDF value (B757-300)	0	0	0	0	0
Subgrade CDF value(B767-400 ER)	4	2	0	0	0
Subgrade CDF value(B777-300 ER)	81	13	0	0	0
Subgrade CDF value(B787-8 (Preliminary))	3	2	0	0	0

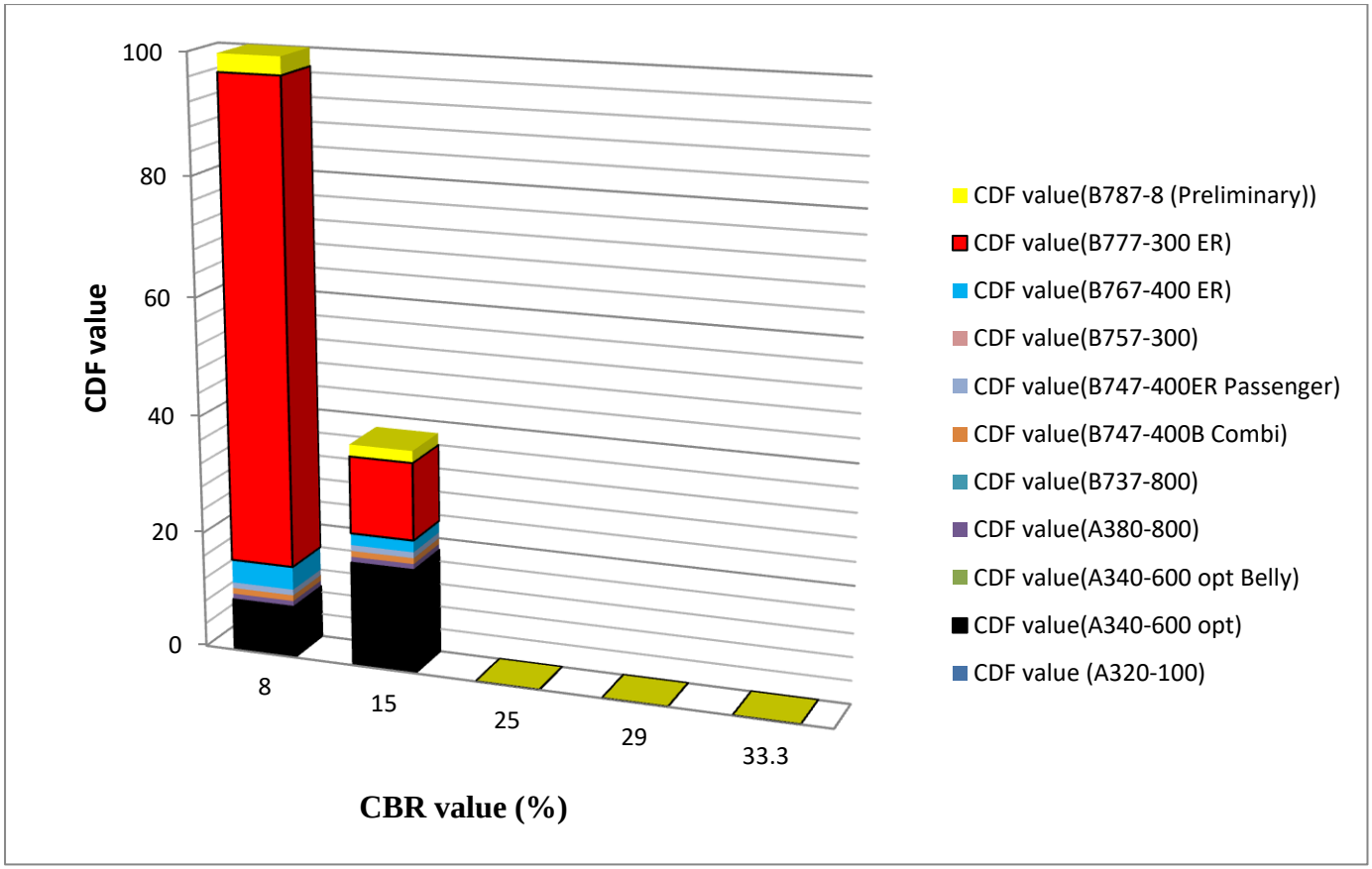

Figure of CBR Value and Subgrade CDF Value for Different Aircraft Category